Poly(arylene imidazolium)s: Towards Stable Hydroxide Ion Exchange Membranes

by

Wei Li

B.Sc. (Hons), University of Waterloo, 2016

Thesis Submitted in Partial Fulfillment
of the Requirements for the Degree of
Master of Science

in the
Department of Chemistry
Faculty of Science

SIMON FRASER UNIVERSITY

Summer 2019

Approval

Name:	**Wei Li**
Degree:	**Master of Science**
Title:	**Poly(arylene imidazolium)s: Towards Stable Hydroxide Ion Exchange Membranes**
Examining Committee:	**Chair:** **Jeffrey Warren** Assistant Professor
	Steven Holdcroft Senior Supervisor Professor
	Dipankar Sen Supervisor Professor
	Bingyun Sun Supervisor Associate Professor
	Timothy Storr Internal Examiner Associate Professor
Date Defended/Approved:	August 22nd, 2019

Abstract

Four novel and sterically-protected arylene imidazole monomers were prepared by the Debus-Radziszewski imidazolium synthesis. Homopolymerization of these monomers was carried out via Yamamoto coupling. Only one of the four monomers yielded high molecular weight poly(arylene imidazole) (PAIM) polymer. Methylation and ethylation of this polymer yield poly(arylene imidazolium), which could be cast into tough, free-standing membranes. By adjusting the degree of methylation from 50% to 100%, the ion exchange capacity (IEC_{cl^-} : number of functional groups per unit mass of polymer) of the membranes were varied from 0 to 2.58 $mmol \cdot g^{-1}$. By controlling the degree of ethylation from 50% to 100%, the IEC_{cl^-} were varied from 0 to 2.40 $mmol \cdot g^{-1}$. The IEC_{cl^-} affected the water uptake and dimensional swelling of membranes. With IEC_{cl^-} increased, both water uptake and dimensional swelling became larger. The chloride ion conductivity of membranes increased up to 15 and 10 $mS \cdot cm^{-1}$ by increasing the IEC_{cl^-} of the methylated and ethylated membranes to 2.58 $mmol \cdot g^{-1}$ and 2.40 $mmol \cdot g^{-1}$, respectively. The membrane with ethylation exhibited more excellent stability in caustic solutions, showing only 2% degradation in 10 M KOH at 80 °C after 168 hours, and longer elongation at break under ambient conditions compared to the membrane with methylation.

Keywords: alkaline anion exchange membrane; steric hindrance; poly(arylene imidazolium); alkylation; hydroxide-stable; organic chemistry

To everyone, who help me in my research project

To my dear family, my friends and teachers

Acknowledgements

I am grateful to my supervisor, Professor Steven Holdcroft, for his guidance, advice, and support through out this research project. He gave me the freedom to investigate new ideas, and inspired me to accomplish more than I had ever imaged. I would also give special thanks to Professor Dipanker Sen and Bingyun Sun for their beneficial feedbacks and advice as supervisory committee members.

Moreover, I would extend my thanks to the previous and present Holdcroft Group members and co-authors for their suggestions and assistance during my time here, especially Dr. Jiantao Fan. I would also like to thanks Dr. Philip Overton for his careful proofreading on the thesis. This thesis would not have been possible without funding from Simon Fraser University.

My deepest and sincerest thanks to all of you.

Table of Contents

List of Figures

List of Tables

List of Schemes

List of Acronyms

2,2'-bipy	2,2'-bipyridine
^{1}H	Proton
^{13}C	Carbon -13
AAEMFC	Alkaline anion exchange membrane Fuel cell
AEM	Anion exchange membrane
AFC	Alkaline fuel cell
DABCO	1,4-diazabicyclo[2.2.2]octane
DCM	Dichloromethane
DFT	Density functional theory
Dm	Degree of methylation
DMF	Dimethylformamide
DMS	Dimethyl sulfide
DMSO	Dimethylsulfoxide
DPn	Degree of polymerization
E_a	Activation energy
EIS	Electrochemical impedance spectroscopy
equiv.	Equivalent(s)
EtOAc	Ethyl acetate
HCl	Hydrochloric acid
HDFE	High-density poly(ethylene)
HOR	Hydrogen oxidation reaction
IEC	Ion-exchange capacity
IEMFCs	Ion-exchange membrane fuel cells
KOH	Potassium hydroxide
MeI	Methyl iodide
mS	Millisiemens
MS	Mass spectroscopy
m/z	Mass-to-charge ratio
NCS	N-Chlorosuccinimide
NMP	N-methyl-2-pyrrolidinone
NMR	Nuclear magnetic resonance
ORR	Oxygen reduction reaction

PAIM	Poly(arylene imidazolium)
PAIM-RR	Poly(arylene imdazolium) with alkylation
PAIM-MX	Poly(arylene imidazolium) (50% methylation)
PAIM-MM	Poly(arylene imidazolium) (100% methylation)
PAIM-EX	Poly(arylene imidazolium) (50% ethylation)
PAIM-EE	Poly(arylene imidazolium) (100% ethylation)
PEM	Proton exchange membrane
PEMFC	Proton exchange membrane fuel cell
QA	Quaternary ammonium
RH	Relative humidity
RT	Room temperature
THF	Tetrahydrofuran
TS	Transition State
W_u	Water uptake (by mass)
δ	Chemical shift
λ	Hydration number (number of water molecule per ion charge)
σ	Ionic conductivity

Chapter 1. Introduction

1.1. Hydrogen fuel cells

The substantial and irreversible environmental effects of greenhouse gas emission and its negative impact on climate change have raised global environmental concerns. Additionally, the decreasing availability of fossil fuels and the increase in cost and uncertainty of imported oil supplies inspire the search for an alternative electric power generation system. One of the significant issues with the use of alternative energy is the energy supplies and demands do not always coincide. For instance, solar panels do not work at night when power is still needed; a cost-effective energy storage system must be applied. Wind-generated power might be located in faraway places; thus, convenient transportation is required.[1] In a situation like this, hydrogen is a promising future storage and transport medium because it can be stored as a compressed gas or liquefied, absorbed onto a porous substrate.[2] Hydrogen can be produced in many ways, such as electrolysis, reforming fossil fuels and biofuels, hydrocarbon cracking or via iron-water vapor reaction.[1,3] Most importantly, hydrogen can be used as fuel for hydrogen fuel cells. Hydrogen fuel cells are an attractive alternative because they convert the chemical energy of a reaction directly into electric energy by redox reaction of hydrogen and oxygen through the electrochemical process.[4,5] The technology is considered green because it involves a zero-emission engine. Contrary to the production of energy by combustion of fossil fuel, no carbon dioxide, methane, nitrous oxide or harmful pollutants are emitted, and they only produce water and heat. Moreover, they operate quietly and efficiently. Hydrogen fuel cells have high efficiency because they do not have moving parts that are not limited by the Carnot efficiencies. The theoretical efficiency can be over 80% in contrast to the limiting efficiency of the Carnot cycle.[6] For instance, the internal combustion engine has efficiency of 25%, and the coal power plant had efficiency 50%.[7] Recently, researchers focus more on the ion exchange membranes as the electrolyte instead of aqueous solutions, because ion exchange membrane fuel cells (IEMFCs) have quick start-up and low cost, they can operate at relatively low temperature and work in any orientation,[4] in addition, there are no more corrosive hazards applied in the fuel cell system. The ion exchange membrane fuel cells (IEMFCs) are further divided into two different types, proton exchange membrane fuel cells (PEMFCs) and alkaline anion

exchange membrane fuel cells (AAEMFCs). The charge carriers in the membrane distinguish them. Protons transport in the PEMFCs, and hydroxide ions transport in the AAEMFCs.

1.1.1. Proton Exchange Membrane Fuel Cells (PEMFCs)

Proton exchange membrane fuel cells consist of two electrodes, an anode, and a cathode, separated by a proton exchange membrane (PEM). The proton exchange membrane prevents the contact of hydrogen and oxygen fuel sources, which would result in direct chemical combustion. Specifically, at the anode, hydrogen diffuses to the catalyst-coated electrode-electrolyte interface undergoing an electrochemical oxidation reaction. The oxidation reaction releases positive charge protons and electrons; the protons transport through the hydrated proton exchange membrane to the cathode by electro-osmotic flow. At the cathode, oxygen reaches catalyst-coated electrode-electrolyte interface undergoing an electrochemical reduction reaction. The reduction reaction combines the incoming electrons from anode and protons transport through the membrane, forming water.[8] Electric current is generated by the flow of electrons through the external circuit, balancing the charge across the cell (Figure 1.1). The two electrochemical half-reactions with overall spontaneous reaction produce a voltage of 1.23 V under standard conditions (Equation 1.1-1.3).[9] Due to its high power density and efficiency with zero-emission, PEMFCs have appealed for a wide range of applications such as vehicle transportation as well as stationary power generations.

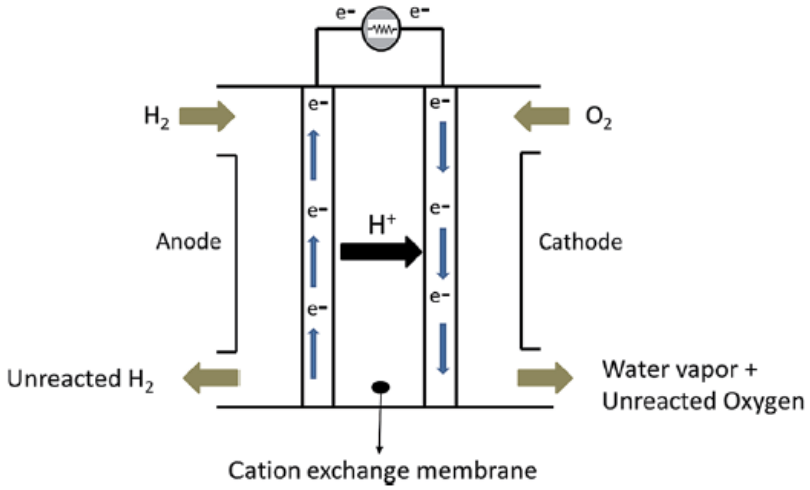

Figure 1.1. Systematic representation of PEMFCs (Adapted).[8]

$$Anode\ reaction: \quad H_2 \rightarrow 2H^+ + 2e^- \qquad E^0 = 0\ V \qquad (1.1)$$

$$Cathode\ reaction: \quad \frac{1}{2}O_2 + 2H^+ + 2e^- \rightarrow H_2O \qquad E^0 = 1.23\ V \qquad (1.2)$$

$$Overall\ reaction: \quad H_2 + \frac{1}{2}O_2 \rightarrow H_2O \qquad E^0 = 1.23 \qquad (1.3)$$

Water management and gas transport are two critical factors that influence the performance of PEMFCs because the proton conductivity is directly proportional to the water content.[8] The water brought by the electro-osmotic flow and the water formed at cathode through the oxygen reduction reaction (ORR) can flood the cathode side. The water can further block the pores in the electrodes and the gas diffusion layer resulting in low fuel cell performance. Back-diffusion plays an essential role in balancing the water on both sides of the electrode; the water gradient created inside the thin membrane between anode and cathode leads to the water back-diffusion from cathode to anode. Back-diffusion decreases the chance of flooding and slows down the anode dry out caused by electro-osmotic flow.[10] Throughout the whole membrane electrolyte, a suitable state of hydration level can be obtained without any special difficulty.[4]

Currently, the most well-known and well-established proton exchange membrane is Nafion™, the perfluorosulfonic acid (PFSA) membrane originally developed by Dupont (Figure 1.2). The strong fluorine-carbon bonds of the hydrophobic polymer backbone make them durable and resistant to chemical attack. The hydrophilic regions around the cluster of ionic sulfonated side-chain lead to the absorption of water and high proton conductivity.

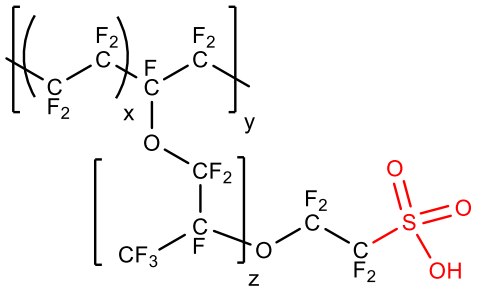

Figure 1.2. Structure of Nafion with sulfonic group labeled red

To facilitate the electrochemical reaction in an acidic environment and avoid catalyst corrosion of PEMFCs,[11] a large and precious amount of platinum (Pt) electro-

catalyst is needed to promote the cathode oxygen reduction reaction (ORR) and the anode hydrogen oxidation reaction (HOR).[8] The ORR at the cathode is five orders of magnitude slower than HOR at the anode. A significant effort has been made to decrease the Pt loading on the cathode.[4] Moreover, PEMFCs are restricted to the use of pure hydrogen as fuel because trace carbon monoxide can poison the platinum catalyst on the anode side. The carbon monoxide poison is preferentially adsorbing to the platinum surface and blocking active sites.[12] Reducing the amount of Pt electrocatalyst loading, looking for practical, alternative and less expensive non-precious metal catalysts, and applying less expensive electrolytes are considered as the pathways to lower the overall cost of the fuel cell system.

1.1.2. Alkaline Anion Exchange Membrane Fuel Cells (AAEMFCs)

An alternative, less expensive non-precious metal catalyst would result in a significant decrease in the overall cost of the fuel cell. It is noteworthy that reaction kinetics at electrodes, especially ORR, is more facile in alkaline conditions than in acidic conditions, such as that found in PEMFCs. In alkaline media, less expensive transition metal catalysts, such as Ag, Co, and Ni, can be used for the electrochemical reactions.[13–15] The AAEMFCs avoid the corrosion problem under acidic conditions, and graphite-based bipolar plates can be replaced with less expensive and robust metal plates.[16,17] Besides, the electro-osmotic flow associated with the ion transport are opposite to fuel crossover, broadening the choices of fuels.[18,19]

Traditional alkaline fuel cells (AFCs) use either aqueous potassium hydroxide (KOH) or sodium hydroxide (NaOH) solution absorbed into an asbestos matrix as the electrolyte. These can operate at a broad range of temperature from 60 °C to 120 °C and possess a high efficiency (fuel to power) in range from 60 to 80%.[4] However, when NASA used the AFC to power the Gemini and Apollo spacecraft in the 1960s, there was a severe problem related to electrolyte and electrode degradation from the use of commercialized fuels. CO_2 in the air reacts with OH^- forming insoluble carbonate and bicarbonate precipitates (Equation 1.4, 1.5).[20] The carbonate and bicarbonate species that precipitate from supersaturated solution fill the pores of electrodes, block the pores, and destroy the active site, leading to an increase in cell resistance and a decrease in current supplied. Also, the effect decreases the number of hydroxide ions available for any half-reaction as they are replaced by the carbonate and bicarbonate ions. Similar to PEMFCs, this has

limited the application of alkaline fuel cells to use of pure hydrogen and oxygen, in order to eliminate the presence of CO_2 contamination.

$$CO_2 + OH^- \rightarrow HCO_3^- \quad (1.4)$$

$$OH^- + HCO_3^- \rightarrow CO_3^{2-} + H_2O \quad (1.5)$$

Today, researchers pay more attention on the development of an AFC electrolyte based on anion exchange membranes (AEMs) instead of 6 M potassium hydroxide or sodium hydroxide solutions. Changing the liquid electrolytes to polymeric anion exchange membranes can eliminate carbonate precipitate formation because the cationic groups are fixed to the polymer chains, and they are not freely mobile. Carbonate precipitate formation is eliminated because there is no liquid-phase for cations such as Na^+, K^+, which combine with carbonate anions to form insoluble Na_2CO_3 and K_2CO_3.[18] There has been an increasing number of publications over the past five years, indicating a growing interest in anionic fuel cell technology.[21] Many researchers have switched their research outlook from an exclusive focus on proton exchange membrane fuel cells to one that includes alkaline anion exchange membrane fuel cells.

Similar to PEMFCs, AAEMFCs consist of two electrodes, an anode, and a cathode, separated by an anion exchange membrane. The membrane prevents the contact of hydrogen and oxygen fuel sources, which would result in chemical combustion. For AAEMFCs, hydroxide ions are available and mobile. The hydrogen is supplied at the anode, and reacts with incoming hydroxide ions, producing water with releasing energy and electrons. The electrons transfer through the external circuit from the anode to the cathode, where the oxygen reacts with electrons and water, forming new hydroxide ions (Figure 1.3). The electron flow from anode to cathode produce electric current and the two electrochemical half-reactions with the overall reaction generate a voltage of 1.23 V under standard conditions (Equation 1.6-1.8).[21,22]

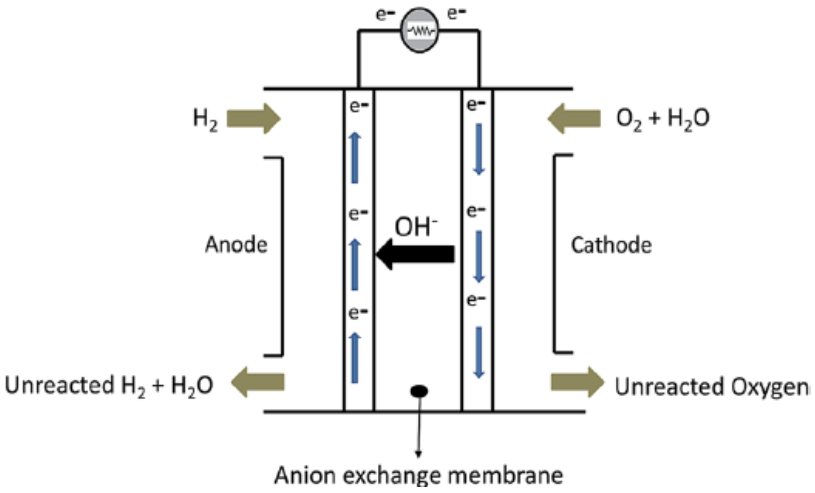

Figure 1.3. Systematic representation of AAEMFCs (Adapted).[8]

$$Anode\ reaction: \quad H_2 + 2OH^- \rightarrow 2H_2O + 2e^- \qquad E^0 = 0.83\ V \qquad (1.6)$$

$$Cathode\ reaction: \quad \tfrac{1}{2}O_2 + H_2O + 2e^- \rightarrow 2OH^- \qquad E^0 = 0.40\ V \qquad (1.7)$$

$$Overall\ reaction: \quad H_2 + \frac{1}{2}O_2 \rightarrow H_2O \qquad E^0 = 1.23\ V \qquad (1.8)$$

Note that, two equivalents of water are produced at the anode while one equivalent of water is consumed at the cathode. Therefore, water management is essential in order to prevent water flooding at the anode and keep the electrode hydrated at the cathode. It is also essential to understand the hydroxide ions migration mechanism. Three main mechanisms describe the hydroxide ions transport in polymer membranes based on acidic proton exchange membrane material (included here as a reference), **(a)** Grotthuss mechanism; **(b)** diffusion or vehicle; **(c)** convection.[13] The Grotthuss mechanism is the primary transport mechanism because hydroxide ions exhibit Grotthuss behavior in aqueous solution compared to protons. In the Grotthuss mechanism, the hydroxide ions diffuse via the formation and cleavage of covalent bonds in a hydrogen-bond network of water molecules. It has been shown that a hyper-coordinating water molecule accompanies the transport of hydrated hydroxide ions. Diffusive transport occurs in the presence of concentration gradient or electrical potential gradient. When the hydroxide ions move through the membrane, convection transport also occurs. The hydroxide ions drag water molecules along with them and form a convective flow of water within the membrane.

1.2. Anion exchange membranes (AEM)

Anion exchange membranes are solid polymer electrolytes consisting of positively charged head groups attached to alkaline and mechanically stable polymer matrix. The positively charged head groups permit the passage of anions such as chloride and hydroxide but repel cations.[23] The polymer backbone provides sufficient mechanical support and must be stable in an alkaline environment. Nitrogen-containing cations are usually chosen to provide ion-conducting sites, which transport hydroxide ions.[24] For instance, poly(2,6-dimethyl 1,4-phenylene) oxide (PPO) (Figure 1.4) containing pendant quaternary ammonium groups, has been used as an anion exchange membrane. The backbone polymer PPO is commercially available and cheap; it can be tailored by chloromethylation and subsequent addition of quaternary ammonium groups. The membrane yields hydroxide ion conductivity of 50 to 100 $mS \cdot cm^{-1}$.[25,26]

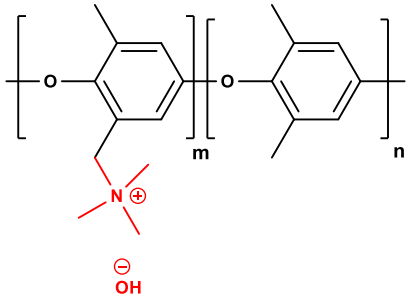

Figure 1.4. Structure of PPO with quaternary ammonium groups labeled red

1.2.1. Properties of AEMs

In order to display excellent performance and long durability in electrochemical devices, the ideal anion exchange membrane candidates should possess the following properties:

- High ionic conductivity
- Sufficient mechanical strength
- High chemical and thermal stability
- Low electrical conductivity
- Low impermeability to gas

- Be as thin as possible (< 50 μm)

The membranes should have high ionic conductivity, preferably 0.1 $mS \cdot cm^{-1}$ or greater at 80 °C in order to support a large current with minimal resistive loses.[6] The membranes should have sufficient mechanical properties. Deterioration or loss of mechanical properties can be observed when membranes swell at high hydration and become brittle at low hydration. Both swelling and brittleness of membranes have a negative impact on fuel cell performance. The membranes need to have excellent chemical and thermal stability during the manufacture and fuel cell performance. The role of the membranes is to serve as conductor for ions and barrier for electrons and gas. In addition, the membranes should prevent fuel crossover under the operating conditions in order to maximize the current efficiency, and offer zero electronic conductivity. Ultimately, they should be as thin as possible, usually less as 50 μm. Thin membranes have low ionic resistance and also alleviate the total cost of the system.[13]

There are many challenges in AAEMFC research, especially anion exchange membranes, including low ionic conductivity compared to acidic proton exchange membranes; and poor alkaline stability. High ionic conductivity can be achieved by increasing the ion-exchange capacity (IEC) of the membranes by introducing more positively charged nitrogen-based cation groups.[27] The IEC represents the number of ionic functional groups per unit mass of polymer, including the counterions (Equation 1.9) in $\frac{mequiv}{g}$ or $\frac{mmol}{g}$. The IEC of membranes must be high to support sufficient ion transport, but also low to prevent the over swelling in aqueous solution. Significantly increasing the IEC of the polymer to a high value leads to a large water swelling. The swelling increases the thickness of the membranes and considerably softens the membrane. All of these damage the membranes' mechanical integrity, resulting in the formation of a physical hole in the membranes during membrane electrode assembly (MEA) process and fuel cell operation. Therefore, it is a great challenge for researchers to find the balance between the ionic conductivity and mechanical strength of the membranes.

$$IEC = \left(\frac{number\ of\ anionic\ pairs\ per\ repeat\ unit}{molecular\ mass\ of\ \ repeat\ unit}\right) \times 1000 \qquad (1.9)$$

1.2.2. Cationic head groups and Degradations

The selection of cationic groups is crucial because it directly influences the chemical stability of the membrane. Numerous cationic groups for anion exchange membrane applications have been reported in the literature (Figure 1.5). The cationic applied groups include quaternary ammonium groups (QA) such as benzyltrialkylammonium,[28] pyridinium,[29] DABCO,[30] guanidinium,[31] imidazolium[28] and benzimidazolium; quaternary phosphonium,[32,33] tertiary sulfonium,[34] and metal complexes (ruthenium and cobalt).[35]

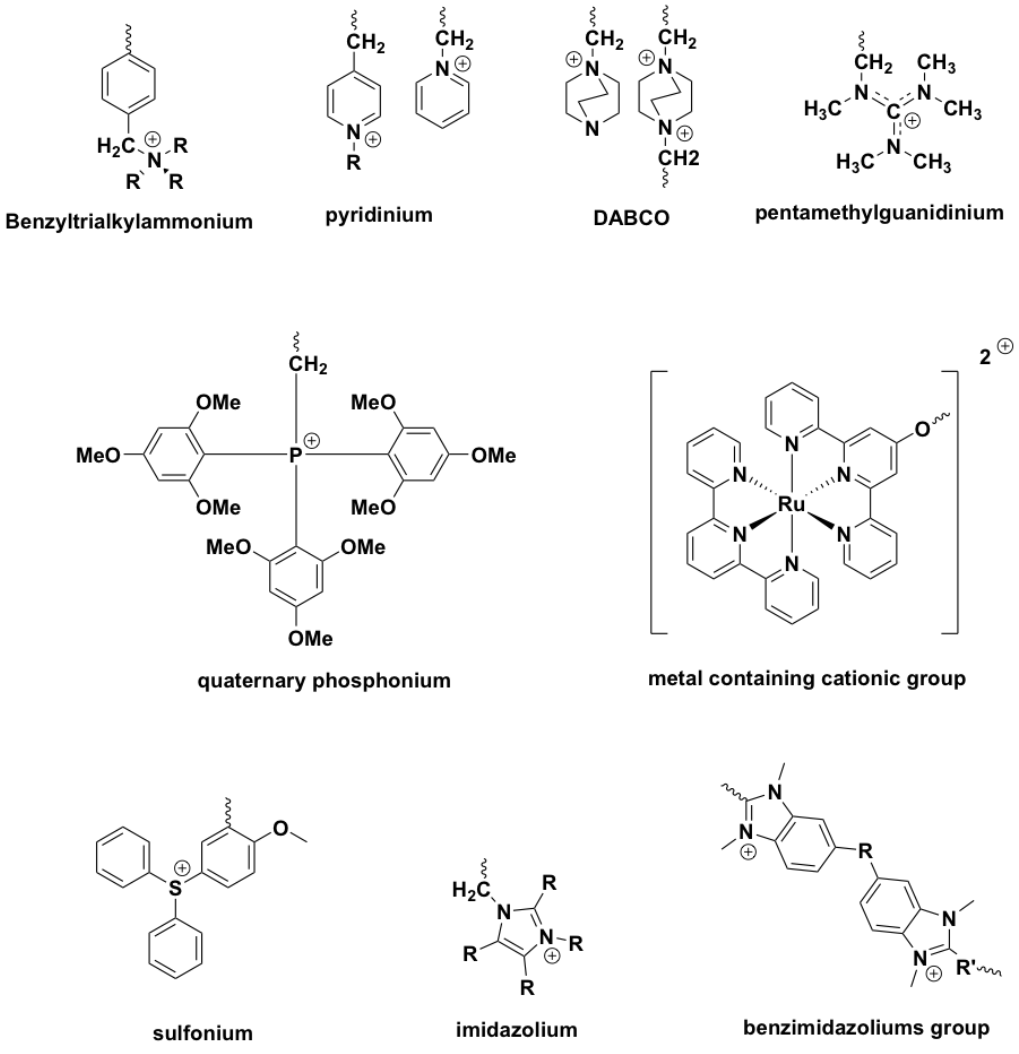

Figure 1.5. Examples of cationic groups used in the literature (pyridinium, DABCO, guanidinium, phosphonium, sulfonium, imidazolium). The counter-anions are omitted for clarity. (Adapted).[18]

In the vast majority of reports, researchers have explored quaternary ammonium and phosphonium cationic polymers, because they are relatively easy to synthesize, and are adaptable to the addition of various functional groups.[36] However, the drawback of inadequate tolerance to the highly alkaline environment has been inhibited the development and commercialization of AEMs.[36] Three chemical degradation routes are found for quaternary ammonium groups in the alkaline environment: β-Hoffmann elimination, S_N2 reaction, and the Ylide reaction.[6,13,20,37] First, β-Hoffman elimination. Here, the nucleophilic hydroxide ion can deprotonate hydrogen from the β-position of the cationic group followed by structural rearrangement. This degradation route produces an alkene, a tertiary amine, and water (Scheme 1.1**a**). In the S_N2 degradation reaction, the nucleophilic hydroxide ion can attack methyl of the cationic group resulting in the formation of tertiary amine and methanol; the hydroxide ion also can attack α-carbon of the cationic group resulting in the formation of tertiary amine and alkyl alcohol (Scheme 1.1**b**). In the Ylide degradation reaction, the nucleophilic hydroxide ion deprotonates the hydrogen from methyl of the cationic group followed by the structural rearrangement. The degradation produces tertiary amine and methanol (Scheme 1.1**c**). Overall, although the backbone of the polymer is intact, the cationic groups on the polymer are gradually lost as a result of degradation, which decreases the IEC resulting in low ionic conductivity of the membranes.

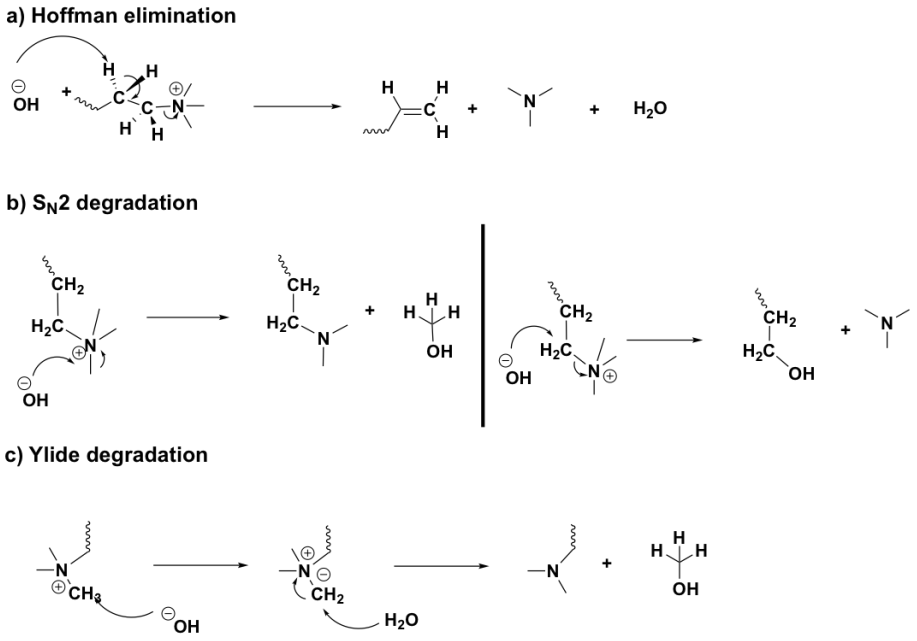

Scheme 1.1. Three degradation routes of trimethylammonium cations: a) Hoffman elimination, b) the S_N2 reaction and c) the Ylide reaction (Adapted).[6]

The search for alkaline-stable AEMs is the primary driver for the study of alternative cationic group chemistry. The Holdcroft group focuses on two cationic groups: benzimidazolium and imidazolium because the access to the hydroxide-reactive site is sterically protected, the presence of π-conjugated structure of heterocyclic ring aids delocalization of the positive charge, thus reducing the prospect of S_N2 substitution and Hofmann elimination reactions.[38,39] Imidazoliums are commonly used in ionic liquids, e.g. 1-butyl-3-methyl imidazolium hydroxide or 1-butyl-2,3-dimethylimidazolium hydroxide.[40,41] They are can be synthesized with a wide range of functional groups (Figure 1.6). Moreover, it has been reported that benzimidazolium and imidazolium-based AAEMs possess higher thermal stability, better mechanical properties and solubility properties compared to the conventional quaternary ammonium (QA)-based AAEMs.[42–45] The benzimidazolium and imidazoliums groups favor solution casting of ionic polymer in the preparation process. They are amenable to pre-functionalization, meaning the ionic functionality can be introduced before the membranes are cast. The uniform percolation of ion clusters throughout the membranes facilitates ion transport. The ion and water mobility across the AEM is reported to be high, which facilitates ionic conductivity of membranes. Also, they can be used in AEM electrolytes as an alkaline ionomer to enhance the ionic contact in the catalyst layer of the fuel cell electrodes.[46]

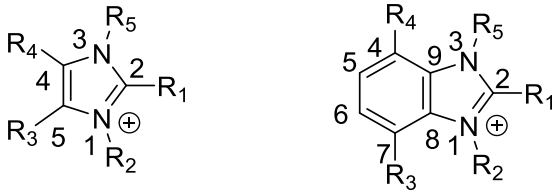

Figure 1.6. Benzimidazolium and imidazolium structures with their assigned functionalized position numbers. Counter-anions are omitted for clarity.

However, similar to ammonium and phosphonium groups, benzimidazolium and imidazolium groups may potentially undergo degradation in the alkaline environment (Scheme 1.2). These mechanisms include the following reactions: a) Ring-opening, b) S_N2, c) Heterocyclic deprotonation, and d) Substituent deprotonation.[47]

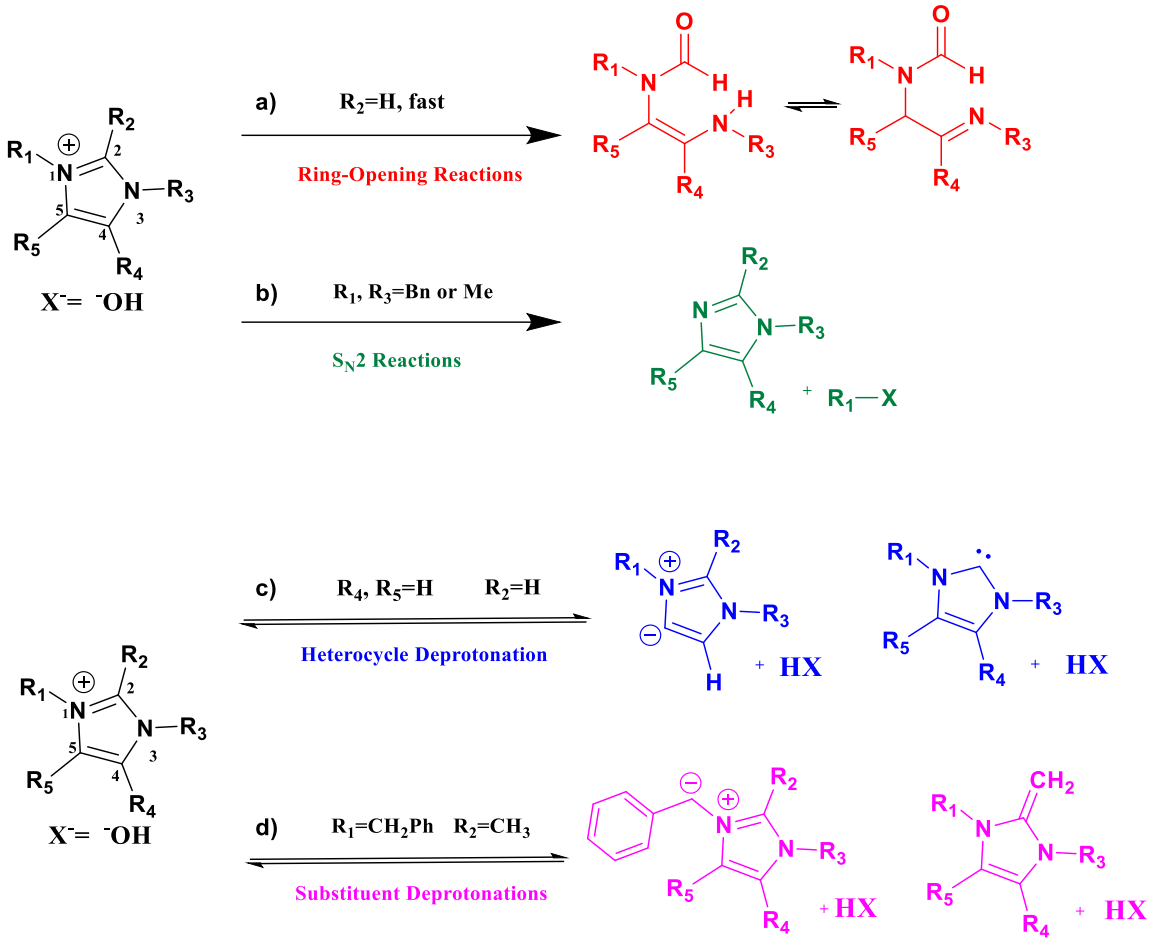

Scheme 1.2. Four possible degradations of benzimidazolium and imidazolium a) Ring-opening, b) S_N2, c) Heterocycle deprotonation and d) Substituent deprotonation. Reactions are shown for imidazolium. (Adapted).[47]

The ring-opening and S_N2 reactions are irreversible degradations, and ring-opening reaction pathway is considered the rate-limiting step.[47] In the ring-opening reaction (Scheme 1.2**a**), the C2-carbon substituent of benzimidazolium or imidazolium is hydrogen. Hydroxide attack on the C2 carbon is very fast, which results in imine-enamine tautomerization. In the S_N2 (Scheme 1.2**b**), the substituent on the nitrogen of benzimidazolium or imidazolium is benzyl or methyl, so either debenzylation or demethylation can occur. Benzyl alcohol or methanol is produced as degradation products. Moreover, heterocycle deprotonation (Scheme 1.2**c**) and substituent deprotonation (Scheme 1.2**d**) are reversible degradations, which both decrease the ionic conductivity of the membranes due to the loss of cationic head groups.

1.2.3. Benzimidazolium and Imidazolium Model Compounds

Pivovar et al. performed density functional theory (DFT) on model compounds of benzimidazolium and imidazolium cations. By comparing the total free energy of the ground state of reaction (cations + OH^-) with the free energy of their transition states (TS), they found that benzimidazolium and imidazolium were more stable with their C2-positions protected by bulky groups, and C4 and C5 substituents of imidazolium were reported to enhance the free energy barriers. Moreover, with C2 protection, the methyl-imidazolium cations analogues were predicted to be more stable than the methyl-benzimidazolium cations, which possessed more extended conjugation.[49] The free energy barriers for ring-opening degradation of methyl-imidazolium derivatives (**1, 2, 4, 5**) were generally larger than their comparable benzimidazolium analogues (**3, 6, 7, 8**) (Table 1.1).

Table 1.1. Comparison of the free energy barrier for ring-opening degradation of benzimidazolium and imidazolium derivatives (1)-(8). The counter-ions are omitted for clarity. (Adapted).[49]

Cations	Free energy barrier for ring-opening degradation (kcal · mol^{-1}) at 80 °C, 1 atm
DMPTMIM **(1)** 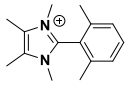	39.2
DMPDMIM **(2)** 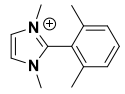	35.9
DMPDMBIM **(3)** 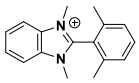	26.5
MPDMIM **(4)** 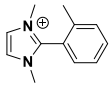	22.5

Cations	Free energy barrier for ring-opening degradation (kcal · mol^{-1}) at 80 °C, 1 atm
PDMIM **(5)** 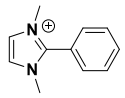	21.9
MPDMBIM **(6)** 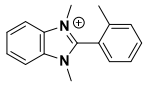	16.5
PDMBIM **(7)** 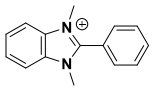	14.7
DMBIM **(8)** 	9.2

Coates et al. performed a stability test of imidazolium model compounds in 1 M KOH, 2 M KOH, and 5 M KOH at 80 °C for 30 days. The C4, C5 substituents were important to the alkaline stability of imidazolium because the degradation of heterocyclic deprotonation can occur. Methyl and phenyl substituents on C4, C5 positions can significantly enhance the stability of imidazolium compared to a hydrogen substituent. The percentage imidazolium cation remaining of methyl and phenyl substituents on C4, C5 were 87% and 80%, which were much higher than hydrogen substituent, for which only 36% remained (Figure 1.7a).[47] By comparing the percentage imidazolium cation remaining of C2 substituents of methyl, isopropyl, phenyl, and 2,6-dimethylphenyl, they found that phenyl and 2,6-dimethylphenyl substituents were effective protecting groups against ring-opening degradation, with higher percentage cation remaining being as high as >99% in 1 M KOH compared to isopropyl and methyl substituents as 95% and 87% (Figure 1.7b).[47] The use of alkyl substituents on the N1 or N3 nitrogen, particular n-butyl, also reduced S_N2 degradation. The report indicated the stability of n-butyl derivatives with the highest percentage imidazolium cation remaining being >99% compared among benzyl, methyl, ethyl and propyl derivatives in 1 M, 2 M and 5 M KOH (Figure 1.7c).[47] The longer alkyl group was reported to decrease the strength of the base by shielding the cations from interaction with the neighbor nucleophile.[47]

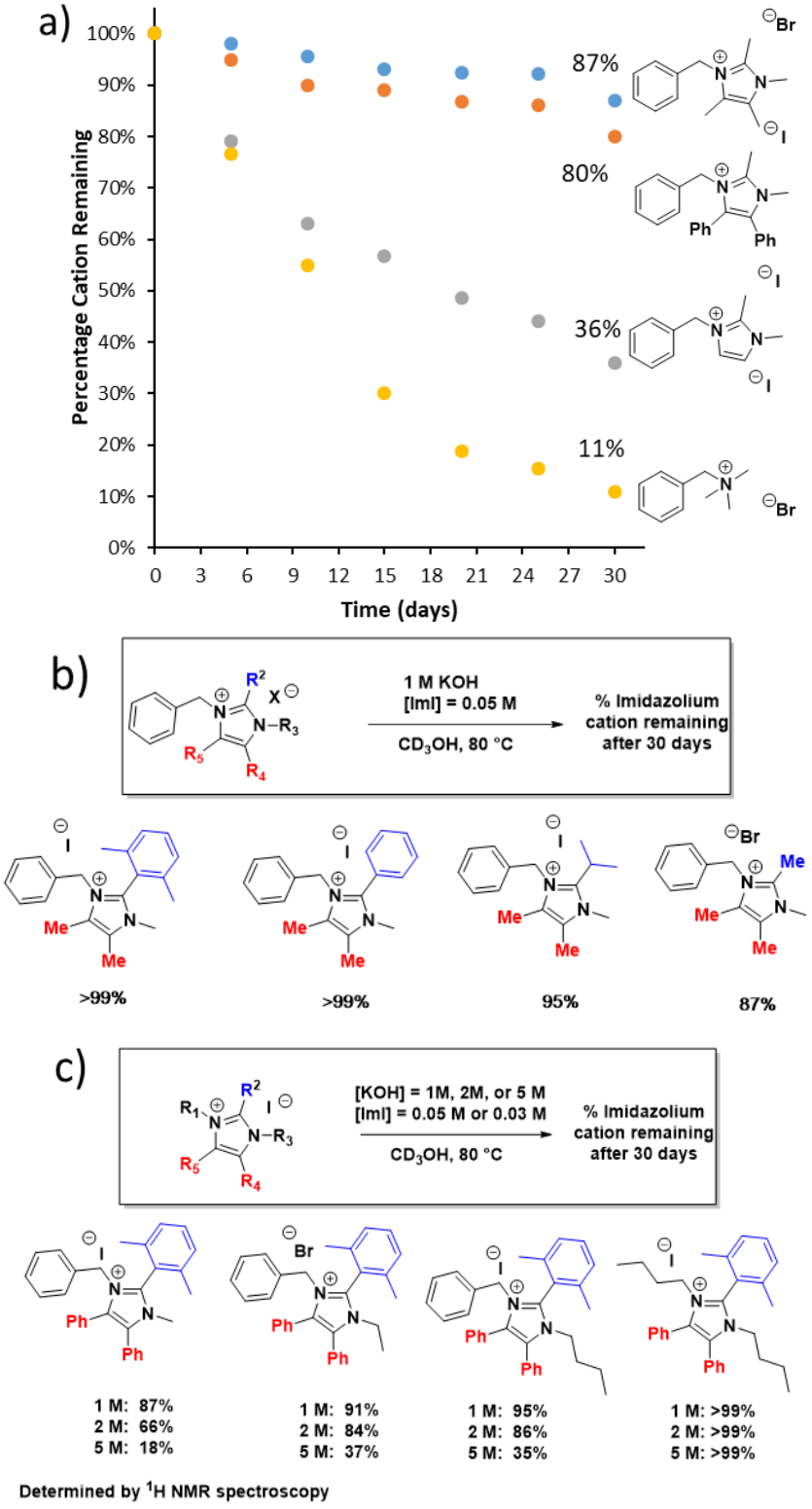

Figure 1.7. ***Influence of a) C4, C5 substituents, b) C2 substituent, and c) N1, N3 substituents on imidazolium stability. Percentage imidazolium cation remaining in 1 M KOH, 2 M KOH, and 5 M KOH at 80 °C for 30 days (Adapted).[47]***

Methyl groups were better than phenyl groups because they can potentially allow the ion exchange capacity (IEC) of the membranes to be increased in order to promote the ionic conductivity. The major strategy for the synthesis of AEMs was to append quaternary ammonium groups to the benzylic position of a polymer backbone.[26,50] However, this functional group was relatively unstable in the highly basic conditions, only 11% cation remains in the above degradation tests,[47] because degradation via deprotonation (Scheme 1.2d) readily occurs.[51] Hence, imidazolium model compounds are useful in the design of AEMs by inserting imidazolium into the polymer backbone. The imidazlium work as an integral component, is of great interest in the context of anion exchange membranes.

1.2.4. Poly(benzimidazoium)s

The benzimidazolium or imidazolium groups are susceptible to nucleophilic attack, which initiates at the C2 position. Previously, in the Holdcroft group, three polymers had been synthesized (Figure 1.8), abbreviated: PDMBI, Mes-PDMBI, and HMT-PDMBI.[48,52–54] Specifically, PDMBI with a phenylene group attached at the C2-position of benzimidazolium was not stable in 2 M KOH at 60 °C, and it was also soluble in water. However, by replacing the phenylene group with a mesitylene group, the resultant polymer, Mes-PDMBI, was found to be stable in 2 M KOH at 60 °C; but still soluble in water. By replacing the mesitylene group (Mes) with hexamethyl-p-terphenylene (HMT), the polymer, HMT-PDMBI, with 89.5% degree of methylation was demonstrated to be stable in 2 M KOH at 60 °C for extended periods *and* insoluble in hot water. The increased stability from PDMBI to Mes-PDMBI is, therefore, owing to the difference in the chemical structure of their repeating unit: PDMBI possesses a phenylene group, Mes-PDMBI possesses an ortho-substituted phenylene group. By examining the dihedral angles between the benzimidazolium and its C2-substituents, phenylene and ortho-substituted phenylene, the angle is found to be increased from 58° to 83°, which significantly enhances steric crowding around the labile C2 position and greatly decreases the possibility of hydroxide attack at the position. In addition, by replacing the mesitylene group with the hexamethyl-p-terphenylene group (HMT), the hydrophobicity of the polymer increases so that HMT-PMBI is insoluble in water at evaluated temperatures. The reduced IEC, the decreased hydrophilic/hydrophobic mass fraction of the polymer primary chain,

and high interconnectivity of the ionic domains all contribute to the exceptional properties of HMT-PMBI.

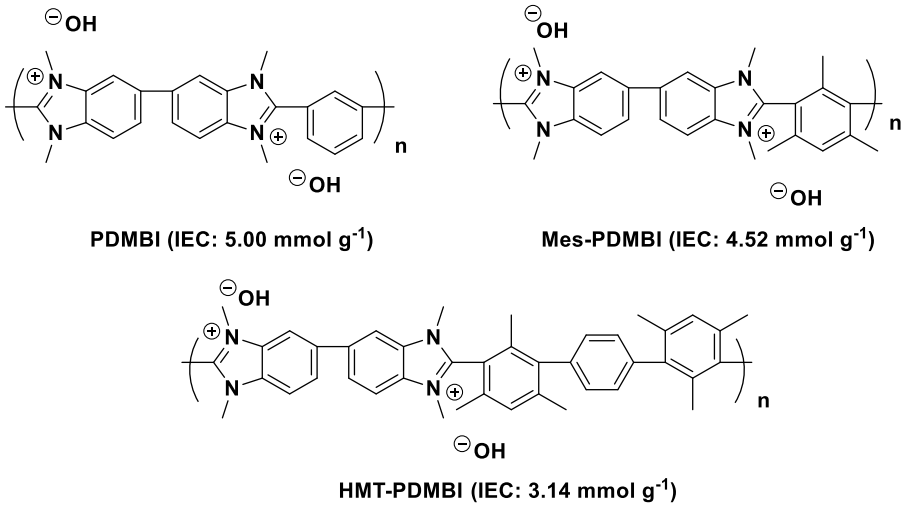

Figure 1.8. ***Three previously developed poly(benzimidazolium)s membranes: PMBI, Mes-PMBI (Mes - Mesityl), and HMT-PMBI (HMT - Hexamethyl-p-terphenyl) with their IEC_{OH^-} values (Adapted).***[48,52,54]

1.2.5. Synthesis of Poly(imidazolium)s

Two different strategies were developed in order to incorporate the imidazolium into polymer chains: **(1)** by the direct formation of heterocyclic rings during the polymerization process, and **(2)** by the synthesis of arylene imidazole monomers and their subsequent polymerization.[55] Base on strategy **(1)**, sterically protected HMT-PMPI was successfully synthesized and characterized by Fan and Holdcroft (Scheme 1.3).[56] The structure of HMT-PMPI followed the structure of HMT-PMBI except that the cationic group was changed from benzimidazolium to imidazolium. HMT-PMPI showed high alkaline stability in 10 M KOH at 80 °C. ^{1}H NMR spectroscopy supports the claim that ring-opening degradation was eliminated. The dihedral angles between mesitylene protecting groups and the imidazolium was 79°.[56] It was comparable with the dihedral angle between mesitylene protecting groups with benzimidazolium, which was 83°.[48] Interestingly, the sterically protecting group on C2-position of imidazolium had no effect on the S_N2 degradation.[56] However, there were a few undesirable properties of HMT-PMPI. The polymer possessed a low degree of polymerization (DP_n = 92) and molecular weight (M_w = 67,000 g·mol^{-1}), because the polymer was obtained by polycondensation, in which three starting material were involved (including a dicarbonyl, dialdehyde and ammonium

acetate). In addition, the membranes swelled excessively and gradually dissolved in water at 80 °C.[56] Therefore; it was necessary to develop a new synthetic route to achieve high molecular weight PAIM polymer with water insolubility at the elevated temperature while maintaining sufficient ion exchange capacity and base-stable imidazolium group within the polymer backbone.

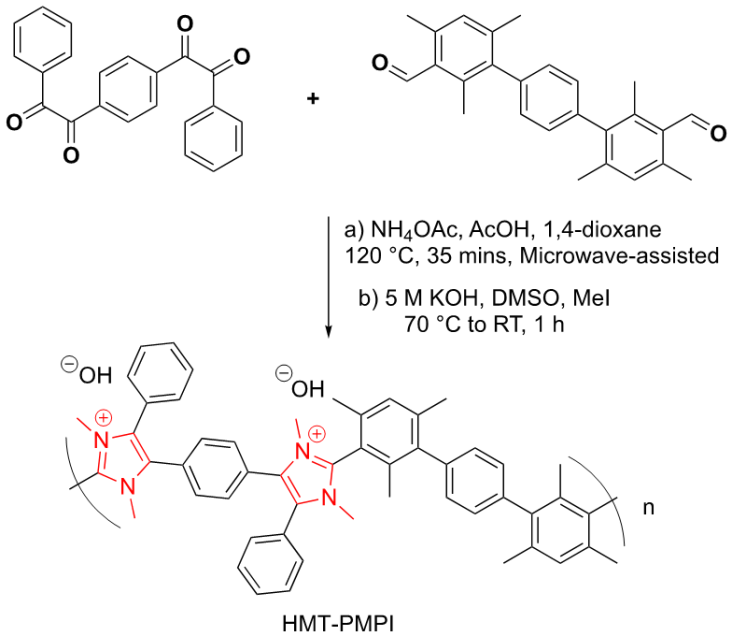

Scheme 1.3. Synthesis of HMT-PMPI (Adapted).[56]

Strategy **(2)** was also explored. The Debus-Radziszewski imidazole synthesis can be used to prepare the imidazole monomer.[55] Three starting materials are involved in the reaction, including a 1,2-diketone, ammonia, and a ketoaldehyde. The 1,2-diketone and ammonia condense producing a dimine, and the dimine further condenses with ketoaldehyde forming imidazole derivatives (Scheme. 1.4).

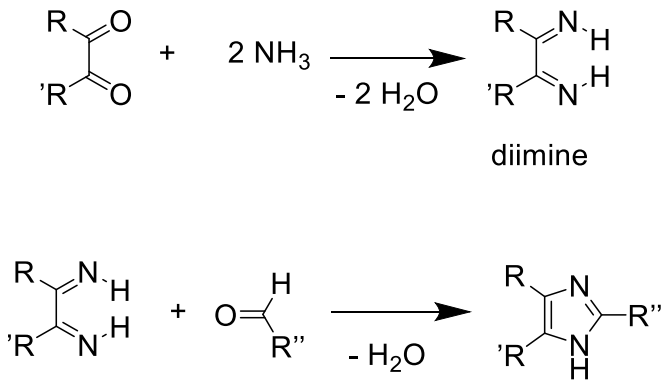

Scheme 1.4. Probable Debus-Radziszewski imidazole synthesis mechanism

The common and general route to obtain polymers is condensation polymerization, in which the polymers form via step-growth kinetics. Condensation polymerization relies on the reaction of a functional group in the monomer. Initially, the polymerization creates dimers and oligomer, but as the polymerization approaches high conversions, large molecular weight polymer is achieved. The challenges of condensation polymerization are long reaction time and high temperature. For great efficiency, microwave-assistance is performed. In this thesis work, Yamamoto polymerization is presented instead of previously reported polycondensation (that involved three monomers).[57–60] Yamamoto polymerization involves carbon-carbon coupling reactions, wherein the polymer is prepared by the dehalogenative polycondensation of the corresponding imidazole monomer using a zero-valent nickel complex, usually, bis(1,5-cyclooctadiene)nickel(0) ($Ni(COD)_2$). This polymerization route is more convenient compared with the polycondensation because only a single, halogen-functionalized monomer is used to form polymers. However, stoichiometric quantities of the expensive nickel complex are required, and solvents need to be anhydrous. Nevertheless, the simplicity of reaction procedures and the known syntheses of other classes of high molecular weight polyaromatics make it an interesting polymerization strategy to explore more.[61,62]

The Yamamoto polymerization involving Ni catalyst contains three essential steps: oxidative addition, disproportionation, and reductive elimination.[60] First, oxidative addition of the di-halogen compound converts the Ni(0) complex to Ni(II) complex coupling with neutral ligands such as 2,2'-bipyridine (Scheme 1.5**a**). Second, disproportionation of Ni(II) complex results in a cis-type complex that involves the exchange of the anionic ligands X to the Ar-X (Scheme 1.5**b**). Lastly, reductive elimination of organonickel (II) complex $NiAr_2Ln$, gives the final carbon-carbon bonds of Ar-Ar and results in a high molecular weight polymer (Scheme 1.5**c**).

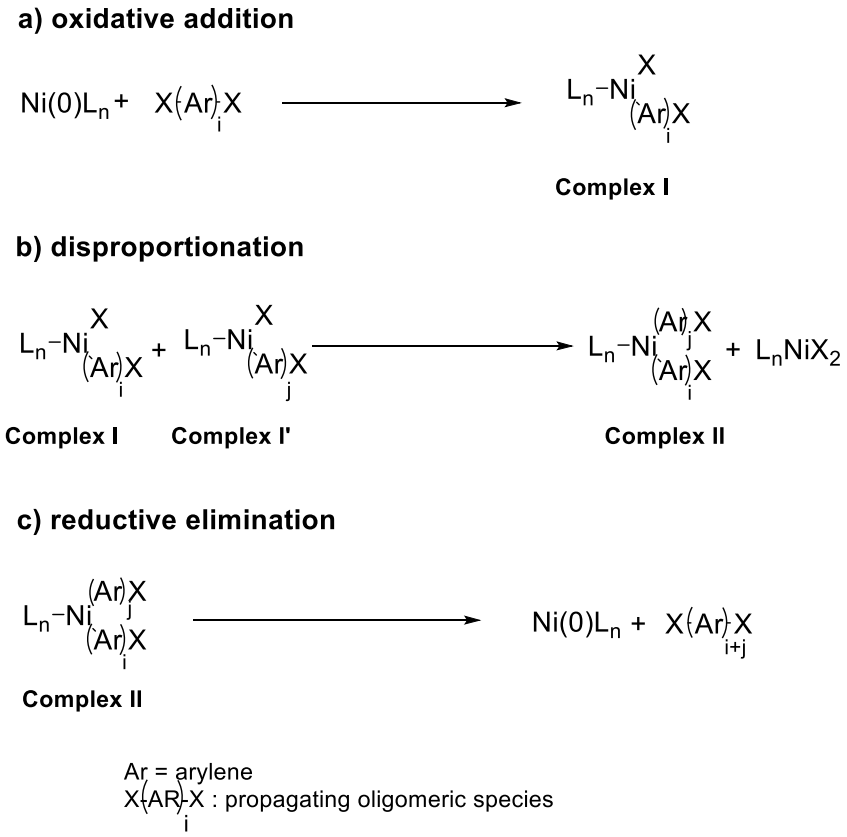

Scheme 1.5. Mechanism of Yamamoto coupling polymerization

1.3. Thesis overview

The purpose of this work is to design, synthesize, and characterize high molecular weight of poly(arylene imidazolium) (PAIM) possessing different alkyl side chains. Four PAIM-based polymers were designed in which the C2-position of the imidazoliums were protected with a 2,6-dimethylphenyl substituent. The four polymers differed in the position of connectivity of the monomers. The C4-, C5-positions of the imidazolium ring possessed phenyl substituents, and the N1-, N3-positions of the imidazolium were alkylated. The designed polymers presented in this work are named as PAIM-RR-1, PAIM-RR-2, PAIM-RR-3, and PAIM-RR-4 (Figure 1.10). In Chapter 2, *Experimental*, the synthetic details of monomers and polymers are described, together with the characterization methods. In Chapter 3, *Results and discussion*, four PAIM based monomers and three polymers synthesized successfully and characterized by ^{1}H spectroscopy. However, among the polymers, only PAIM-RR-1 with methyl and ethyl side chains could be cast to form free-standing membranes – as this was the only polymer with high molecular weight. The IEC_{cl-}

, water uptake, dimensional swelling, chloride conductivity, chemical stability, thermal and physical properties of these membranes are all described in details. Through the characterizations of the membranes, exceptional understandings of advantages and disadvantages of these materials can be found. Chapter 4, describes the overall conclusions and suggestions for future work.

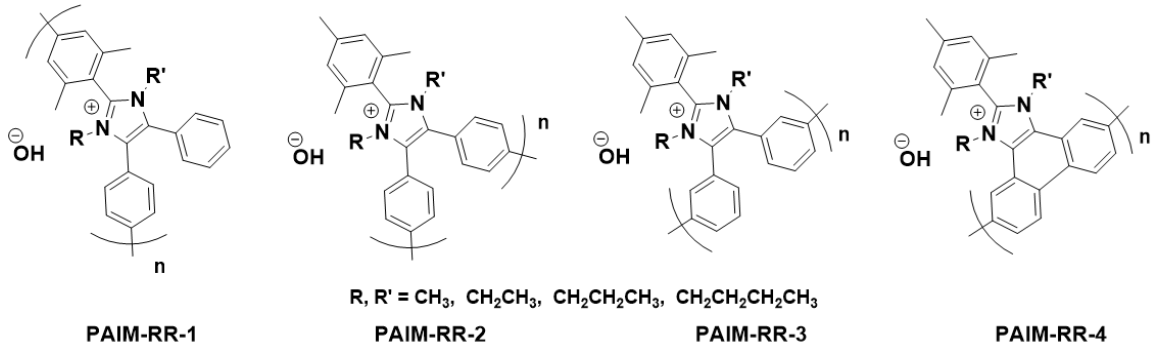

Figure 1.9. Four proposed poly(arylene imidazolium) polymers (PAIM-RR)

Chapter 2. Experimental

2.1. Materials

All the chemicals were purchased from Sigma Aldrich and used as received unless specified otherwise. 2-Bromo-5-chloro-1,3-dimethylbenzene (98%) were purchased from Combi-Blocks. Tetrakis(triphenylphosphine)palladium (99%) and bis(1,5-cyclooctadiene)nickel(0) (99%) were purchased from Strem Chemicals. Potassium carbonate (ACS grade), sodium chloride (ACS grade), hexanes (ACS grade), dimethyl sulfoxide (spectro-grade) and diethyl ether (ACS grade) were purchased from ACP Chemical Inc.. Acetic acid (glacial) was purchased from Caledon Laboratories Ltd. Methylene chloride (ACS grade), acetone (ACS grade), methanol (ACS grade) and tetrahydrofuran were purchased from Fisher Scientific. Dimethyl sulfoxide (ACS grade) and magnesium sulfate were purchased from BDH Chemicals. Anhydrous ethanol was purchased from Commercial Alcohol Inc. Basic aluminum oxide (Brockmann I 50-200 µm, 60 Å) was purchased from Acros Organics. Dimethylsulfoxide-d6 (99.9%-D), dichloromethane-d2 (99.8%-D), and chloroform-d (99.8%-D) were purchased from Cambridge Isotope Laboratories; Deionized water was purified using a Millipore Gradient Milli-Q® water purification system at 18.2 MΩ cm. Nuclear Magnetic resonance (NMR-^{1}H and ^{13}C) spectra were obtained on a 400 and 500 MHz Bruker AVANCE III running IconNMR under Top Spin 2.1 instruments, and the ^{1}H NMR solvent peaks for DMSO-d6, CD_2Cl_2-d_2, $CDCl_3$–d were set to 2.50 ppm, 5.32 ppm, and 7.26 ppm, respectively and the ^{13}C NMR solvent peaks for CD_2Cl_2-d_2 and $CDCl_3$-d were set to 54.00 ppm and 77.23 ppm, respectively.

2.2. Synthesis

2.2.1. Synthesis of PAIM-RR-1

Synthesis of 4-chloro-2,6-dimethylbenzaldehyde[63]

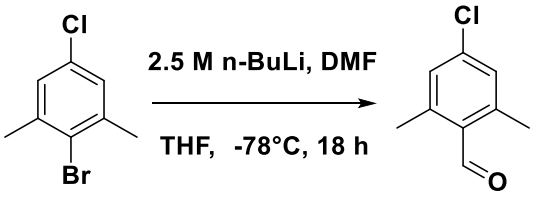

In a 400 mL Schlenk flask, 2-bromo-5-chloro-1,3-dimethylbenzene (1.00 equiv., 60.5 mmol, 13.3 g) and anhydrous tetrahydrofuran (200 mL) were added and cooled to -78 °C. The flask was evacuated and refilled with argon three times. N-butyllithium in 2.5 M hexane (1.10 equiv., 66.6 mmol, 27.0 mL) was then added within 10 minutes. The mixture was stirred for 2 hours at -78 °C and dimethylformamide (2.00 equiv., 121 mmol, 9.37 mL) was added to the slightly orange suspension. The resulting orange solution was then allowed to reach room temperature for 18 hours while stirring under nitrogen. Water (50 mL) was added, and the mixture was then stirred for another 10 minutes, after that, the solvent was removed under reduced pressure. The remaining gel was further dissolved in methylene chloride (2 × 100 mL) and washed with water (2 × 100 mL). The organic layers were dried over magnesium sulfate, filtrated, and concentrated. The crude product was thermally recrystallized from hexane : ethyl acetate 6:1 by volume, obtained colorless needles product 42% yield (25.6 mmol, 4.32 g). ^{1}H NMR (400 MHz, $CDCl_3$-d, ppm) δ: 10.52 (s, 1H), 7.07 (s, 2H), 2.57 (s, 6H). ^{13}C NMR (125 MHz, $CDCl_3$-d, ppm) δ: 192.29, 143.09, 138.78, 130.98, 129.65, 20.42.

Synthesis of 1-chloro-4-(phenylethynyl)benzene

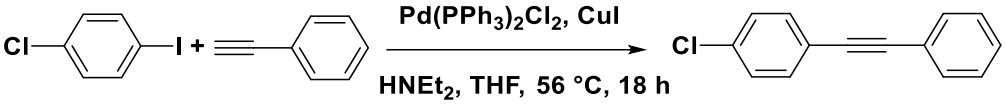

A 50 mL Schlenk flask was charged with 1-chloro-4-iodo-benzene (1.00 equiv., 50.3 mmol, 12.0 g) and $Pd(PPh_3)_2Cl_2$ (0.100 %, 5.03 x 10^{-2} mmol, 35.3 mg) and the flask was evacuated and refilled with argon three times. Diethylamine (6.00 equiv., 301.8 mmol, 31.0 mL) and THF (5 mL) were then injected to dissolve the solids with addition of phenylacetylene (1.00 equiv., 50.3 mmol, 5.60 mL) and CuI (0.100 %, 5.03 x 10^{-2} mmol, 9.58 mg) under argon. The solution was heated and stirred for 18 hours at 56 °C; after

that, a brown-orange solid formed at the bottom of the flask. The reaction mixture was precipitated from 10% HCl (300 mL) and filtered, yielded a yellow-orange solid. The solid was then dissolved in diethyl ether (600 mL), washed with 10% NH_4Cl (50 mL), water (2 × 100 mL) and brine (100 mL). The organic layer was dried over magnesium sulfate and evaporated under reduced pressure. The crude product was further purified by Celite filtration with petroleum ether (300 mL) under heating with active carbon for 4 hours. After filtration and evaporation under pressure, the yielded product was recrystallized from hexane, obtained light brown crystals 92% yield (46.3 mmol, 9.84 g). ^{1}H NMR (400 MHz, CD_2Cl_2-d_2, ppm) δ: 7.56-7.46 (m, 4H), 7.41-7.32 (m, 5H), ^{13}C NMR (125 MHz, CD_2Cl_2-d_2, ppm) δ: 134.86, 133.45, 132.17, 129.34, 129.09, 129.07, 123.57, 122.51, 90.85, 88.71.

Synthesis of 4-chlorobenzil[64]

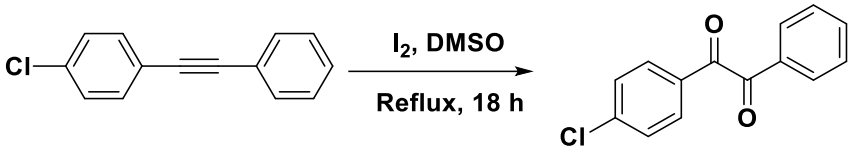

A 500 mL round bottom flask was charged with 1-chloro-4-(phenylethynyl)benzene (1.00 equiv., 39.2 mmol, 8.34 g) and I_2 (1.10 equiv., 43.1 mmol, 10.9 g) in DMSO (130 mL). After heating at reflux for 18 hours, the reaction mixture was precipitated from 1% sodium thiosulfate solution (600 mL) and obtained an orange precipitate. The precipitate was filtered, dissolved in methylene chloride (500 mL) and washed with water (2 × 200 mL). The organic layer was then dried over magnesium sulfate, evaporated under reduced pressure, obtained a yellow-orange solid. The yellow-orange crude solid was further purified by recrystallization from methanol, obtained yellow crystals 67% yield (28.9 mmol, 7.06 g). ^{1}H NMR (400 MHz, $CDCl_3$-d, ppm) δ: 7.94 (dd, *J* = 17.0, 8.4 Hz, 4H), 7.67 (t, *J* = 7.4 Hz, 1H), 7.56-7.41 (m, 4H). ^{13}C NMR (125 MHz, $CDCl_3$-d, ppm) δ: 193.96, 193.14, 141.71, 135.14, 132.98, 131.55, 131.34, 130.06, 129.56, 129.20.

Debus-Radziszewski imidazole synthesis[64]

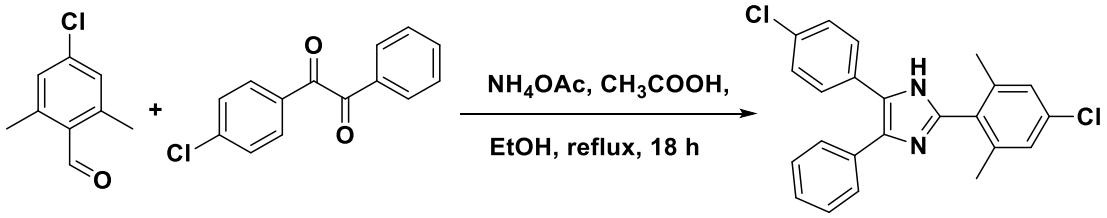

A 500 mL round bottom flask was charged with 4-chloro-2, 6-dimethylbenzaldehyde (1.00 equiv., 6.13 mmol, 1.03 g), 4-chlorobenzil (1.00 equiv., 6.13 mmol, 1.50 g) and ammonium acetate (8.00 equiv., 49.1 mmol, 3.78 g) in acetic acid (45 mL) and ethanol (200 mL). After refluxing for 18 hours, the reaction mixture was precipitated from water (1 L) with stirring. The yellow precipitate was filtered, dissolved in methylene chloride (700 mL) and washed with water (2 × 500 mL). The organic layer was then dried over magnesium sulfate and evaporated under reduced pressure to obtain a pink solid. The crude solid product was further washed with hexane and recrystallized from methanol to obtain white solid product 77% yield (4.73 mmol, 1.86 g). The ^{1}H NMR and ^{13}C were shown in Figure A1 and A2, ^{1}H NMR (400 MHz, CD_2Cl_2-d_2, ppm) δ: 9.39 (s, 1H), 7.62-7.03 (m, 11H), 2.19 (s, 6H). ^{13}C NMR (125 MHz, $CDCl_3$-d, ppm) δ: 144.86, 140.96, 135.11, 129.99, 129.65, 129.18, 129.04, 128.52, 127.91, 20.35.

Synthesis of 2-(4-chloro-2, 6-dimethylphenyl)-4-(4-chlorophenyl)-1-methyl-5-phenyl-1*H*-imidazole

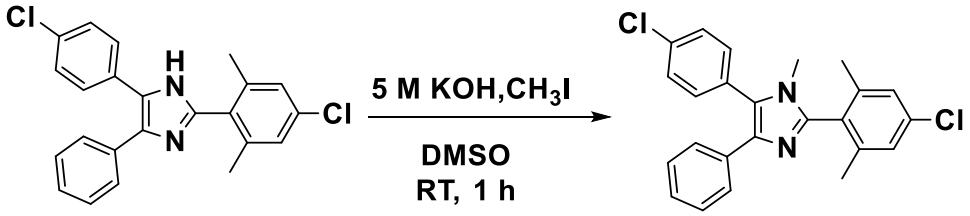

In a 250 mL round bottom flask, 2-(4-chloro-2, 6-dimethylphenyl)-4-(4-chlorophenyl)-5-phenyl-1*H*-imidazole (1.00 equiv., 3.17 mmol, 1.25 g) and 5 M KOH (3.10 equiv., 9.83 mmol, 1.96 mL) were added in DMSO (100 mL). The solution changed color from light yellow to dark green and then to dark yellow in 10 minutes. After 30 minutes, Iodomethane (3.20 equiv., 10.1 mmol, 0.623 mL) was added in dropwise. Another 30 minutes later, the reaction mixture was precipitated from 2 M KOH (500 mL). The brown precipitate was filtered, washed with excess water and dissolved in methylene chloride (700 mL). The organic layer was then washed with water (2 × 500 mL), dried over magnesium sulfate, and evaporated under reduced pressure to obtain a pale solid. The solid was further purified by flash chromatography on basic alumina using ethyl acetate. A white solid was obtained 82% yield (2.58 mmol, 1.05 g). The ^{1}H and ^{13}C NMR were shown in Figure A3 and A4, ^{1}H NMR (400 MHz, CD_2Cl_2-d_2, ppm) δ: 7.55-7.44 (m, 5H), 7.42-7.33 (m, 2H), 7.24-7.13 (m, 4H), 3.13 (d, J = 2.7 Hz, 3H), 2.15 (s, 6H). ^{13}C NMR (125 MHz, CD_2Cl_2-d_2, ppm) δ: 146.19, 145.99, 141.48, 138.34, 136.80, 135.47, 135.36, 135.18,

134.41, 132.89, 132.19, 131.71, 131.39, 130.59, 130.07, 129.93, 129.91, 129.74, 129.36, 128.70, 128.44, 128.24, 127.93, 127.29, 126.92, 31.64, 20.14.

Synthesis of 2-(4-chloro-2, 6-dimethylphenyl)-4-(4-chlorophenyl)-1-ethyl-5-phenyl-1*H*-imidazole

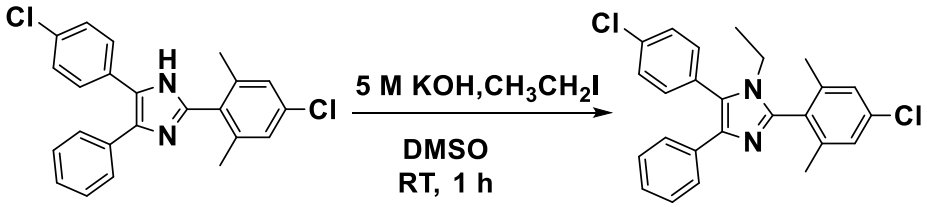

In a 250 mL round bottom flask, 2-(4-chloro-2, 6-dimethylphenyl)-4-(4-chlorophenyl)-5-phenyl-1*H*-imidazole (1.00 equiv., 1.73 mmol, 0.730 g) and 5 M KOH (3.10 equiv., 5.37 mmol, 1.07 mL) were added in DMSO (80 mL). The solution changed color from light yellow to dark green and then to dark yellow in 10 minutes. After 30 minutes, Iodoethane (3.20 equiv., 5.53 mmol, 0.444 mL) was added in dropwise. Another 30 minutes later, the reaction mixture was precipitated from 2 M KOH (500 mL). The pale precipitate was filtered, washed with excess water and dissolved in methylene chloride (600 mL). The organic layer was then washed with water (2 × 300 mL), dried over magnesium sulfate and evaporated under reduced pressure to obtain pale solid. The solid was further purified by flash chromatography on basic alumina using ethyl acetate. A white solid was obtained 76% yield (1.31 mmol, 0.554 g). The ^{1}H and ^{13}C NMR were shown in Figure A5 and A6, and ^{1}H NMR (400 MHz, CD_2Cl_2-d_2, ppm) δ: 7.59-7.37 (m, 7H), 7.26-7.10 (m, 4H), 3.56 (q, *J* = *7.2* Hz, 2H), 2.19 (s, 6H), 0.88 (t, *J* = *7.2* Hz, 3H). ^{13}C NMR (125 MHz, CD_2Cl_2-d_2, ppm) δ: 145.20, 141.37, 137.10, 135.32, 134.44, 133.07, 132.11, 131.98, 131.57, 130.35, 130.00, 129.80, 129.42, 129.32, 128.68, 128.33, 128.06, 127.17, 39.77, 20.30, 16.23.

50% methylated Polymer (PAIM-MX)[60]

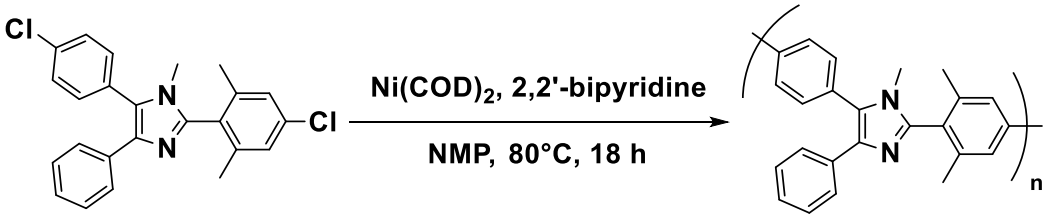

A 20 mL Schlenk flask was charged with 2,2'-bipyridine (2.41 equiv., 0.591 mmol, 0.0924 g) and the flask was evacuated and refilled with argon three times. Bis(1,5-cyclooctadiene)nickel(0) (2.42 equiv., 0.591 mmol, 0.163 g) was transferred into the flask, and the flask was evacuated and refilled with argon three times again. Anhydrous N-methyl-pyrrolidone (5 mL) was added, and the catalyst solution was heated up to 60 ˚C for 30 minutes. In a separate 20 mL flask, 2-(4-chloro-2,6-dimethylphenyl)-4-(4-chlorophenyl)-1-methyl-5-phenyl-1*H*-imidazole monomer (1.00 equiv., 0.245 mmol, 0.100 g) and anhydrous N-methyl-pyrrolidone (5 mL) were added. The flask was evacuated and refilled with argon three times. After the catalyst solution was heated for 30 minutes, the monomer solution was then transferred to the catalyst solution and heated up to 80 °C while stirring for 18 hours. The reaction mixture was then cooled to room temperature and poured into 6 M HCl (200 mL) to consume the nickel catalyst. The white fiber-like precipitate was filtered and washed with 2 M potassium carbonate solution (100 mL), water (100 mL) and acetone (100 mL). A pale solid was obtained 96% yield (0.235 mmol, 0.0791 g). The product was further dissolved in methylene chloride (5 mL) in a 10 mL vial and evaporated; a yellow membrane was formed shown in Figure A7. The ^{1}H NMR was shown in Figure A8, PAIM-MX: ^{1}H NMR (400 MHz, CD_2Cl_2-d_2, ppm) δ: 7.86-7.17 (m, 11H), 3.28-3.18 (m, 3H), 2.30-2.23 (m, 6H).

50% ethylated Polymer (PAIM-EX)[60]

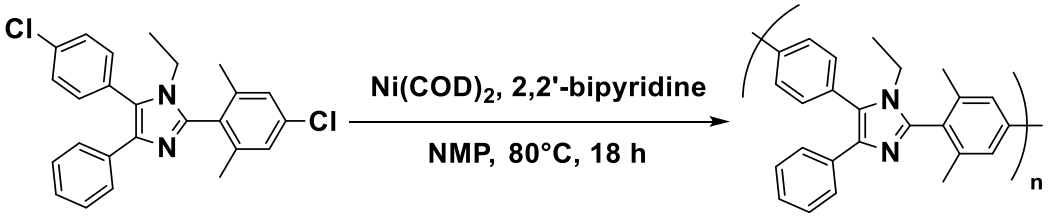

A 20 mL Schlenk flask was charged with 2,2'-bipyridine (2.41 equiv., 2.41 mmol, 0.376 g), and the flask was evacuated and refilled with argon three times. Bis(1,5-cyclooctadiene)nickel(0) (2.42 equiv., 2.41 mmol, 0.663 g) was transferred into the flask, and the flask was evacuated and refilled with argon three times again. Anhydrous N-methyl-pyrrolidone (10 mL) was added, and the catalyst solution was heated up to 60 ˚C for 30 minutes. In a separate 20 mL flask, 2-(4-chloro-2,6-dimethylphenyl)-4-(4-chlorophenyl)-1-ethyl-5-phenyl-1*H*-imidazole monomer (1.00 equiv., 0.997 mmol, 0.420 g) and anhydrous N-methyl-pyrrolidone (15 mL) were added. The flask was evacuated and refilled with argon three times. After the catalyst solution was heated for 30 minutes, the monomer solution was then transferred to the catalyst solution and heated up to 80 °C

while stirring for 18 hours. The reaction mixture was then cooled to room temperature and poured into 6 M HCl (400 mL) to consume the nickel catalyst. The white fiber-like precipitate was filtered and washed with 2 M potassium carbonate solution (300 mL), water (200 mL) and acetone (200 mL). A pale solid was obtained 92% yield (0.916 mmol, 0.321 g). The ^{1}H NMR was shown in Figure A9, PAIM-EX: ^{1}H NMR (400 MHz, CD_2Cl_2-d_2, ppm) δ: 7.89-7.12 (m, 11H), 3.79-3.58 (m, 2H), 2.34-2.24 (m, 6H), 1.89-1.63 (m, 2H), 1.12-0.84 (m, 3H).

Fully methylated polymer (PAIM-MM)

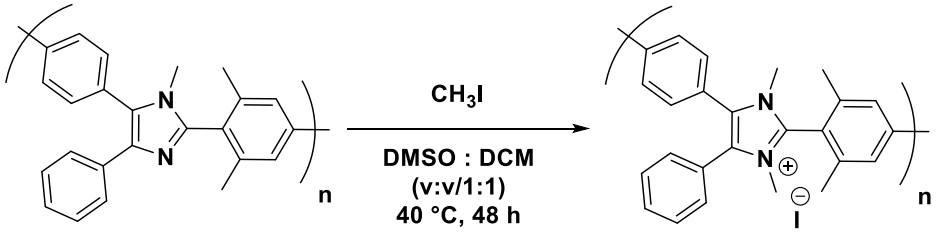

A 40 mL round bottom flask was charged with 50% methylated polymer PAIM-MX (1.00 equiv., 0.184 mmol, 0.0620 g) in methylene chloride (4 mL) and N-methyl-2-pyrrolidone (4 mL). Iodomethane (20.0 equiv., 3.68 mmol, 0.229 mL) was added, and the reaction mixture was heated at 40 °C for 48 hours. The reaction mixture was then precipitated from ethyl acetate (150 mL), washed with acetone (100 mL), obtained a red-orange solid PAIM-MM 99% yield (0.182 mmol, 0.0640 g). The ^{1}H NMR was shown in Figure A10, PAIM-MM: ^{1}H NMR (400 MHz, DMSO-d_6, ppm) δ: 8.10-7.46 (m, 11H), 3.70-3.43 (m, 6H), 2.47-2.27 (m, 6H).

Fully ethylated polymer (PAIM-EE)

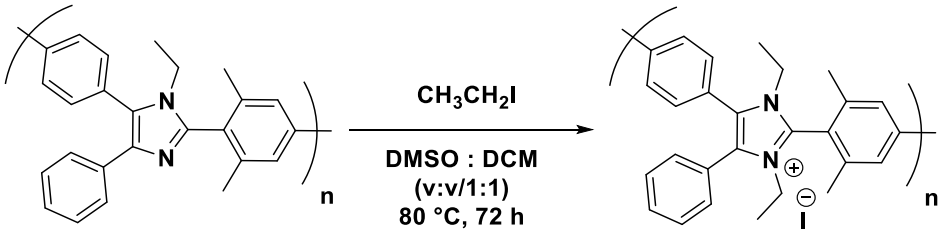

A 40 mL pressure vessel flask was charged with 50% ethylated polymer PAIM-EX (1.00 equiv., 0.858 mmol, 0.301 g) in methylene chloride (10 mL) and N-methyl-2-pyrrolidone (10 mL). Iodoethane (20.0 equiv., 17.1 mmol, 1.37 mL) was added, and the reaction mixture was heated at 80 °C for 72 hours. The reaction mixture was then precipitated from ethyl acetate (300 mL), washed with acetone (200 mL), obtained red-orange solid PAIM-EE 97% yield (0.830 mmol, 0.315 g). The ^{1}H NMR was shown in Figure

A11, PAIM-EE: ^{1}H NMR (400 MHz, DMSO-d_6, ppm) δ: 8.02-7.49 (m, 11H), 4.09-3.95 (m, 4H), 2.43-2.29 (m, 6H), 1.14-0.85 (m, 6H).

2.2.2. Synthesis of PAIM-RR-2

Synthesis of 1,2-bis(4-chlorophenyl)ethyne[65]

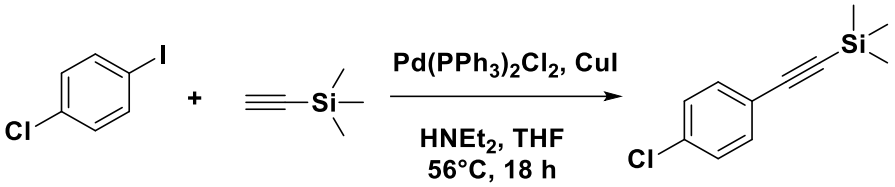

In a 50 mL Schlenk round bottle flask, 1-chloro-4-iodo-benzene (1.00 equiv., 63.7 mmol, 15.2 g) and $Pd(PPh_3)_2Cl_2$ (0.100%, 6.37 × 10^{-2} mmol, 0.0500 g) were added and the flask was evacuated and refilled with argon three times. Diethylamine (6.00 equiv., 382 mmol, 39.5 mL) and THF (6 mL) were then injected to dissolve the solids with addition of trimethylsilylacetylene (1.02 equiv., 65.0 mmol, 9.25 mL) and CuI (0.100 %, 6.37 x 10^{-2} mmol, 12.0 mg) under argon. The solution was heated at 56 °C with stirring for 18 hours; after that, a brown pale solid was formed at the bottom of the flask within one hour. Diethyl ether (500 mL) was added to the reaction mixture and stirred for 30 minutes. The brown solid was then filtered, and the filtrate was washed with 10% NH_4Cl (2 × 50 mL), water (2 ×100 mL) and brine (100 mL). The organic layer was further dried over magnesium sulfate, evaporated under reduced pressure, obtained an orange solid 97% yield (61.8 mmol, 12.9 g). ^{1}H NMR (400 MHz, $CDCl_3$-d, ppm) δ: 7.41 (d, *J* = 8.6 Hz, 2H), 7.29 (d, *J* = 7.8 Hz, 2H), 0.27 (s, 9H).

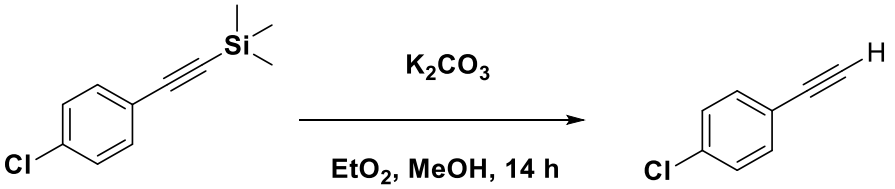

((4-Chlorophenyl)ethynyl)trimethylsilane (1.00 equiv., 76.6 mmol, 16.0 g), degassed diethyl ether (100 mL) and methanol (50 mL) were added into a 250 mL round bottle flask covered with aluminum foil. After the solution was stirred for 30 minutes, potassium carbonate (1.50 equiv., 115 mmol, 15.9 g) was added to the solution, and the reaction mixture was stirred at room temperature for 14 hours. A brown solid was obtained after the reaction mixture was evaporated under reduced pressure. The solid was

dissolved in diethyl ether (500 mL) and washed with water (2 × 200). The organic layer was then dried over magnesium sulfate, filtered, and evaporated under reduced pressure, yielded a brown solid. The solid was further purified by Celite filtration with petroleum ether (400 mL) under heating with active carbon for 18 hours. After the solvent was evaporated under reduced pressure, pale-orange solid was obtained 87% yield (66.6 mmol, 9.10 g). ^{1}H NMR (400 MHz, $CDCl_3$-d, ppm) δ: 7.42 (d, *J* = 8.6 Hz, 2H), 7.30 (d, *J* = 8.6 Hz, 2H), 3.10 (s, 1H).

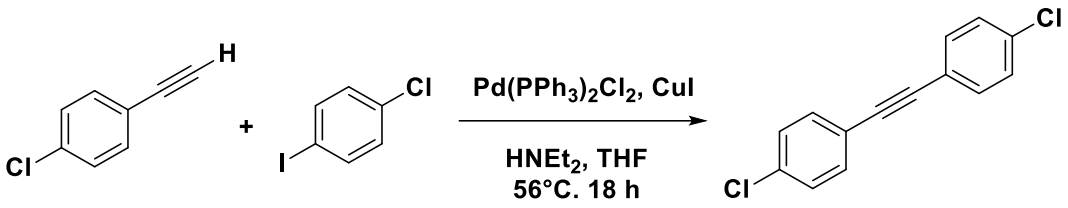

1-chloro-4-iodo-benzene (1.20 equiv., 101 mmol, 24.0 g) and $Pd(PPh_3)_2Cl_2$ (0.100%, 8.39 × 10^{-2} mmol, 60.0 mg) were added into a 50 mL Schlenk round bottom flask, and the flask was degassed with argon three times. Diethylamine (6.00 equiv., 505.2 mmol, 52.0 mL) and THF (8 mL) were then injected to dissolve the solids with addition of 1-chloro-4-ethynylbenzene (1.00 equiv., 84.2 mmol, 11.5 g) and CuI (0.100%, 8.42 × 10^{-3} mmol, 160 mg) under argon. The solution was heated at 56 °C with stirring for 18 hours; after that, an orange solid was formed at the bottom of flask within one hour. Diethyl ether (500 mL) was added to the reaction mixture and stirred for 30 minutes. The orange solid was filtered, and the filtrate was washed with 10% NH_4Cl (2 × 100 mL), 1 M HCl (2 × 100 mL), water (2 × 100mL) and brine (100 mL). The organic layer was dried over magnesium sulfate, evaporated under reduced pressure, obtained a yellow solid. The solid was further purified by Celite filtration with hexane under heating with active carbon for 18 hours. After evaporation under reduced pressure, a light yellowish crystal was obtained 40% yield (33.7 mmol, 8.32 g). ^{1}H NMR (400 MHz, $CDCl_3$-d, ppm) δ: 7.45 (d, *J* = 8.6 Hz, 4H), 7.33 (d, *J* = 8.6 Hz, 4H). ^{13}C NMR (125 MHz, $CDCl_3$-d, ppm) δ: 134.7, 132.9, 128.8, 121.6, 89.3.

Synthesis of 1,2-bis(4-chlorophenyl)ethane-1,2-dione[64]

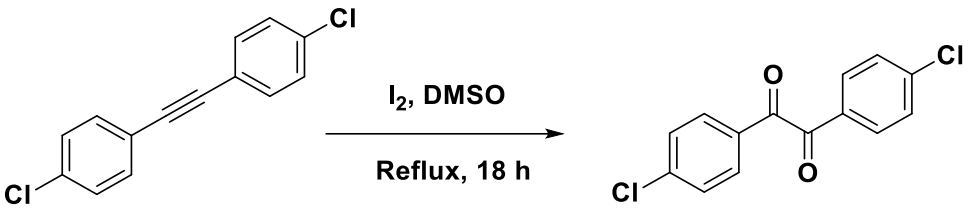

In a 500 mL round bottle flask, 1,2-bis(4-chlorophenyl)ethyne (1 equiv., 33.0 mmol, 8.15 g) and I_2 (1.10 equiv., 36.3 mmol, 9.20 g) were added in dimethyl sulfoxide (110 mL). After heating at reflux for 18 hours, the solution was precipitated from 1% sodium thiosulfate (600 mL), and the yellow precipitate was filtered. The precipitate was then dissolved in methylene chloride (450 mL) and washed with water (2 × 200 mL). The organic layer was dried over magnesium sulfate, evaporated under reduced pressure, obtained a yellow solid. The yellow crude solid was further purified by recrystallization from hexane, obtained a yellow crystals 46% yield (11.8 mmol, 3.29 g). ^{1}H NMR (400 MHz, $CDCl_3$-d, ppm) δ: 7.92 (d, *J* = 8.7 Hz, 4H), 7.51 (d, *J* = 8.7 Hz, 4H). ^{13}C NMR (125 MHz, $CDCl_3$-d, ppm) δ: 192.40, 141.86, 131.30, 131.13, 129.54.

Debus-Radziszewski imidazole synthesis[64]

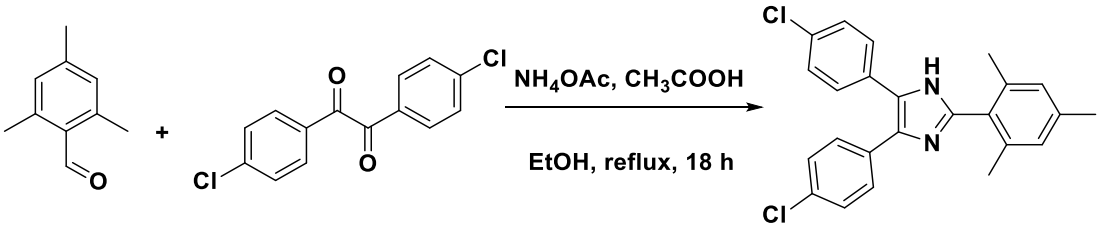

A 500 mL round bottom flask was charged with 2,4,6-trimethylbenzaldehyde (1.20 equiv., 8.34 mmol, 1.01 mL), 1,2-bis(4-chlorophenyl)ethane-1,2-dione (1.00 equiv., 6.95 mmol, 1.94 g) and ammonium acetate (10.0 equiv., 69.5 mmol, 5.35 g) in acetic acid (50 mL) and ethanol (200 mL). After heating at reflux for 18 hours, the reaction mixture was precipitated from the water (1 L) with stirring. The yellow precipitate was filtered, dissolved in methylene chloride (500 mL) and washed with water (2 × 300 mL). The organic layer was then dried over magnesium sulfate, evaporated under reduced pressure to obtain a pink crude solid. The crude solid was further washed with hexane to obtain white solid 45% yield (3.12 mmol, 1.27 g), The ^{1}H NMR was shown in Figure B1, ^{1}H NMR (400 MHz, $CDCl_3$-d, ppm) δ: 9.20 (s, 1H), 7.48-7.45 (m, 4H), 7.31 (d, *J* = 17.7 Hz, 4H), 6.91 (s, 2H), 2.35 (s, 3H), 2.19 (s, 6H).

Synthesis of 4,5-bis(4-chlorophenyl)-2-mesityl-1-methyl-1*H*-imidazole

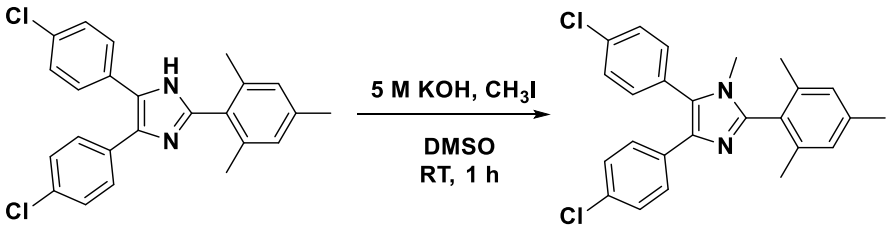

In a 250 mL round bottom flask, 4,5-bis(4-chlorophenyl)-2-mesityl-1*H*-imidazole (1.00 equiv., 3.11 mmol, 1.27 g) and 5 M KOH (3.00 equiv., 9.33 mmol, 1.87 mL) were added in dimethyl sulfoxide (100 mL). The solution changed color from light yellow to dark green and then to dark yellow in 10 minutes. After 30 minutes, Iodomethane (3.10 equiv., 9.64 mmol, 0.600 mL) was added in dropwise. Another 30 minutes later, the reaction mixture was precipitated from 2 M KOH (500 mL)). The brown precipitate was filtered, washed with excess water and dissolved in methylene chloride (500 mL). The organic layer was washed with water (2 × 500 mL), dried over magnesium sulfate, evaporated under reduced pressure to obtain a pale solid. The solid was further purified by flash chromatography on basic alumina using methylene chloride. A white solid was obtained 61% yield (1.90 mmol. 0.802 g). The ^{1}H and ^{13}C NMR were shown in Figure B2 and B3, ^{1}H NMR (400 MHz, CD_2Cl_2-d_2, ppm) δ: 7.53-7.46 (d, 4H), 7.36 (d, *J* = 8.5 Hz, 2H), 7.19 (d, *J* = 8.5 Hz, 2H), 7.00 (s, 2H), 3.13 (s, 3H), 2.36 (s, 3H), 2.12 (s, 6H). ^{13}C NMR (125 MHz, CD_2Cl_2-d_2, ppm) δ: 147.73, 139.84, 139.06, 136.95, 135.24, 134.36, 132.82, 132.26, 130.55, 129.98, 128.77, 128.52, 128.24, 128.22, 31.62, 21.56, 20.08.

Yamamoto homo-polymerization[60]

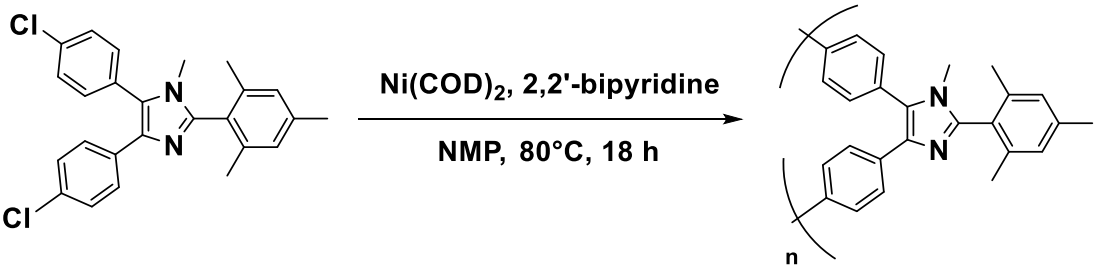

A 20 mL Schlenk flask was charged with 2,2'-bipyridine (2.41 equiv., 0.572 mmol, 0.0893 g). The flask was evacuated and refilled with argon three times. Bis(1,5-cyclooctadiene)nickel(0) (2.42 equiv., 0.572 mmol, 0.157 g) was transferred into the flask, and the flask was evacuated and refilled with argon three times again. Anhydrous N-methyl-pyrrolidone (5 mL) was added, and the catalyst solution was heated up to 60 ˚C for 30 minutes. In a separate 20 mL flask, 4,5-bis(4-chlorophenyl)-2-mesityl-1-methyl-1*H*-

imidazole monomer (1.00 equiv., 0.237 mmol, 0.100 g) and anhydrous N-methyl-pyrrolidone (5 mL) were added. The flask was evacuated and refilled with argon three times. After the catalyst solution was heated for 30 minutes, the monomer solution was then transferred to the catalyst solution and heated at 80 °C while stirring for 18 hours. The reaction mixture was cooled to room temperature and poured into 6 M HCl (200 mL) to consume the nickel catalyst. The precipitate was then filtered and washed with 2 M potassium carbonate solution (100 mL), water (100 mL) and acetone (100 mL). A yellow-brown solid was obtained. The solid was further dissolved in methylene chloride (5 mL) and evaporated under reduced pressure. A yellow powder was formed. The ^{1}H NMR was shown in Figure B4. ^{1}H NMR (400 MHz, CD_2Cl_2-d_2, ppm) δ: 7.93-6.84 (m, 10H), 3.39-3.19 (m, 3H), 2.37 (s, 3H), 2.18 (s, 6H).

2.2.3. Synthesis of PAIM-RR-3

Synthesis of 1,2-bis(3-chlorophenyl)ethyne[65]

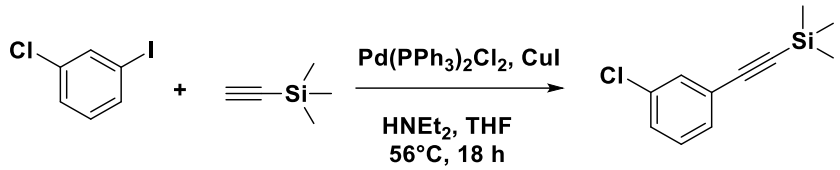

In a 50 mL Schlenk round bottle flask, 3-chloro-iodo-benzene (1.00 equiv., 33.5 mmol, 7.99 g) and $Pd(PPh_3)_2Cl_2$ (0.100%, 3.35 × 10^{-2} mmol, 0.0235 g) were added, and the flask was evacuated and refilled with argon three times. Diethylamine (6.00 equiv., 201 mmol, 21.0 mL) and THF (3 mL) were then injected to dissolve the solids with addition of trimethylsilylacetylene (1.02 equiv., 34.2 mmol, 5.00 mL) and CuI (0.100 %, 3.35 x 10^{-2} mmol, 6.40 mg) under argon. The solution was heated at 56 °C with stirring for 18 hours; after that, a grey pale solid was formed at the bottom of the flask within one hour. Diethyl ether (300 mL) was added to the reaction mixture and stirred for 30 minutes. The grey pale solid was filtered, and the filtrate was washed with 10% NH_4Cl (2 × 50 mL), water (2 × 100 mL) and brine (100 mL). The organic layer was further dried over magnesium sulfate, evaporated under reduced pressure, obtained orange oil liquid 74% yield (24.9 mmol, 5.20 g). ^{1}H NMR (400 MHz, $CDCl_3$-d, ppm) δ: 7.48-7.45 (m, 1H), 7.37-7.19 (m, 3H), 0.25 (s, 9H).

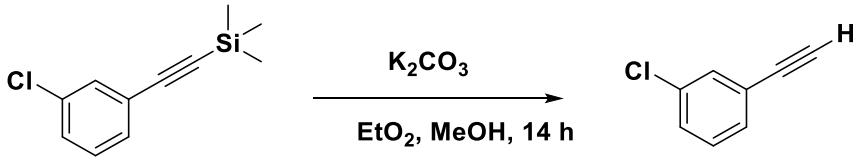

((3-chlorophenyl)ethynyl)trimethylsilane (1.00 equiv., 24.9 mmol, 5.20 g), degassed diethyl ether (90 mL) and methanol (30 mL) were added into a 250 mL round bottle flask covered with aluminum foil. After the solution was stirred for 30 minutes, potassium carbonate (1.50 equiv., 37.4 mmol, 5.16 g) was added to the solution, and the reaction mixture was stirred at room temperature for 14 hours. A red-orange oil was obtained after the reaction mixture was evaporated under reduced pressure. The oil was dissolved in diethyl ether (200 mL) and washed with water (2 × 200). The organic layer was further dried over magnesium sulfate and evaporated under reduced pressure, obtained a yellow oil 86% yield (21.4 mmol, 2.92 g). ^{1}H NMR (400 MHz, $CDCl_3$-d, ppm) δ: 7.51-7.50 (m, 1H), 7.43-7.34 (m, 2H), 7.28-7.27 (m, 1H), 3.13 (s, 1H).

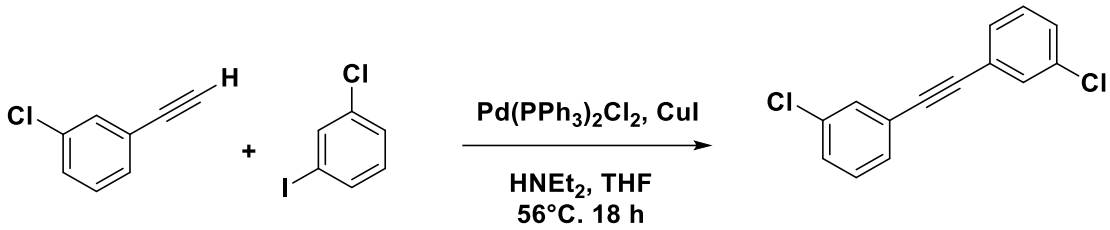

3-chloro-iodo-benzene (1.20 equiv., 35.2 mmol, 8.39 g) and $Pd(PPh_3)_2Cl_2$ (0.100 %, 2.94 × 10^{-2} mmol, 0.0206 g) were added into a 50 mL Schlenk round bottom flask, and the flask was degassed with argon three times. Diethylamine (6.00 equiv., 176 mmol, 18.2 mL) and THF (3 mL) were then injected to dissolve the solids with addition of 1-chloro-3-ethynylbenzene (1.00 equiv., 29.4 mmol, 4.01 g) and CuI (0.100 %, 2.94 × 10^{-2} mmol, 5.00 mg) under argon. The solution was heated at 56 °C with stirring for 18 hours; after that, an orange-colored solid was formed at the bottom of flasks within one hour. Diethyl ether (500 mL) was added to the reaction mixture and stirred for 30 minutes. The orange solid was then filtered, and the filtrate was washed with 10% NH_4Cl (2 × 100 mL), 1 M HCl (2 × 100 mL), water (2 × 100 mL) and brine (100 mL). The organic layer was dried over magnesium sulfate, evaporated under reduced pressure obtained a red oil. Column The oil was further purified by column chromatography on silica using hexane, obtained colorless oil 60% yield (17.6 mmol, 4.36 g). ^{1}H NMR (400 MHz, $CDCl_3$-d, ppm) δ: 7.46-7.41 (m, 2H), 7.39-7.35 (m, 2 H), 7.34-7.25 (m, 4 H). ^{13}C NMR (125 MHz, $CDCl_3$-d, ppm) δ: 134.5, 132.8, 129.0, 128.7, 128.2, 121.5, 89.2.

Synthesis of 1,2-bis(3-chlorophenyl)ethane-1,2-dione[64]

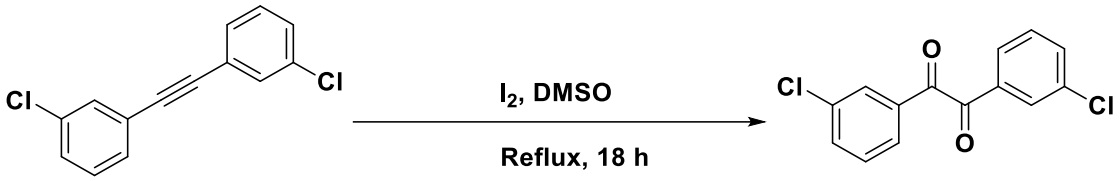

In a 50 mL round bottle flask, 1,2-bis(3-chlorophenyl)ethyne (1.00 equiv., 10.0 mmol, 2.80 g) and I_2 (1.10 equiv., 11.0 mmol, 2.78 g) were added in dimethyl sulfoxide (35 mL). After heating at reflux for 18 hours, the solution was precipitated from 1% sodium thiosulfate (600 mL), and the yellow precipitate was filtered. The precipitate was dissolved in methylene chloride (450 mL) and washed with water (2 × 200 mL). The organic layer was then dried over magnesium sulfate, evaporated under reduced pressure, obtained a yellow solid. The yellow solid was further recrystallized from methanol obtained yellow crystals 65% yield (6.48 mmol, 1.81 g). ^{1}H NMR (400 MHz, CD_2Cl_2-d_2, ppm) δ: 7.97 (t, *J* = 1.9 Hz, 2H), 7.84 (ddd, *J* = 7.8, 1.6, 1.1 Hz, 2H), 7.68 (ddd, *J* = 8.0, 2.2, 1.1 Hz, 2H), 7.50 (t, *J* = 7.9 Hz, 2H). ^{13}C NMR (125 MHz, CD_2Cl_2-d_2, ppm) δ: 192.74, 135.94, 135.57, 134.79, 131.11, 130.09, 128.78.

Debus-Radziszewski imidazole synthesis[64]

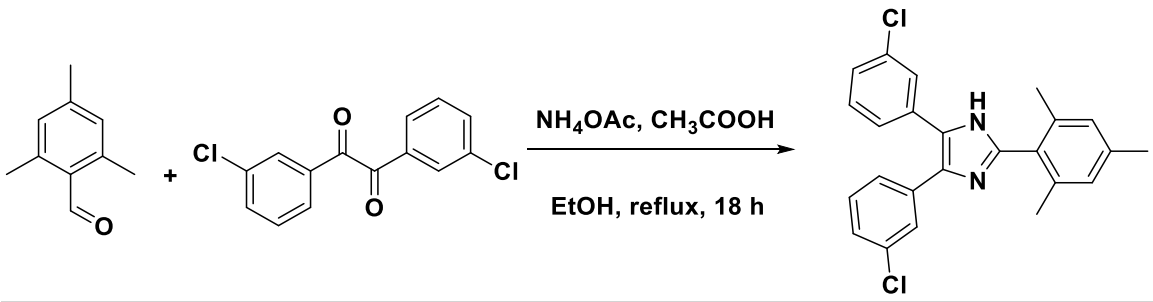

A 500 mL round bottom flask was charged with 2,4,6-trimethylbenzaldehyde (1.20 equiv., 19.3 mmol, 2.62 mL), 1,2-bis(3-chlorophenyl)ethane-1,2-dione (1.00 equiv., 16.1 mmol, 4.50 g) and ammonium acetate (10.0 equiv., 161 mmol, 12.4 g) in acetic acid (80 mL) and ethanol (300 mL). After heating at reflux for 18 hours, the reaction mixture was precipitated from the water (1 L) with stirring. The yellow precipitate was filtered, dissolved in methylene chloride (500 mL), and washed with water (2 × 400 mL). The organic layer was then dried over magnesium sulfate, evaporated under reduced pressure to obtain brown pale crude solid. The crude solid was further washed with hexane to obtain white solid 53% yield (8.37 mmol, 3.41 g). The ^{1}H NMR was shown in Figure B5, ^{1}H NMR (400

MHz, CD_2Cl_2-d_2, ppm) δ: 9.31 (s, 1H), 7.67-7.22 (m, 8H), 6.97-6.92 (m, 2H), 2.34 (s, 3H), 2.17 (s, 6H).

Synthesis of 4,5-bis(3-chlorophenyl)-2-mesityl-1-methyl-1H-imidazole

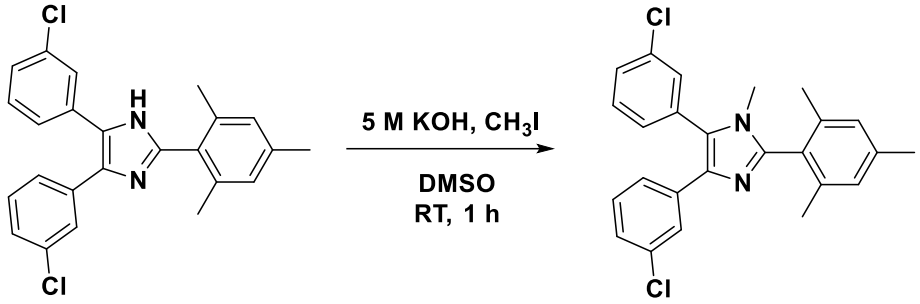

In a 500 mL round bottom flask, 4,5-bis(3-chlorophenyl)-2-mesityl-1*H*-imidazole (1.00 equiv., 2.63 mmol, 1.07 g) and 5 M KOH (3 equiv., 7.88 mmol, 1.51 mL) were added in dimethyl sulfoxide (100 mL). The solution changed color from light yellow to dark green and then to dark yellow in 10 minutes. After 30 minutes, Iodomethane (3.10 equiv., 8.15 mmol, 0.508 mL) was added in dropwise. Another 30 minutes later, the reaction mixture was precipitate from 2 M KOH (500 mL). The brown precipitate was filtered, washed with excess water and dissolved in methylene chloride (800 mL). The organic layer was then washed with water (2 × 500 mL), dried over magnesium sulfate and evaporated under reduced pressure to yield a pale solid. The solid was further purified by flash chromatography on basic alumina using methylene chloride. A white solid was obtained 72% yield (1.89 mmol, 0.798 g). The ^{1}H and ^{13}C NMR were shown in Figure B6 and B7, ^{1}H NMR (400 MHz, CD_2Cl_2-d_2, ppm) δ: 7.65-7.64 (m, 1H), 7.50-7.40 (m, 3H), 7.36-7.27 (m, 2H), 7.16-7.09 (m, 2H), 6.99 (s, 2H), 3.13 (s, 3H), 2.35 (s, 3H), 2.10 (s, 6H). ^{13}C NMR (125 MHz, CD_2Cl_2-d_2, ppm) δ: 147.86, 139.91, 139.06, 137.56, 136.78, 135.43, 134.63, 133.76, 131.29, 131.08, 129.94, 129.81, 129.45, 128.79, 128.43, 128.09, 127.21, 126.68, 125.17, 31.67, 21.57, 20.07.

Yamamoto homo-polymerization[60]

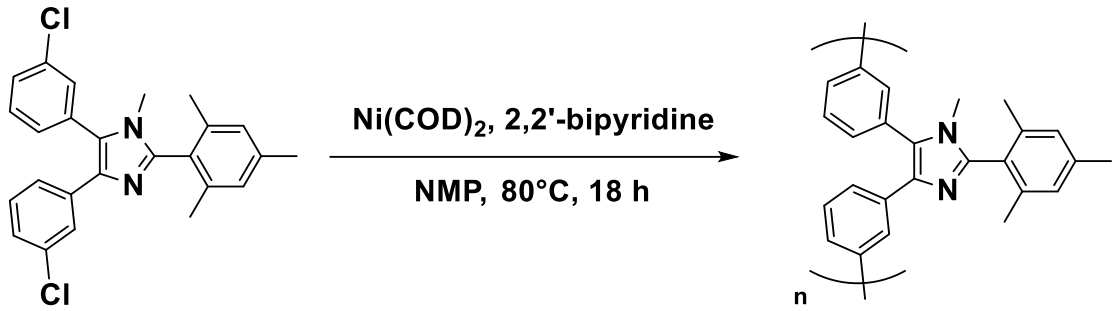

A 20 mL Schlenk flask was charged with 2,2'-bipyridine (2.41 equiv., 0.650 mmol, 0.101 g). The flask was evacuated and refilled with argon three times. Bis(1,5-cyclooctadiene)nickel(0) (2.42 equiv., 0.651 mmol, 0.179 g) was transferred into the flask, and the flask was evacuated and refilled with argon three times again. Anhydrous N-methyl-pyrrolidone (5 mL) was added, and the catalyst solution was heated up to 60 ˚C for 30 minutes. In a separate 20 mL flask, 4,5-bis(3-chlorophenyl)-2-mesityl-1-methyl-1*H*-imidazole monomer (1.00 equiv., 0.270 mmol, 0.114 g) and anhydrous N-methyl-pyrrolidone (5 mL) were added. The flask was evacuated and refilled with argon three times. After the catalyst solution was heated for 30 minutes, the monomer solution was then transferred to the catalyst solution and heated up to 80 °C while stirring for 18 hours. The reaction mixture was then cooled to room temperature and poured into 6 M HCl (200 mL) to consume the nickel catalyst. The precipitate was filtered and washed with 2 M potassium carbonate solution (150 mL), water (100 mL) and acetone (100mL). A yellow-brownish solid was obtained. The solid was further dissolved in methylene chloride (5 mL) and evaporated under reduced pressure. A yellow powder was formed. ^{1}H NMR was shown in Figure B8. ^{1}H NMR (400 MHz, CD_2Cl_2-d_2, ppm) δ: 8.21-6.99 (m, 10H), 3.40-3.12 (m, 3H), 2.37 (s, 3H), 2.22-2.12 (m, 6H).

2.2.4. Synthesis of PAIM-RR-4

Synthesis of 2, 7-dichlorophenanthrene-9, 10-dione[66]

In a 250 mL round bottle flask, phenanthrene-9,10-dione (1.00 equiv., 6.34 mmol,1.32 g) was added in 98% sulphuric acid (50 mL). The solution was stirred for 30 minutes, and N-Chlorosuccinimide (3.00 equiv., 19.0 mmol, 2.54 g) was added. The reaction mixture was agitated at room temperature. After 18 hours, the reaction mixture was poured into an ice/water bath, and the precipitate was filtered and further recrystallized from ethyl acetate : methylene chloride 1:1 by volume. A deep red solid was obtained 30% yield (1.90 mmol, 0.527 g). The ^{1}H NMR was shown in Figure B9 ^{1}H NMR (400 MHz, CD_2Cl_2-d_2, ppm) δ: 8.12 (d, *J* = 2.4 Hz, 2H), 7.96 (d, *J* = 8.6 Hz, 2H), 7.72 (dd, *J* = 8.6, 2.4 Hz, 2H).

Debus-Radziszewski imidazole synthesis[67]

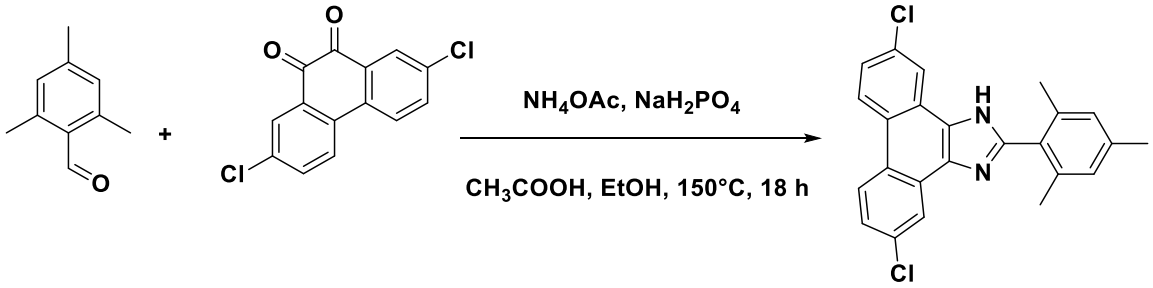

A 200 mL pressure vessel was charged with 2,4,6-trimethylbenzaldehyde (1.00 equiv., 0.540 mmol, 0.0800 mL), 2,7-dichlorophenanthrene-9,10-dione (1.00 equiv., 0.540 mmol, 0.150 g), ammonium acetate (2.00 equiv., 1.08 mmol, 83.5 mg) and NaH_2PO_4 (0.03 g) in acetic acid (5 mL) and ethanol (10 mL). After heating at 150 °C for 18 hours, the reaction mixture was poured into the water (100 mL) with stirring, and the pale orange precipitate was filtered. The precipitate was further dissolved in methylene chloride (200 mL) and washed with water (2× 200 mL) and brine (2× 100 mL). The pale layer was dried over magnesium sulfate, evaporated under reduced pressure, obtained pale solid. The crude solid was further washed with hexane to obtain white solid 61% yield (0.333 mmol, 0.135 g). The ^{1}H NMR was shown in Figure B10, ^{1}H NMR (400 MHz, CD_2Cl_2-d_2, ppm) δ:

8.66 (t, *J* = 8.8 Hz, 2H), 8.57 (d, *J* = 2.3 Hz, 1H), 8.26 (d, *J* = 2.3 Hz, 1H), 7.67 (dt, *J* = 9.0, 2.1 Hz, 2H), 7.06 (s, 2H), 2.39 (s, 9H).

2.3. Methods

2.3.1. Membrane Fabrication and Anion exchange Process

Membrane cast by casting table

A 10 wt% polymer solution was prepared in a vial by dissolving PAIM-RR-1 power in DMSO. The polymer solution was obtained by stirring it at 80 °C for 18 hours and sonicating for 10 minutes in a water bath. The polymer solution was further filtered through a 0.45 m glass fiber filter and cast onto the plate. The DMSO was evaporated in a casting oven at 80 ˚C for 12 hours, and a dried membrane was obtained. The membranes were then peeled off from the plate and soaked in 300 mL distilled water to remove residual DMSO and salts. The membrane was further sandwiched between two filter paper with glass plates and dried under reduced pressure at 80 ˚C for 18 hours. The thickness of the membrane was 19±2 μm.

Anion Exchange process

By converting the membranes from its iodide form to other forms, the membranes were treated with different salt solutions. By exchanging the counterion from iodide to chloride, the iodide-containing membranes were soaked into 300 mL deionized water and exchanged with fresh deionized water three times in 24 hours. The membranes were then immersed in 300 mL 1 M NaCl solution and exchange with fresh 1 M NaCl three times in 24 hours. In the end; the membranes were washed with 300 mL deionized water to remove residual NaCl. The membranes were then soaked in water for 48 hours before any characterizations.

2.3.2. Molecular Weight, UV Absorption

The molecular weight and absorption wavelength, are measured by the Malvern OMNISEC GPC. The Malvern OMNISEC GPC applied advanced tetra detection analysis by simultaneously using four detectors including refractive index (dn/dc), photodiode array (PDA) (dA/dc), static light scattering (Molecular Weight) and viscosity (Specific Viscosity),

advanced tetra detection analysis was applied. The running conditions were, solvent DMF with 0.01 M lithium bromide, at flow rate 1 mL·min^{-1} under 50 ˚C for 45 minutes.

2.3.3. Degree of Methylation

The controlled, partial methylation of the remaining basic nitrogen was performed in methylene chloride and dimethyl sulfoxide. The degree of methylation was performed under a specific equivalent of methyl iodide at a specific temperature over an adjustable range of time. The degree of methylation was determined by proton integration of ^{1}H NMR spectra with error in 5 % and calculated using Equation (1) below. ^{1}H NMR spectra were baseline corrected using the "Full Auto (Polynomial Fit)" function in MestReNova 10.0. The degree of methylation was calculated by first setting the integration area between 2.38-2.23 ppm to 6.00 H as a reference, which represents the two methyl groups of the mesitylene groups. Then 3.61-3.51 ppm integration area were integrated to provide the value "x" that correspond to the N-methyl-resonances of the charged imidazoliums groups.

$$dm\ (\%) = \frac{\left[\left(3 - \frac{x}{2}\right) + x\right]}{6} \times 100\% \qquad (1)$$

2.3.4. Ion Exchange Capacity

Back titration can be used to determine the IECs of AAEMs. However, the membranes need to expose to acid and base, which may cause high and low pH-derived degradation leading discrepancies between IECs. NMR data can be used to determine the IECs with soluble AEMs. The IECs of the membranes were calculated from the degree of alkylation, determined by the ^{1}H NMR spectroscopy shown in the equation (2). X^- represents the counterion. dm represents the percent fraction of the degree of methylation. MR_{100} is the mass of one repeating unit in 100% dm with the counterion, and MR_{50} is the mass of one repeating unit in 50% dm. For instance, dm is 0.87 if the degree of methylation is 87%, MR_{100} is $\frac{386.92\ g}{repeat\ unit}$, MR_{50} is $\frac{336.44\ g}{repeat\ unit}$, and the IEC_{cl^-} of the membrane is 1.98 $\frac{mmol}{g}$.

$$IEC_{x-}(\frac{mmol}{g}) = \frac{\left(\frac{1000\ mmol}{1mol}\right) \times (dm - 0.5)}{(dm - 0.5) \times MR_{100} + (1 - dm) \times MR_{50}} \qquad (2)$$

2.3.5. Water Uptake, Dimensional Swelling and Hydration Number

By measuring the change of mass before and after the membranes were soaked in deionized water at room temperature, the water uptake of the membrane in its chloride form was determined. The membranes were dried under reduced pressure at 80 °C until constant weights of dry membranes were recorded. The membranes were then immersed in deionized water at room temperature for 24 hours. The wet membranes were then taken out of the water, gently wiped with Kimtech precision wipe and quickly transferred to a mass balance to measure the wet mass. The water uptake was calculated by equation (3).

$$Water\ uptake\ (W_u) = \frac{W_{wet} - W_{dry}}{W_{dry}} \times 100\% \quad (3)$$

The dimensional swelling (D_s) of membranes was measured the same as water uptake, which by measuring the change in length and thickness in percentage. The dimensional swelling was obtained by equation (4).

$$Dimensional\ Swelling\ (D_s) = \frac{(L_{wet})^2 T_{wet} - (L_{dry})^2 T_{dry}}{(L_{dry})^2 T_{dry}} \times 100\% \quad (4)$$

where W_{wet}, $L_{wet,}$ T_{wet}, and W_{dry}, $L_{dry,}$ T_{dry} are the weights, lengths, and thickness of membranes at membrane wet and dry states. Six entries from different locations of the membrane were measured. The final result was the average of the six trials, and the standard deviation defined the uncertainty.

The hydration level (λ), or the number of water molecules per cation functional group, was calculated using equation (5).

$$\lambda = \frac{n(H_2O)}{n(NR_4{}^+)} = \frac{W_u}{m(H_2O) \times IEC} \quad (5)$$

where $n(H_2O)$ is the number of waters, $n(NR_4{}^+)$ is the number of cation groups, W_u is the water uptake of the membrane, $m(H_2O)$ is the molar mass of water, and IEC is the ion exchange capacity in $mol \cdot g^{-1}$.

2.3.6. Ionic Conductivity

The ionic resistance of the membranes was measured at the in-plane direction by electrochemical impedance spectroscopy. The membrane samples were hydrated before the conductivity measurements. The chloride conductivity of the wet membranes was measured under ambient conditions and also measured at % RH decreasing from 95% to 30%, and temperature decreasing from 80 ˚C to 30 ˚C. A frequency range 100 MHz to 10^7 MHz with 100 mV amplitude was set on a Solartron SI 1260 impedance/gain-phase analyzer. The membrane samples were sandwiched between Pt metal electrodes mounted in a Teflon frame. The membranes were equilibrated for 30 minutes for a change of temperature or relative humidity. When the temperature and humidity both changed, the cell was equilibrated for 2 hours before any measurements. The resistance was measured and fitted with a Randle circuit model.

The conductivity was calculated using equation (6).

$$\sigma\left(\frac{S}{cm}\right) = \frac{L(cm)}{R_m(\Omega) \times A(cm^2)} \tag{6}$$

where σ is the conductivity ($\frac{S}{cm}$), L is the distance in centimeter between the two Pt electrodes (length of the cavity) used to measure the potential; R_m is the membrane resistance (Ω) acquired from Randles circuit, A is the cross-section area of membrane in square cm. $A(cm^2) = T(cm) \times W\ (cm)$, where T and W are the thickness and width in centimeter of the membrane. For each membrane, four measurements of three different position of the membrane were taken, and the standard deviation was used as the uncertainty.

2.3.7. Stability in Alkaline Solutions

The membranes in chloride form were immersed in alkaline solutions in closed HDPE containers. The membranes were exposed to 1.0 M, 2.0 M, 5.0 M, 7.0 M and 10.0 M aqueous KOH solution at 80 °C for 168 hours. Then the membranes were washed with deionized water to remove excess potassium hydroxide. The membranes were further immersed in 1 M NaCl (30 mL) solution and exchanged with fresh 1 M NaCl five times in 48 hours. Afterward, the membranes were washed with deionized water (3 × 30 mL) and

dried under reduced pressure at 80 ˚C until constant masses of membranes were achieved. The structures were obtained from ^{1}H NMR in DMSO-d_6. The relative amount of imidazoliums remaining was calculated through the ^{1}H NMR data using the equation (7).

$$Relative\ imidazolium\ Remaining\ (\%) = \frac{\frac{X_c}{X_c + Y_c + Z_c}}{\frac{X_i}{X_i + Y_i + Z_i}} \times 100 \quad (7)$$

where X_c represents the integration area for the alkylation peak, Y_c and Z_c represent the integration areas for the degradation peaks. X_i, Y_i, and Z_i express the integration areas for the initial sample without any caustic treatment (Table 2.1).

Table 2.1. Chemical shift ranges of the alkylation peaks and degradation peaks for PAIM-MM and PAIM-EE

PAIM-RR-1	Chemical shift range for Xc	Chemical shift range for Yc	Chemical shift range for Zc
PAIM-MM	3.70-3.45 ppm	3.44-3.37 ppm	3.30-3.10 ppm
PAIM-EE	4.15-3.75 ppm	3.67-3.49 ppm	3.28-3.13 ppm

2.3.8. Mechanical Strength and Thermal Stability

The mechanical strength of the membranes was measured under ambient conditions (21 ˚C, 42% RH). The dried membrane samples were cut to barbell shapes (9.53 mm × 3.18 mm) using a standard ASTM D638-4 cutter. The prepared membranes were examined by a single column system (Instron 3344 Series) at a rate of 5.00 mm·min^{-1}. Six samples were tested, the average of tensile strength (the magnitude of stress applied to the film just before breaking), average of elongation at break (percent increased observed in AEM length), and average of Young's moduli (the elastic nature of membranes calculated by the slope of the stress-strain curve in the 0.5%-2.0% strain region) were obtained. The standard deviations were showed as uncertainty. A Thermogravimetric analyzer (TGA Q50, TA Instrument, USA) was used to explore the thermal degradation behavior of the membranes. The membranes in chloride form (3-10 mg) were measured under the nitrogen atmosphere with a heating rate of 5 ˚C·min^{-1} from 100 ˚C to 800 ˚C.

Chapter 3. Result and Discussion

3.1. Synthesis

3.1.1. Synthesis of PAIM-RR-1

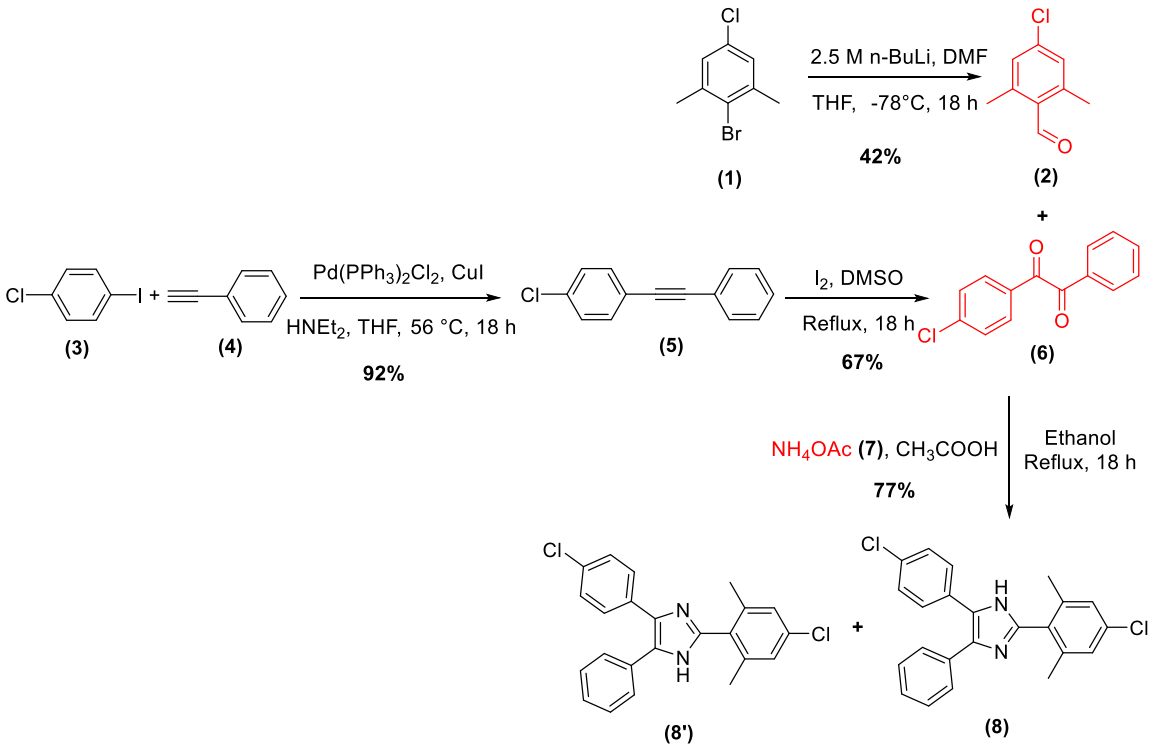

Scheme 3.1. The synthetic route to prepare the imidazole (8)

The PAIM-RR-1 polymers were designed with imidazolium group incorporated into the polymer backbone. Base on the dihalogenated monomer involved in Yamamoto polymerization, the monomer structure was proposed with one halogen group on C4 or C5 substituents, and the other halogen attached to the mesitylene at the C2 substituent. PAIM-RR-1 was synthesized by the Debus-Radziszewski imidazole synthesis, mono-alkylation, Yamamoto homo-polymerization, followed by the full alkylation.

In the Debus-Radziszewski imidazole synthesis, three starting materials were required: 4-chloro-2,6-dimethylbenzaldehyde **(2)**, 4-chloro-benzil **(6)** and ammonium acetate **(7)** (Scheme 3.1). 4-Chloro-2,6-dimethylbenzaldehyde **(2)** was obtained by lithium-halogen exchange of 2-bromo-5-chloro-1,3-dimethylbenzene **(1)** followed by the addition of DMF under nitrogen. In the reaction, the organolithium reagent used was 2.5

M n-butyllithium solution in hexanes, which was relatively stable under exclusion of air and humidity. Lithiation via the bromide occurred faster than chloride because the interexchange rate of bromide was faster than chloride (Inter-exchange rate: Iodide > Bromide > Chloride),[68] and the un-lithiated chloride was further applied in the Yamamoto homo-polymerization. The percentage yield for the reaction is 95% in the literature,[63] which is much higher than the percentage yield obtained in this work, only 42%. A possible explanation of the low yield is that the reaction was carried out at the elevated temperature close to -78 °C (dry ice/acetone) instead of -100 °C in the literature. The elevated temperature causes the mechanism of lithium-halogen exchange to radical cleavage and formation so that the free radical can rearrange to form the radical by-products, resulting in low percentage yield.[69] 4-Chloro-benzil **(6)** was obtained by the synthesis of 1-chloro-4-(phenylethynyl)benzene **(5)** through the Sonogashira coupling of 1-chloro-4-iodobenze **(3)** with phenylacetylene **(4)**, followed by the oxidation reaction.[70,71,64] In the Sonogashira coupling, $Pd(II)(PPh_3)_2Cl_2$ was used as the Pd source catalyst instead of $Pd(PPh_3)_4$, because it was much more air and moisture stable than $Pd(PPh_3)_4$. Iodide in 1-chloro-4-iodobenze participated in the oxidative addition because the iodide aryl bond posses a lower electron density compared with chloride aryl bond.[65,72] Moreover, chloride acting as an electron withdrawing group, further reduced the electron density of the aryl iodide bond and facilitated the oxidative addition. The organic solvent tetrahydrofuran was treated as secondary solvent, because 1-chloro-4-iodobenze **(3)** and phenylacetylene **(4)** had better solubility in tetrahydrofuran than in diethylamine at 56 °C. The addition of tetrahydrofuran significantly promoted the reactivity of Sonogashira reaction and increased the percentage yield from 86% to 92%. There were many oxidation reactions to turn the internal alkynes to 1,2-diketones such as potassium permanganate,[73] ruthenium,[74] chromium[75] and cobalt oxidants[76] and sulfur trioxide-dioxane complex.[77] However, most of the reactions suffered harsh reaction conditions, low product yield, tedious isolation procedures and use of expensive and detrimental metal precursors. Molecular iodine and dimethyl sulfoxide were chosen because they were inexpensive, non-toxic, and have non-metallic nature. The tautomers, 2-(4-chloro-2, 6-dimethylphenyl)-5-(4-chlorophenyl)-4-phenyl-1*H*-imidazole **(8)** and 2-(4-chloro-2, 6-dimethylphenyl)-4-(4-chlorophenyl)-5-phenyl-1*H*-imidazole **(8')** were then successfully obtained through the Debus-Radziszewski imidazole synthesis due to the presence of the labile hydrogen on the nitrogen atom. In addition, the coupling reaction of trisubstituted imidazole is known to be solvent specific.[70,78] Ethanol was used because it gave the best percentage yield (77%) compared to other solvents like 1,4-dioxane

(68%), methanol (62%), and glacial acetic acid (54%). The crude monomer was conveniently purified by washing with hexane, filtration, and recrystallization from methanol. The synthesis of the monomer with a good percentage yield was achieved without the need of purification techniques such as column chromatography.

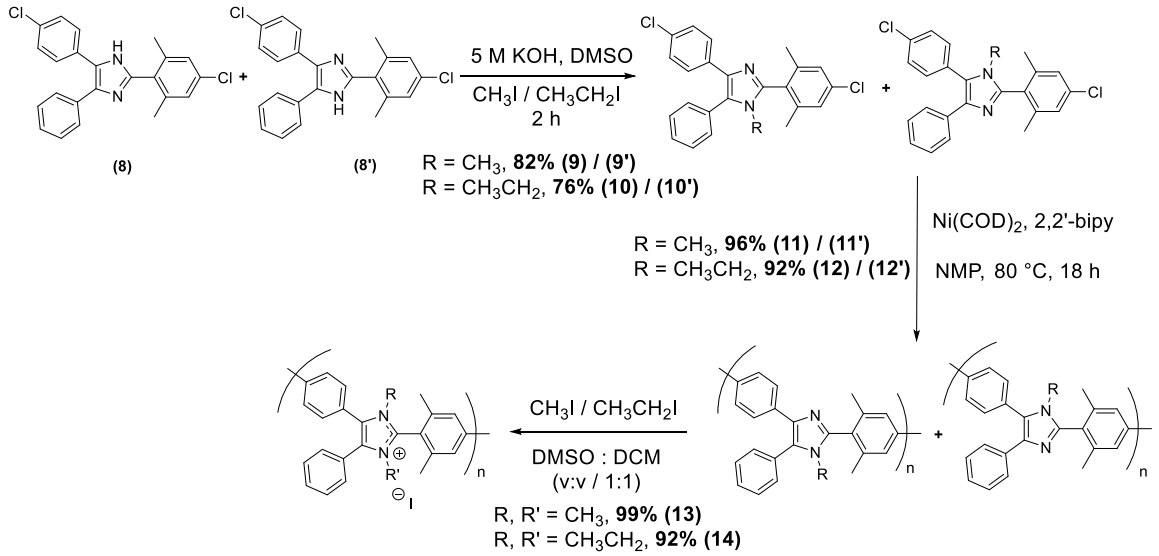

Scheme 3.2. The synthetic route to prepare the PAIM-MM (13) and PAIM-EE (14)

As shown in Scheme 3.2, the acidic proton of the monomer **(8)** was deprotonated by 5 M potassium hydroxide followed by mono-alkylation. The mono-alkylated monomer favored on the Yamamoto homo-polymerization because both of the acidic monomers without any alkylation and the fully alkylated charged monomer were problematic on solubility in polar aprotic solvents such as DMF and NMP. Surprisingly, the percentage yields of the alkylation decreased from 82% to 76% when the length of the alkylated side chain increased from methyl to ethyl. The alkylated monomers were successfully synthesized and proven by ^{1}H NMR spectroscopy. There were broad peaks in multiplets between δ = 7.54 - 7.14 ppm, corresponding to the eleven protons from aromatic groups - nine protons from C4, C5 phenyl groups labeled as **H^{a}**, and two protons from the mesitylene protecting group labeled as **H^{b}**. There exists a narrow peak, singlet at δ = 2.15 ppm, corresponding to the six methyl protons from the mesitylene protecting groups labeled as **H^{c}**. Two conformations of monomer are possible due to the tautomerization. For the methylated monomer, there were significant peaks **(H^{d}, H^{d*})** (singlet at δ = 3.13 ppm), corresponding to the three methyl protons (Figure 3.1a). For the ethylated monomer, there were peaks **(H$^{d'}$)** in quartet at δ = 3.56 ppm and peaks **(H$^{e'}$)** in triplet at δ = 0.88 ppm, corresponding to the five ethyl protons (Figure 3.1b).

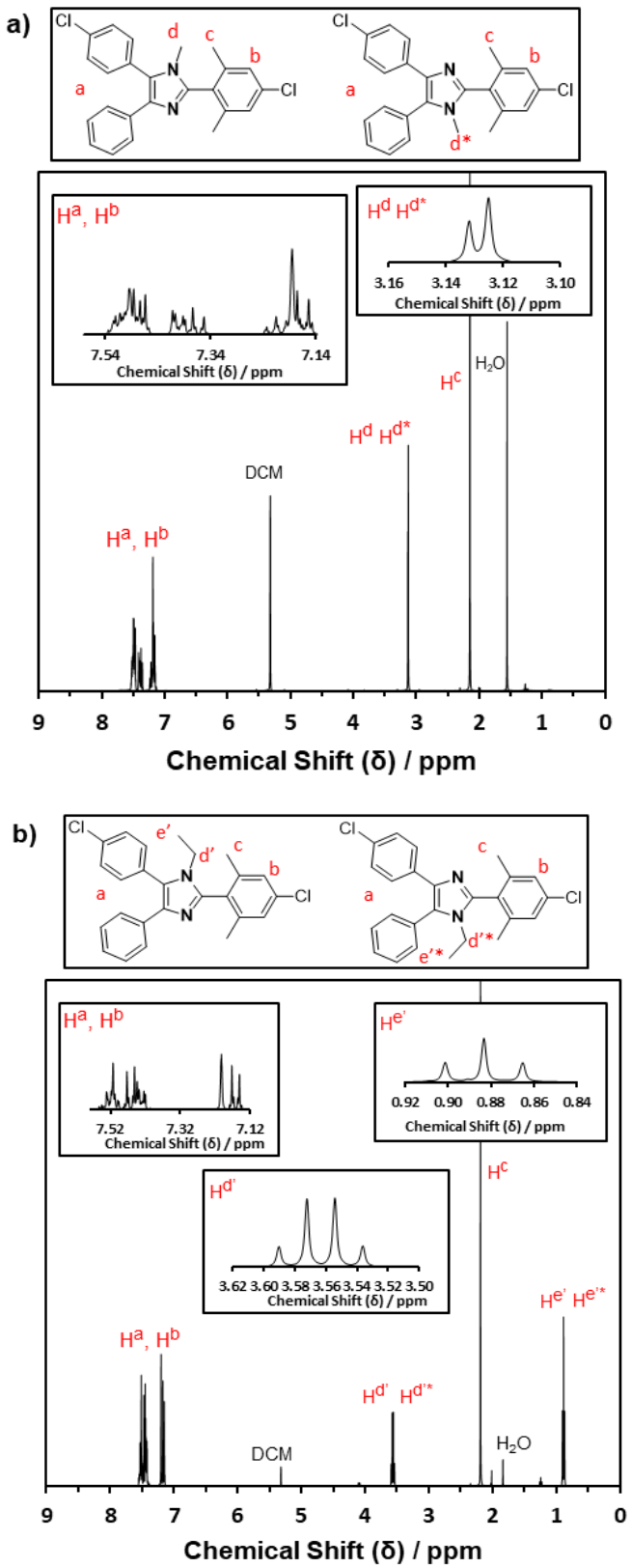

Figure 3.1. ***Two conformations of the methylated and ethylated monomers monomer and their ^{1}H NMR spectra.***

Yamamoto homo-polymerization was convenient because it required only one type of monomer, **(9)** or **(10)**, which showed great solubility in polar aprotic solvents, such as dimethylformamide (DMF) and N-methyl-2-pyrrolidone (NMP). The percentage yields of the polymerization decreased gradually from 96% to 92% as the length of alkyl side chain increased. A solvent mixture, methylene chloride, and dimethyl sulfoxide with volume ratio 1 to 1, was used for the full alkylation of the polymer because the mono-alkylated polymers **(11)** and **(12)** were soluble in methylene chloride; however, the full alkylated polymers **(13)** and **(14)** were soluble in dimethyl sulfoxide. The reaction conditions were varied from full methylation to full ethylation by increasing the temperature from 40 °C to 80 °C and extending the time from 48 hours to 72 hours. The percentage yields for both fully alkylation were approximately the same; 99% for full methylation, and 97% for full ethylation. The obtained molecular weight of PAIM-RR-1 was much higher than the originally reported HMT-PMPI. The Degree of Polymerization (DPn) for PAIM-MM-1 was 641 (M_w = 225300 g·mol^{-1}) with DPI 1.69, whereas, the Degree of Polymerization (DPn) for HMT-PMPI was 92 (M_w = 67000 g·mol^{-1}) with DPI 1.39. This proved that the Yamamoto homo-polymerization was successful in achieving higher molecular weight polymers. The UV absorbance was also measured through a PDA detector, PAIM-RR-1 possessed a maximum absorbance peak at 295 nm.

Remarkably, the PAIM-RR-1 ionic polymer showed excellent solubility in DMSO, which favored easy characterization of the polymer using ^{1}H NMR spectroscopy (Figure 3.2, DMSO-d_6 as NMR solvent). Similar to the ^{1}H NMR spectra of monomers, broad peaks **H^a** and **H^b** in multiplets between δ = 7.97 – 7.25 ppm were observed, corresponded to the eleven protons from the aromatic group. A peak **H^c** in doublet at δ = 2.43 ppm, attributed to the six protons from the two mesitylene methyl groups. For PAIM-MM, peaks **H^d** in multiplets between δ = 3.61 - 3.51 ppm, represented the methyl protons next to the nitrogen of imidazolium (-NCH_3^d). For PAIM-EE, a broad peak **H$^{d'}$** in singlet at δ = 3.80 ppm, expressed the methylene (-$NCH_2^{d'}$-) protons next to nitrogen of imidazolium. A narrow peak **H$^{e'}$** in doublet at δ = 0.90 ppm, corresponded to the methyl protons (-$CH_2CH_3^{e'}$) next to the methylene groups. As the length of alkylation increased, the chemical shifts of alkyl protons were further shielded or upfield, because the nucleus of protons experienced weaker magnetic fields when they were further away from the positively charged nitrogen of imidazolium.

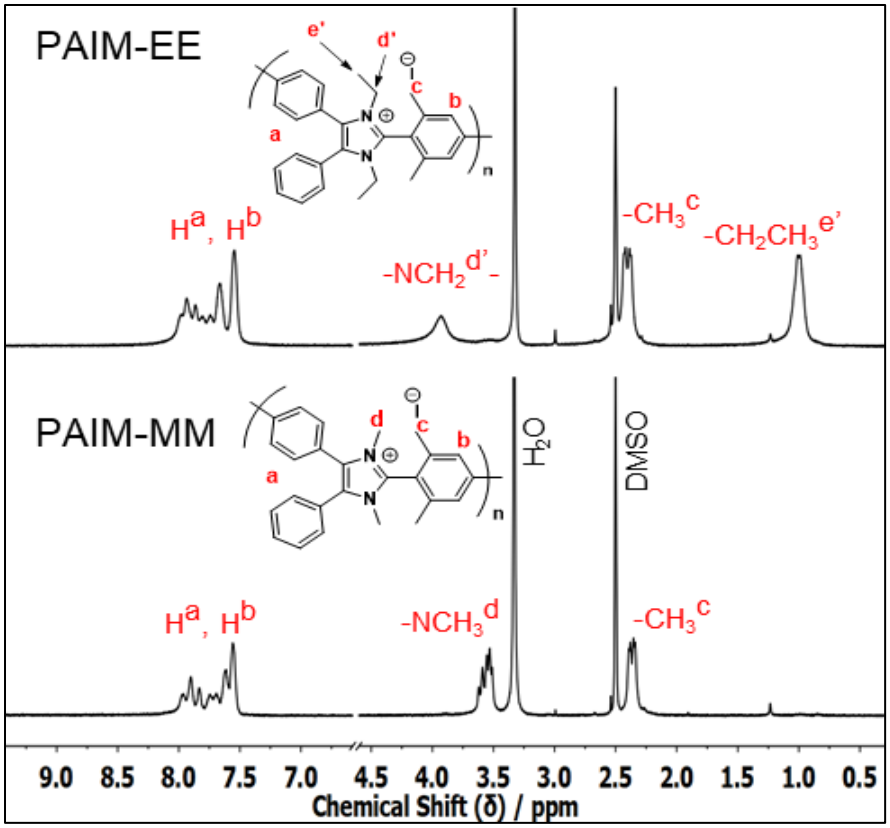

Figure 3.2. Stacked ^{1}H NMR spectra of PAIM-MM and PAIM-EE

Proton integration can be used to prove the degree of alkylation. For PAIM-MM, six-proton integration between 3.70 - 3.45 ppm proved the 100% degree of methylation because of the six methyl proton (2 × $-NCH_3{}^d$) on each imidazolium. The degree of methylation is specifically explained in section 3.3.1. For PAIM-EE, four-proton integration between 4.15 – 3.75 ppm and six-proton integration between 1.30 – 0.89 ppm proved the 100% degree of ethylation because of the four methylene protons (2 × $-NCH_2{}^{d'}-$) and six methyl protons (2 × $-CH_3{}^{e'}$) on each imidazolium. Besides, the polymers had a statistical configuration due to the asymmetric monomers. The obtained structure of the polymer was random on account of junctions. For instance, the head of the monomer can join with another head of the monomer, the tail of the monomer can join with another tail of the monomer, and the head of the monomer can join with the tail of another monomer, lead to the whole proton peaks appearing as multiplets in the ^{1}H NMR spectra (Figure 3.3).

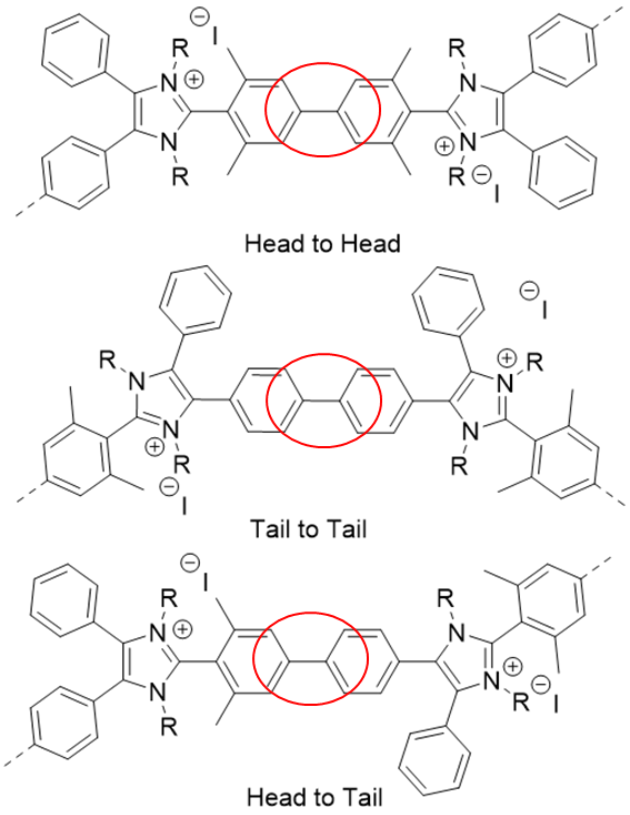

Figure 3.3. Head-to-head, tail-to-tail and head-to-tail conformations of the PAIM-RR-1

3.1.2. Attempted Synthesis of PAIM-RR-2, PAIM-RR-3, PAIM-RR-4

The synthetic route described above provided more potential ways to develop new PAIM-based polymers. The imidazolium cationic group may also be designed as a pendant group that is exposed from the hydrophobic polymer backbone. The conductivity may be greatly promoted by increasing the hydrophilic/hydrophobic phase separation because the imidazolium cationic group can interconnect and form narrow ionic channels to enhance the conductive network for ion transport. Based on dihalogenated monomer involved in Yamamoto homo-polymerization, the corresponding monomer structures of PAIM-RR-2, PAIM-RR-3, and PAIM-RR-4 were proposed and differentiated by the locations of halogen groups. The monomer PAIM-RR-2 possessed phenyl groups on the C4 and C5 positions of the imidazolium. Both of the halogen groups were on para positions with respect to C4 and C5 of imidazolium. PAIM-RR-3 monomer also had phenyl groups on C4 and C5 of imidazolium, but both of the halogen groups were on meta positions with respect to C4 and C5 of the imidazolium. By linking the ortho-carbons of the aromatics positioned at C4 and C5, a fused framework, PAIM-RR-4 monomer was proposed. PAIM-

RR-4 monomer may eliminate the significant distortion from the planarity, and the monomer may have good stability as a radical cation upon electro-oxidation.[67]

Three distinct di-chlorobenzil derivatives were prepared including 1,2-bis(4-chlorophenyl)ethane-1,2-dione, 1,2-bis(3-chlorophenyl)ethane-1,2-dione and 2, 7-dichlorophenanthrene-9, 10-dione for Debus-Radziszewski imidazole synthesis . ^{1}H and ^{13}C spectroscopy fully characterized these di-chlorobenzils. Both the 1,2-bis(4-chlorophenyl)ethane-1,2-dione, and 1,2-bis(3-chlorophenyl)ethane-1,2-dione were prepared through Sonogashira coupling with trimethylsilane (TMS) protection, deprotection by potassium carbonate, and second Sonogashira coupling, followed by the oxidation reaction. For the ^{1}H NMR spectrum of 1,2-bis(4-chlorophenyl)ethane-1,2-dione, peaks **H^{a}** and **H^{b}** represented eight protons from the aromatic group. The aromatic protons experienced two distinct environments due to the symmetric structure and there were four aromatic protons in each environment (Figure 3.4 a). For the ^{1}H NMR spectrum of 1,2-bis(3-chlorophenyl)ethane-1,2-dione, peaks **H^{a}**, **H^{b}**, **H^{c},** and **H^{d}** showed eight protons from aromatic groups. The aromatic protons experienced four distinct environments due to the symmetric structure, and there were two aromatic protons in each environment (Figure 3.4 b). 2,7-dichlorophenanthrene-9,10-dione was also successfully synthesized through chlorination of phenanthrene-9,10-dione with N-chlorosuccinimide (NCS) at acidic conditions. For the ^{1}H NMR spectrum of 2, 7-dichlorophenanthrene-9, 10-dione, peaks **H^{a}**, **H^{b}** and **H^{c}** expressed six protons from the aromatic group. The aromatic protons experienced three distinct environments due to the symmetric structure and there were two aromatic protons in each environment (Figure 3.4 c).

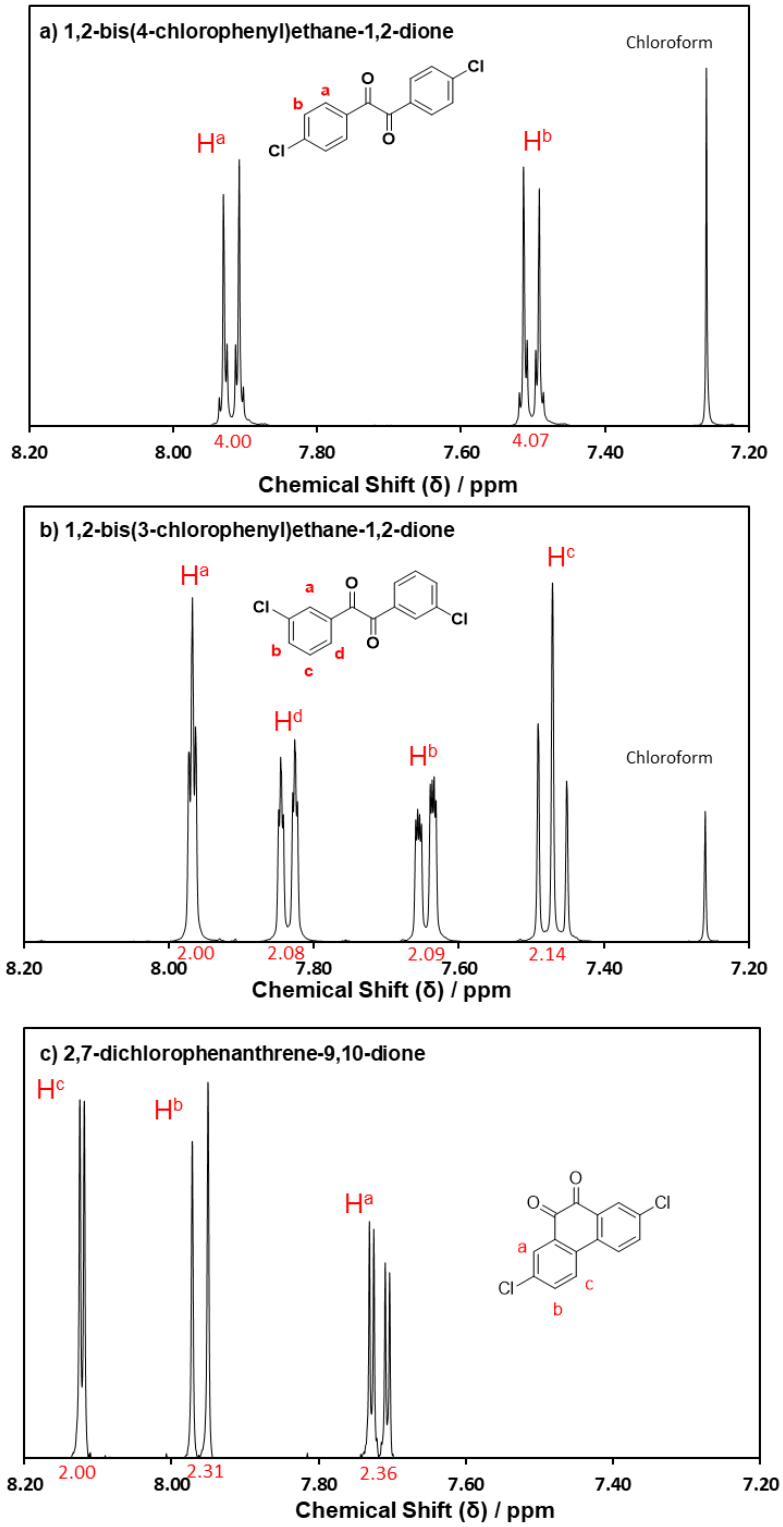

Figure 3.4. ***^{1}H NMR spectra (8.20 ppm to 7.20 ppm) of three benzils with chloride groups located at para and meta positions relative to the dicarbonyl, and with linking the ortho-carbons of the aromatics positioned at C4 and C5 (Proton positions assigned and proton integration are labeled in red)***

The imidazole monomers were then successfully synthesized by Debus-Radziszewski imidazole synthesis involving 2,4,6-trimethylbenzaldehyde, the di-chlorobenzil derivatives, and ammonium acetate.[64] However, the mono-methylation for PAIM-RR-3 were unsuccessful due to the solubility issue of the monomer in DMSO. Furthermore, they were fully characterized by ^{1}H and ^{13}C spectroscopy. For ^{1}H NMR spectrum of PAIM-RR-2 monomer, four distinct peaks in doublet, doublet, double and singlet between δ = 7.56 ppm - 6.96 ppm, corresponding to the ten protons from the aromatic group. A narrow peak **H^{a}** in singlet at δ = 3.13 ppm, represented three methyl protons next to nitrogen. There were also two narrow peaks **H^{b}** and **H^{c}** in singlet at δ = 2.36 ppm, 2.11 ppm, corresponded nine methyl protons from mesitylene protection groups (Figure 3.6a). For ^{1}H NMR spectrum of PAIM-RR-3 monomer, six distinct peaks in multiplets between δ = 7.76 ppm - 6.96 ppm, corresponded to the ten protons from the aromatic group. Similar to PAIM-RR-2 monomer, a narrow peak **H^{a}** in singlet at δ = 3.13 ppm, represented three methyl protons next to nitrogen. There were also two narrow peaks **H^{b}** and **H^{c}** in singlet at 2.36 ppm, and 2.11 ppm, attributed to the nine methyl protons from mesitylene protecting groups (Figure 3.6b). For the ^{1}H NMR spectrum of PAIM-RR-4 monomer without alkylation, there were five distinct peaks in triplet, doublet, doublet, doublet of triplet and singlet between δ = 8.80 ppm –7.00 ppm, attributed to the eight protons from the aromatic group. There was a peak **H^{a}** in singlet at δ = 2.39, represented nine methyl protons on mesitylene protection groups (Figure 3.6c).

Although the monomers of the designed PAIM-based polymers were successfully prepared, the synthesis of the desired high molecular weight polymers was unsuccessful. The obtained polymers possess low molecular weight so that they could not be cast as membranes. The Degree of Polymerization (DPn) for PAIM-RR-2 is 20 (M_w = 6900 g·mol^{-1}), and for PAIM-RR-3 is 15 (M_w = 5100 g·mol^{-1}). Confirmation of low molecular weight are also obtained by ESI mass spectrometry. In MS analyses, the relative abundance mass to charge ratio (m/Z) only account to four de-halogenated repeating units, as shown in Figure B11. In addition, PAIM-RR-3 could not be obtained by Yamamoto homo-polymerization due to the solubility issue of the monomer in the polar aprotic solvents, such as DMF, and DMAc, NMP, etc. Courageous conjectures were made for the low molecular weight of polymers, in particular, electronic effect, uneven electronic structures of imidazole were formed. Both halogen groups on C4 and C5 aromatic rings withdrew electron density away from imidazole, in another word, the polarizability was excessively

distributed on one side of imidazole, Comparing with PAIM-RR-1 monomer, even electronic structure of imidazole was obtained, one halogen group was on mesityl group with electron donating methyl groups and the other was on C4 or C5 aromatic that withdrew the electron density away from imidazole, in another word, the polarizability was moderately distributed around the imidazole.

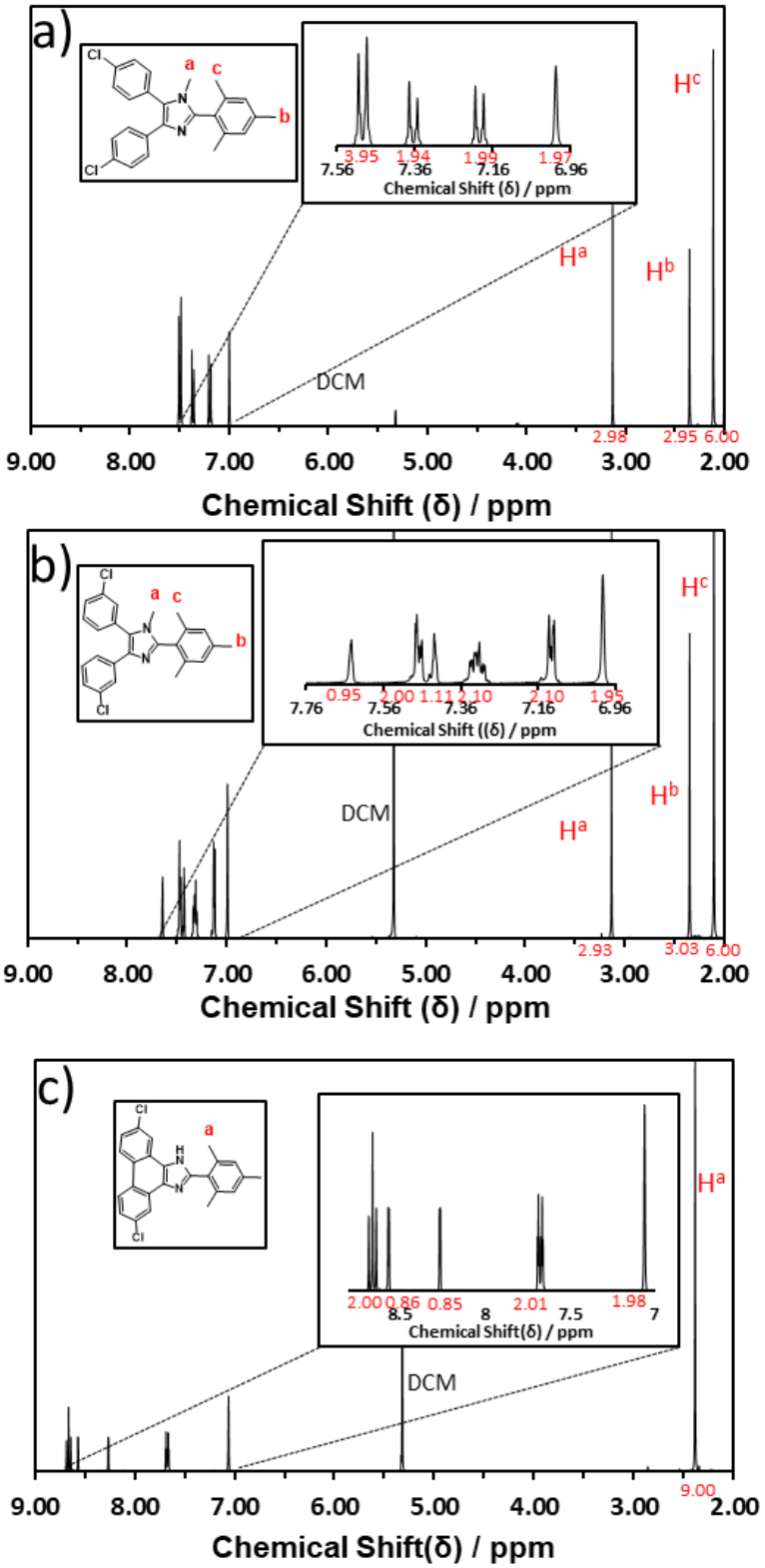

Figure 3.5. ***^{1}H NMR spectra (9.00 ppm to 2.00 ppm) of a) PAIM-RR-2, b) PAIM-RR-3 and c) PAIM-RR-3 monomers (Proton positions assigned and proton integration are labeled in red)***

3.2. Characterizations

3.2.1. Degree of Methylation

Membranes with degree of methylation 66%, 78%, 84%, 87%, 94%, 97% were prepared. The specific equivalent of methyl iodide, temperature, and range of time to achieve a certain degree of methylation were shown in Table A1. Specifically, the degree of methylation can reach to 84% when 20 equivalent of methyl iodide was added at room temperature for 18 hours, and the degree of methylation can reach 97% when 20 equivalent of methyl iodide was added, and the reaction was run at 40 °C for 48 hours.

The polymers were characterized by ^{1}H NMR (DMSO-d_6 as NMR solvent), the proton integration of the N-methyl resonances provided the quantification of the degree of methylation (dm), and the dm can be calculated by equation (1) (2.4.3). There were two distributed units in polymers as the degree of methylation increased, one unit is 50% dm imidazole (Figure 3.6, labeled in blue), and the other unit is 100% dm or fully methylated imidazolium (Figure 3.6, labeled in red).

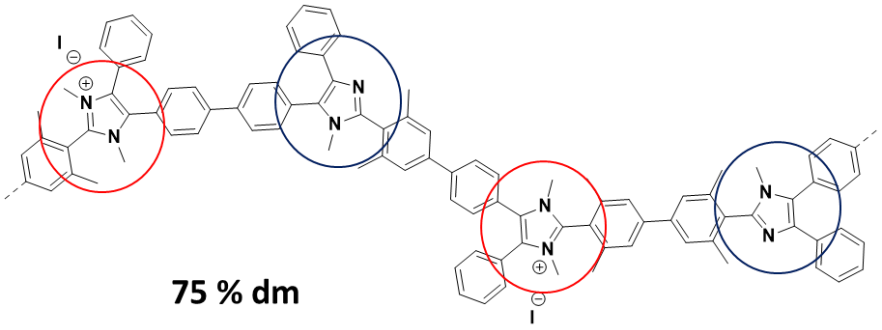

Figure 3.6. Two distributed units in the polymer as the degree of methylation increased (50% dm imidazole labeled in blue and 100% dm imidazolium labeled in red)

The stacked ^{1}H NMR spectrum of degree of methylation was obtained for analysis. In aromatic regions, as the degree of methylation increased, the two small peaks at δ = 7.26 ppm, 7.16 ppm gradually diminished. In methyl region, the peaks at δ =3.17 ppm, corresponding to the three methyl protons of imidazole, gradually diminished with increased peaks at δ =3.56 ppm. The peaks at δ =3.56 ppm corresponded to the six methyl protons of imidazolium (Figure 3.7). The downfield methyl proton peaks can be explained by the generated positive charged imidazolium, which is electron deficient. The positively charged imidazolium withdrew electron density away from the nuclei by induction and

conjugation, the nuclei experienced more external magnetic field, and therefore they were de-shielded. The protons experienced higher external magnetic field, and they need higher frequency to achieve resonance; therefore, the chemical shift shifted downfield (higher ppm).

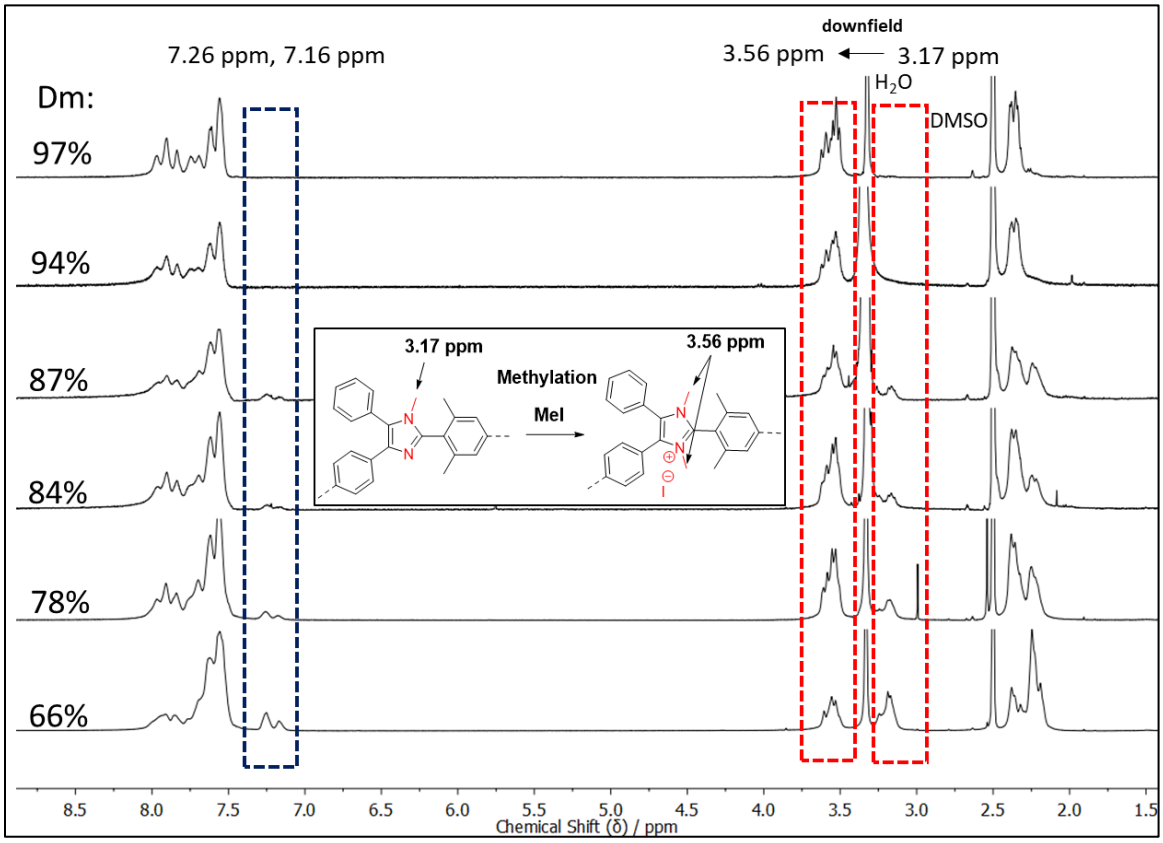

Figure 3.7. ***^{1}H NMR (400 MHz, DMSO-d6) spectra of diminished aromatic peaks labeled in blue and downfield methyl peaks label in red as the degree of methylation increased from 66% to 97%***

The PAIM-MM based AAEMs were fabricated via solution casting with the thickness thinner than 8 µm. All membranes with the degree of methylation greater than 84% were flexible and transparent after washing with water, 1 M KOH, and 1 M HCl solutions (Figure 3.8). Moreover, the membranes can be cut into the desired shape for further characterizations.

Figure 3.8. Colorless, flexible and transparent PAIM-MM (87 % dm) membrane

3.2.2. Ion Exchange Capacity, Water Uptake and Dimensional Swelling

The iodide form of the PAIM-MM membranes was exchanged to chloride form by the anion exchange process (2.4.1). Based on the degree of methylation, IEC_{cl^-} was obtained by equation (2) (2.4.4). The IEC_{cl^-} of PAIM-MM membranes increased from 0.54 $mmol \cdot g^{-1}$ to 2.45 $mmol \cdot g^{-1}$ when the degree of methylation increased from 62% to 97% (Figure 3.9). When the alkyl chain length increased from methyl to ethyl, the IEC_{cl^-} decreased from 2.58 $mmol \cdot g^{-1}$ to 2.40 $mmol \cdot g^{-1}$. Comparing solubility in water at 80 °C, fully methylated PAIM-MM membrane (IEC_{cl^-}: 2.58 $mmol \cdot g^{-1}$) yielded a better result than fully methylated HMT-PMBI membrane (IEC_{cl^-}: 2.97 $mmol \cdot g^{-1}$), because the fully methylated PAIM-MM membrane was not soluble in water at 80 °C due to the lower IEC_{cl^-}. Thus, PAIM-RR-1 with different degrees of methylation and ethylation can be prepared with desired IEC_{cl^-} targets (Table A1).

The ion exchange capacity affected water uptake and dimensional swelling of the membranes. When the IEC_{cl^-} increased from 0.54 $mmol \cdot g^{-1}$ to 2.45 $mmol \cdot g^{-1}$ as the degree of methylation increased, the water uptake of membranes increased from 3% to 32% (Figure 3.9). In opposite, the water uptake of membranes decreased from 32% to 26% and the dimensional swelling decreased from 13% to 10% when the length of alkyl side chain increased from methyl to ethyl. In addition, the hydration level (λ) of the methylated (λ =7) and the ethylated (λ =6) membranes difference by one under ambient conditions. As the ion exchange capacity increased, the imidazolium clusters turned larger, and the hydrophilic channel became more continuous. Both of them expanded the overall PAIM hydrophilic domain and consequently improved the water content associated properties.[33,79] Both the methylate and ethylated PAIM membranes show relatively small

water uptake and dimensional swelling in comparison with conventional quaternary ammonium based membranes, making them good candidates for fuel cell applications.[80]

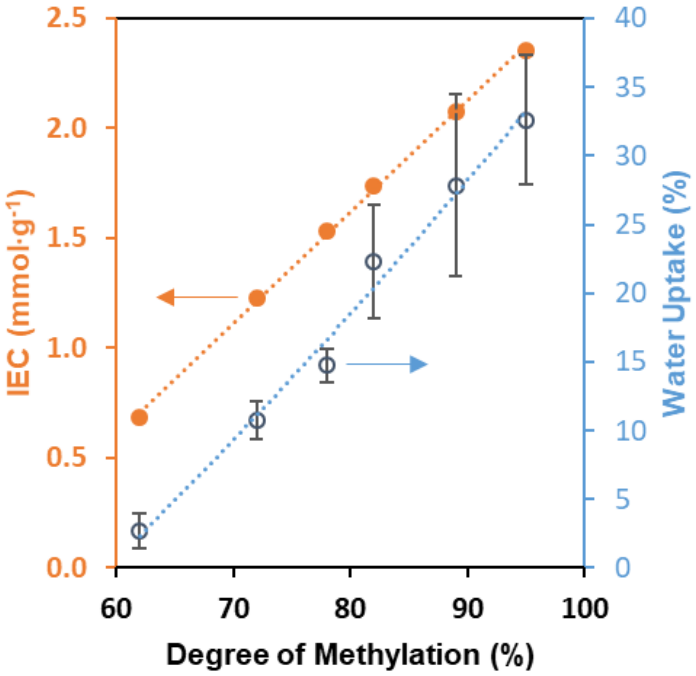

Figure 3.9. ***IEC_{Cl^-} and water uptake both increased with respect to the increased degree of methylation***

3.2.3. Chloride Ion Conductivity

The chloride ion conductivity of the membranes was measured in the fully hydrated condition at 23 °C (RT) unless specified otherwise. Considering the plot of chloride conductivity vs. degree of methylation (Figure 3.10), the chloride conductivity did not increase until the degree of methylation was greater than 82%. The ionic conductivity increased from 5 $mS \cdot cm^{-1}$ to 15 $mS \cdot cm^{-1}$ as the degree of methylation increased from 82% to 97% (figure 3.10). That is, as the degree of methylation increased, more cationic imidazolium were formed, which greatly facilitated the transport of chloride ions. However, for fully methylated HMT-PMPI, the chloride conductivity was 10 $mS \cdot cm^{-1}$.[56] By changing the alkyl side chain from methyl to ethyl, the ionic conductivity dropped from 15 $mS \cdot cm^{-1}$ to 10 $mS \cdot cm^{-1}$. The lower conductivity of the PAIM-EE membrane might be attributed to its lower ion exchange capacity and water uptake.

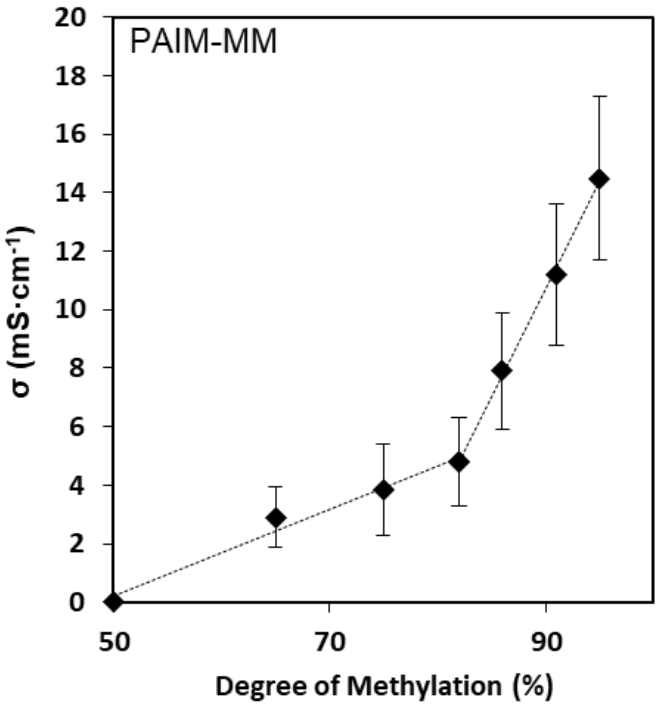

Figure 3.10. Chloride conductivity increased with respect to the increased degree of methylation

PAIM-EE membrane was chosen to explore more on its properties of chloride conductivity by changing the temperature at different relative humidity. The chloride conductivity of membrane increased with increased temperature at 95% relative humidity because the polymer created a more extensive free volume when the temperature increased.[81,82] The polymeric chains were more flexible, and the membrane absorbed more water at the higher temperature. A more swollen membrane structure and wider ion transferring channel, improved overall mobility of ions and polymer chains, consequently more favorable ion transfer.[83,84] Obviously, the ionic conductivity of the membrane also depended on the relative humidity, the results showed an exponential increase in humidity-dependent conductivity as relative humidity increased from 30% to 95% (Figure 3.11).

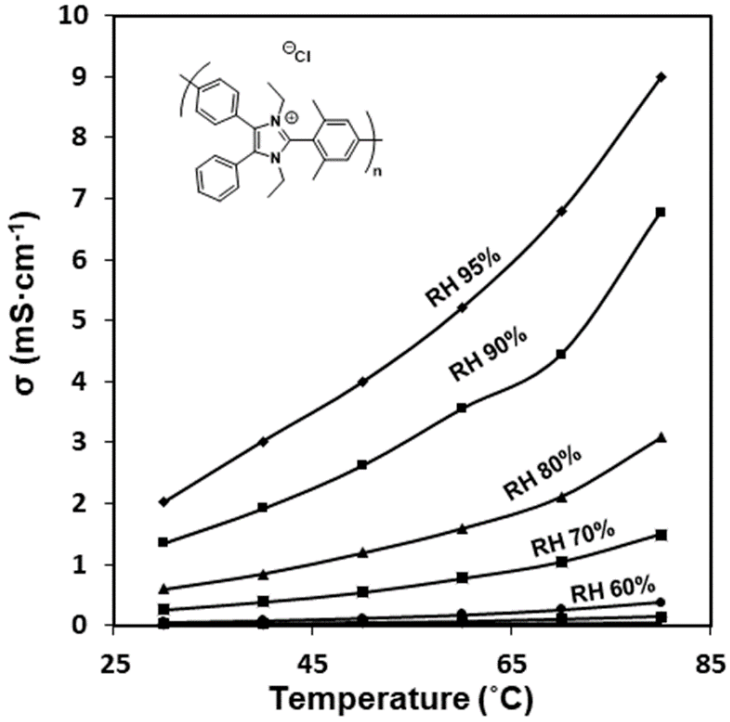

Figure 3.11. a) Chloride conductivity increases with increased temperature AND relative humidity (RH)

Arrhenius plots of chloride conductivity as a function of temperature at different relative humidity can be used to calculate the activation energy of ion transport (*Ea*). Activation energy represents the energy barrier for the anion migration from one point to another based on the Grotthuss mechanism.[72,73] As the Arrhenius equation (3.1),

$$log(\sigma) = \frac{-Ea \times 1000}{RT} \qquad (3.1)$$

The activation energy of ion transport (E_a) in kJ·mol^{-1} can be evaluated from equation $b = \frac{-E_a}{R}$, $E_a = -b \times \mathrm{R}$ that b is the slope of the linear regression (figure 3.12) of $log(\sigma)$ vs. $\frac{1000}{T}$. σ is ionic conductivity, and R is the gas constant (8.3145 J·K^{-1}·mol^{-1}).[27,87]

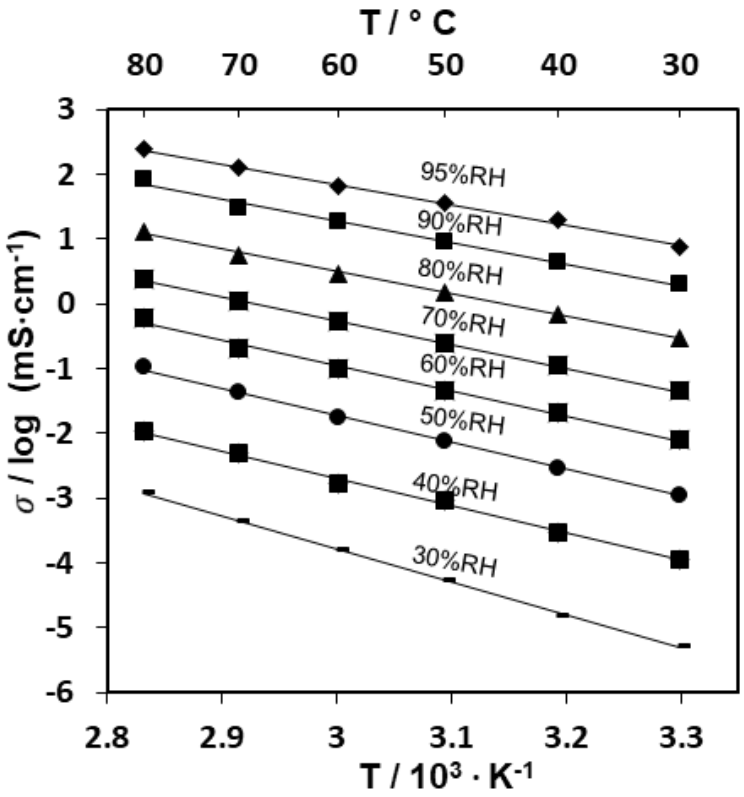

Figure 3.12. Arrhenius plot of chloride conductivity at different temperature AND relative humidity (RH)

The activation energies of PAIM-EE were calculated in the range from 26 to 44 kJ·mol^{-1}. By decreasing the relative humidity, the energy barrier for ion transport through the polymer increased. The membrane at the highest relative humidity (95%) had the lowest activation energy 25.9 kJ·mol^{-1}, which 25.9 kJ·mol^{-1} of activation energy was required for the chloride conduction (Figure 3.13). As the relative humidity decreased over the range from 95% to 30%, activation energy increased linearly (approximately 1.5 kJ·mol^{-1}) until the relative humidity declined to 40%. The activation energy increased dramatically from 35.2 kJ·mol^{-1} to 42.5 kJ·mol^{-1} (7.3 kJ·mol^{-1}) as the relative humidity decreased from 40% to 30%. This suggested that at RH < 40%, a change in the hydration level of the membrane caused a significant change in the activation of chloride transport for PAIM-EE.

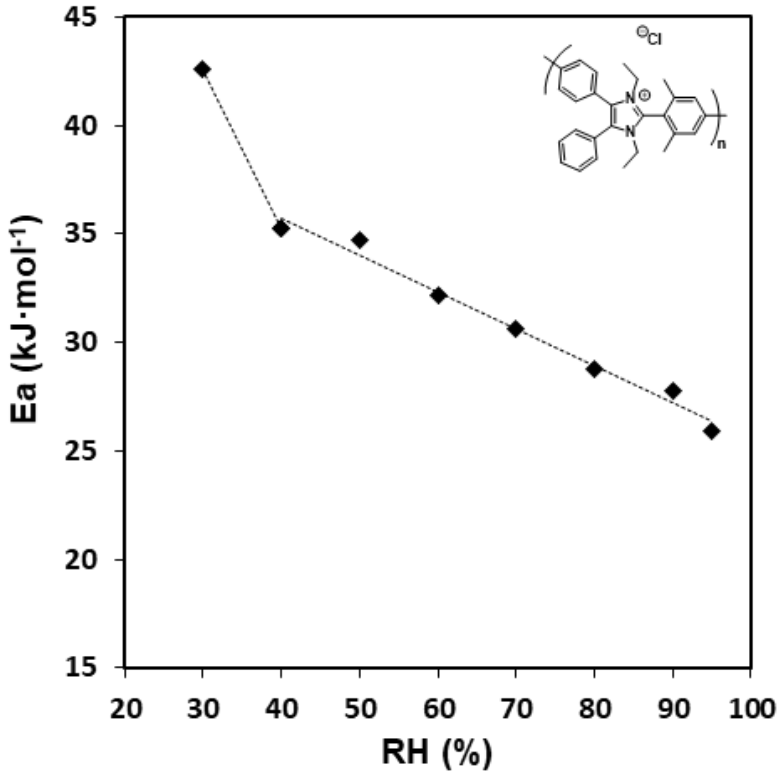

Figure 3.13. The corresponding calculated activation energy at a given relative humidity (RH)

3.2.4. Alkaline Stability

AEMs with long term stability under caustic conditions is critical for fuel cell applications. For PAIM-MM, all of the membranes became brittle and discolored from transparent colorless to pale yellow. As the concentration of the KOH solution increased, the physical degradation of the membranes appeared to be worse. There was no ring opening degradation because no amine protons as the ring opening degradation product were observed in the range of 4.00 ppm to 6.75 ppm. However, de-alkylation occurred, where the degradation peaks were at δ =7.26 ppm, 7.16 ppm, and 3.17 ppm. As the concentration of the KOH solution increased, two small aromatic peaks gradually appeared at δ = 7.26 ppm and 7.16 ppm. The peaks of methyl protons of imidazolium at δ = 3.56 ppm gradually upfield to δ = 3.17 ppm that corresponded to the methyl protons of imidazole (Figure 3.14). For PAIM-EE, all of the membranes were flexible except the membranes in 10 M KOH; all membranes were transparent without any discoloration. Similar to PAIM-MM membrane, there was no ring opening degradation because no amine protons peaks as the ring opening degradation product were observed in the range of δ =

4.00 ppm to 6.75 ppm. However, partial de-alkylation occurred, where the degradation peaks were at δ = 3.60 ppm, 3.20 ppm corresponding to the ethyl protons of imidazole (Figure A12).

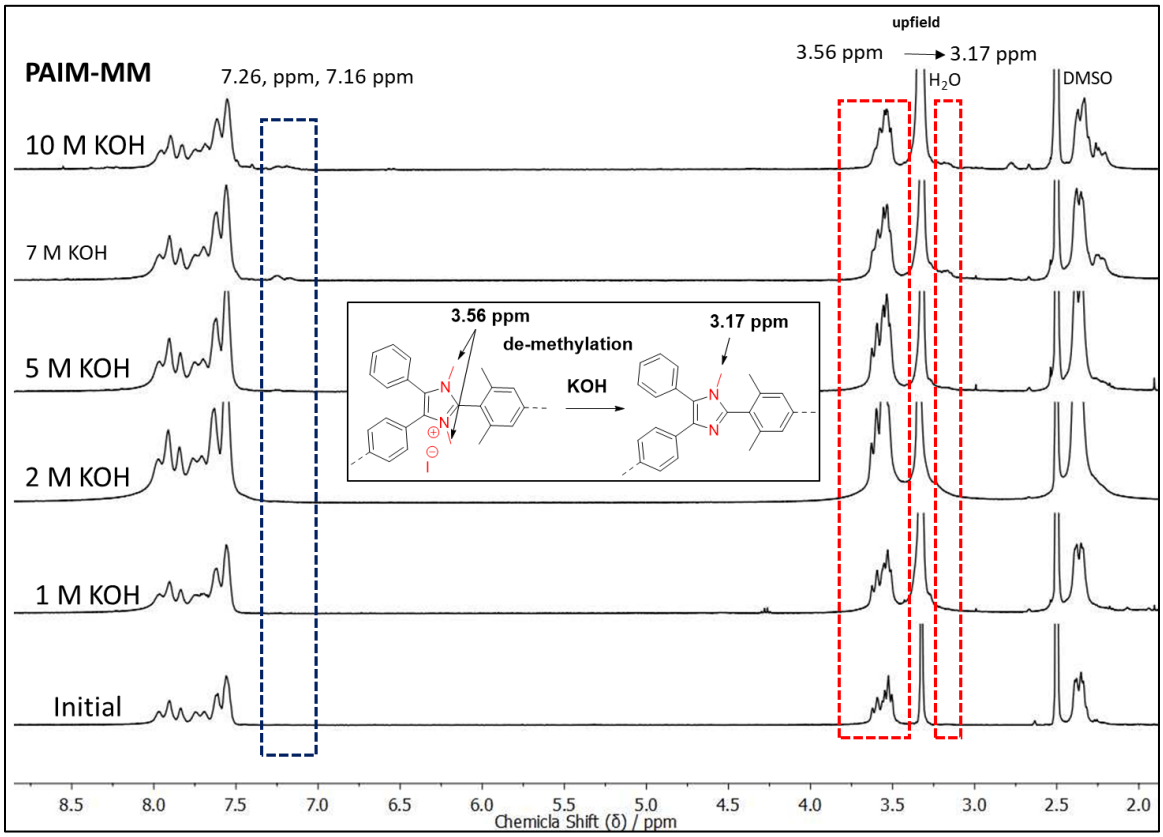

Figure 3.14. De-methylation degradation of PAIM-MM in different concentrations of KOH as aromatic peak appeared and methyl peaks upfield

The amount of imidazolium remaining in the membranes after exposure to different concentrations of KOH was calculated using the equation (7) (2.4.7). A plot of relative imidazolium remaining of PAIM-MM and PAIM-EE vs. concentration of KOH was obtained (Figure 3.15). For PAIM-MM, the relative imidazolium remaining was 92% in 1 M KOH, 91% in 2 M KOH, 90% in 5 M KOH, 89% in 7 M KOH and 87% in 10 M KOH at 80 °C for 168 hours. For PAIM-EE, the relative imidazolium remaining were 99% in 1 M KOH, 99% in 2 M KOH, 99% in 5 M KOH, 99% in 7 M KOH and 98% in 10 M KOH at 80 °C for 168 hours. Compared with PAIM-MM, PAIM-EE showed better alkaline stability in different concentrations of KOH at 80 °C for 168 hours, where the relative imidazolium remaining only decreased by 2% from the initial (100%) to 10 M KOH (98%). However, the relative imidazolium remaining of PAIM-MM decreased by 13% from the initial (100%) to 10 M KOH (87%). From the obtained results, the stability of PAIM-RR to a high caustic solution

was promoted with increased length of alkyl side chains from methyl to ethyl, the increased length of alkyl side chain does shield the positively charge nitrogen from the attack of a hydroxide ion and prevent the S_N2 degradation.

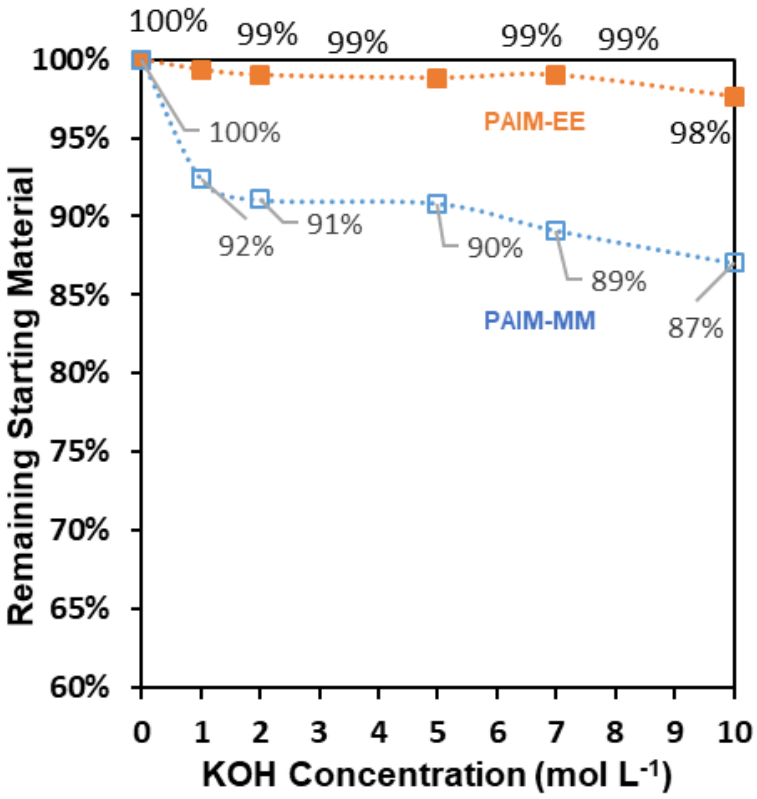

Figure 3.15. Relative imidazolium remaining of PAIM-MM and PAIM-EE at different concentrations of KOH

3.2.5. Mechanical Properties and Thermal Stability

AEMs must have adequate mechanical strength and durability for application in the fuel cell. A plot of stress vs. strain was obtained (Figure 3.16). For PAIM-MM membrane, tensile strength was 62 MPa, elongation at break was 32%, and Young's modulus was 966 MPa. For PAIM-EE membrane, tensile strength was 53 MPa, elongation at break was 47%, and Young's modulus was 883 MPa. Compared with PAIM-MM membrane, the tensile strength of PAIM-EE membrane decreased by 9 MPa with increased elongation at break by 15%. The values of Young's modulus for methylated and ethylated PAIM membranes were comparable. Moreover, compared with HMT-PMPI that had tensile strength 43.5 MPa and the elongation at break 44.3%, PAIM-EE membrane possesses higher tensile strength and approximately the same elongation at break.

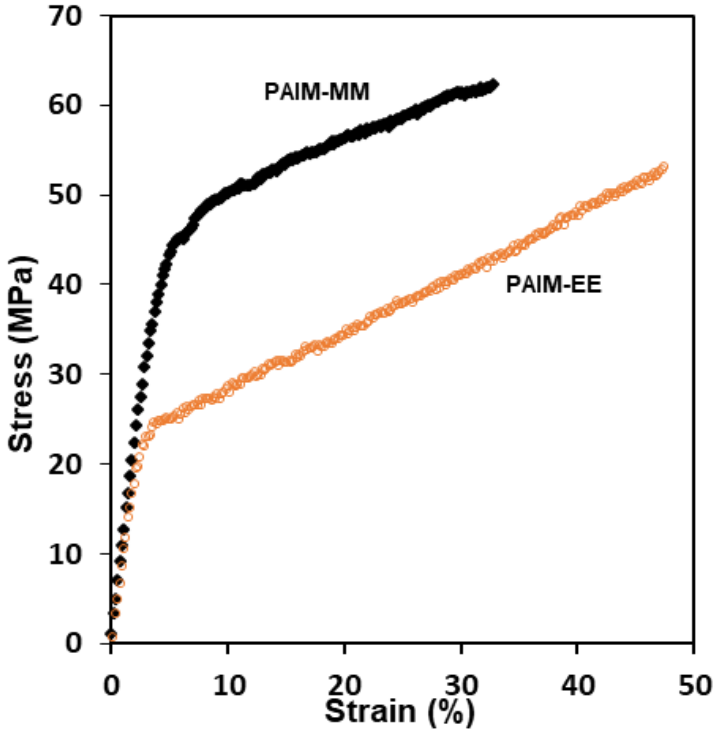

Figure 3.16. Stress versus strain for the dry PAIM-MM and PAIM-EE membranes

In order to form ionic conducting ionomer for use in a fuel cell, the thermal stability of the polymer must be investigated. A plot of weight percentage vs. temperature was obtained (Figure 3.17). Both of the membranes have the same thermal degradations until 190 °C because the membrane samples were preheated to remove the water and dimethyl sulfoxide absorbed. As the temperature increased, a two-step membrane degradation in chloride form was observed. The first 15% weight loss occurred from 200 °C to 320 °C, which represented the decomposition of imidazolium groups.[88] The second 72% weight loss occurred from 330 °C to 520 °C, which related to the thermal degradation of the polymer backbone, the break of carbon–nitrogen, and carbon-carbon bonds.

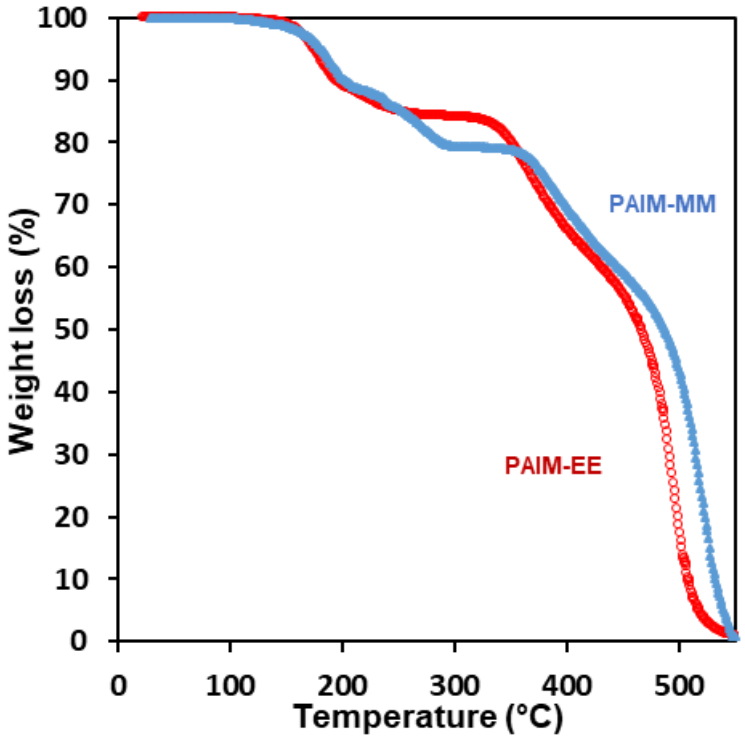

Figure 3.17. Two steps thermal degradation of PAIM-MM and PAIM-EE membranes

3.2.6. Data Summary

Table 3.1. Water uptake, swelling ratio, IEC, λ, and mechanical properties of PAIM-MM and PAIM-EE.

PAIM-RR	PAIM-MM	PAIM-EE
Water uptake (wt %)	32.6 ± 4.3	26.9 ± 3.3
Swelling (%)	13.0 ± 0.8	10.7 ± 0.9
IEC_{Cl^-}[a] (mmol · g^{-1})	2.58	2.41
λ[b]	7	6
σ_{Cl^-}[c] (mS · cm^{-1})	15.2 ± 4.3	9.82±3.26
Ts[d] (MPa)	62.3 ± 5.2	53.6 ± 7.5
Ea[e] (%)	32.1 ±10.7	47.3 ±6.4
Modulus[g] (MPa)	965 ± 132	883 ±151

Water uptake and swelling ratio of PAIM-RR are all measured in chloride form. [a] Theoretical ion exchange capacity of PAIM-RR. [b]Hydration level, [H2O]/[Cl-] molar ration, [c] Ionic conductivity of PAIM-RR in chloride form at 23 °C in water. [d] Tensile strength of PAIM-RR in chloride form in the dry state. [e] Elongation at break. [g] Young's modulus of PAIM-RR.

Chapter 4. Conclusion and Future Work

4.1. Conclusion

In this work, all four imidazolium monomers were synthesized, and PAIM-RR-1 with methyl and ethyl side chains were successfully obtained and cast as an anion exchange membrane. The PAIM-RR-1 found to have high molecular weight compared to HMT-PMPI, and the fully methylated PAIM-MM was discovered insoluble in water at 80 °C due to the lower IEC_{cl^-}. By adjusting the degree of methylation from 50% to 100%, the IEC_{cl^-} of PAIM-RR-1 can be easily altered from 0 $mmol \cdot g^{-1}$ to 2.58 $mmol \cdot g^{-1}$. By changing the alkyl side chain from methyl to ethyl, the IEC_{cl^-} of PAIM-RR-1 can be reduced from 2.58 $mmol \cdot g^{-1}$ to 2.41 $mmol \cdot g^{-1}$. The IEC_{cl^-} of PAIM-RR-1 affected the water uptake and dimensional swelling of membranes. The water uptake of methylated membranes increased from 3% to 32% as the IEC_{cl^-} raise from 0.91 $mmol \cdot g^{-1}$ to 2.45 $mmol \cdot g^{-1}$. As the alkyl side chain of PAIM-RR-1 changed from methyl to ethyl, the water uptake decreased from 32% to 26%, and the dimensional swelling also slightly dropped from 13% to 10%. The chloride conductivity of methylated membranes increased from 5 to 15 $mS \cdot cm^{-1}$ by increasing the degree of methylation from 82% to 97%. The chloride conductivity was suppressed from 15 $mS \cdot cm^{-1}$ to 10 $mS \cdot cm^{-1}$ by changing the alkyl side chain from methyl to ethyl. The ethylated PAIM-EE membrane showed better alkaline stability even in 10 M KOH and higher elongation at break at ambient condition compared with PAIM-MM. All of the properties of PAIM-RR-1 illustrate the PAIM materials are good candidates as an anion exchange membrane.

4.2. Future Work

Further study on alkaline stability of PAIM-RR-1 with propyl and butyl alkyl side chains might lead to a full picture of chemical degradation (Figure 4.1). Theoretically, the alkaline stability will be higher because by introducing longer length of alkyl side chain from methyl, ethyl groups to propyl, butyl groups, the steric hindrances are further enhanced by shielding the attack of neighbor hydroxide attack. Moreover, the alkaline stability test was performed in 168 hours interval. By extending the degradation time from 168 hours to 240 hours or even longer, the chemical degradation mechanism of PAIM-RR-1 will be fully explored. The degradation products can be further separated and

analyzed by the High-performance Liquid Chromatography (HPLC) and Mass Spectroscopy (MS).

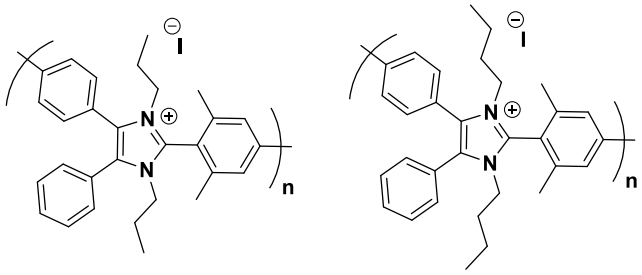

Figure 4.1. Propylated and butylated PAIM-RR-1

The Yamamoto co-polymerization of imidazolium monomer with 1,3-dichlorobenzene and 1,3,5-trichlorobenzene might also greatly promote the chemical and physical properties of membranes (Figure 4.2). Through the copolymerization, there is an introduction of benzene in the polymer backbone; theoretically, it improves the physical properties of the membranes. As the hydrophobicity of polymers was enhanced and the two adjacent imidazolium cations are further apart in the distance; theoretically, it also increased thermal and chemical stability of the membrane.[48,54]

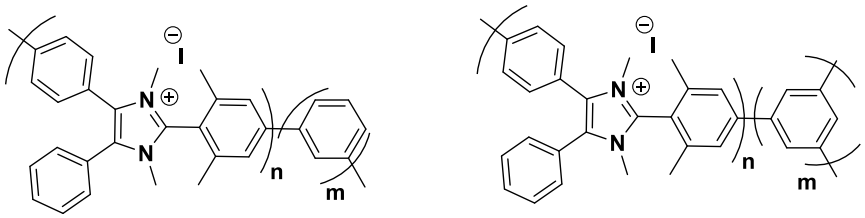

Figure 4.2. Yamamoto copolymerized with 1,3-dichlorobenzene and 1,3,5-trichlorobenzene

References

(1) Revankar, S. T.; Majumdar, P. *Fuel Cells: Principles, Design, and Analysis*; CRC Press, 2016.

(2) Fu, J.; Zhang, J.; Song, X.; Zarrin, H.; Tian, X.; Qiao, J.; Rasen, L.; Li, K.; Chen, Z. *Energy Environ. Sci.* **2016**, *9* (2), 663–670.

(3) Panwar, N. L.; Kaushik, S. C.; Kothari, S. *Energy Rev.* **2011**, *15* (3), 1513–1524.

(4) Larminie, J.; Dicks, A. *Fuel Cell Systems Explained*, 2nd ed.; J. Wiley: Chichester, West Sussex, 2003.

(5) Hassanzadeh, H.; Mansouri, S. H. *Efficiency of Ideal Fuel Cell and Carnot Cycle*; 2004.

(6) Wang, Y.-J.; Qiao, J.; Baker, R.; Zhang, *J. Chem. Soc. Rev.* **2013**, *42* (13), 5768.

(7) Howell, J. R.; Buckius, R. O. *Fundamentals of Engineering Thermodynamics*; McGraw-Hill Book Co.: New York, 1987.

(8) Qin, C.; Wang, J.; Yang, D.; Li, B.; Zhang, C. *Catalysts* **2016**, *6* (12), 197.

(9) Maurya, S.; Shin, S.-H.; Kim, Y.; Moon, S.-H. *RSC Adv.* **2015**, *5* (47), 37206–37230.

(10) Bhattacharya, P. K. *Directions* **2015**, *15* (1), 1-33.

(11) Shao, Y.; Yin, G.; Gao, Y. *J. Power Sources* **2007**, *171* (2), 558–566.

(12) Baschuk, J. J.; Li, X. Int. J*. Energy Res***. 2001**, *25* (8), 695–713.

(13) Merle, G.; Wessling, M.; Nijmeijer, K. *J. Membr. Sci.* **2011**, *377* (1–2), 1–35.

(14) Cao, Y.-C.; Wang, X.; Scott, K. *J. Power Sources* **2012**, *201*, 226–230.

(15) Chen, J.-C.; Chen, P.-Y.; Chen, H.-Y.; Chen, K.-H. *Polymer* **2018,** *141*, 143–153.

(16) Davies, D. P.; Adcock, P. L.; Turpin, M.; Rowen, S. J. *J. Appl. Electrochem*. **2000**, *30*, 101-105.

(17) Wind, J.; Späh, R.; Kaiser, W.; Böhm, G. *J. Power Sources* **2002**, *105* (2), 256–260.

(18) Varcoe, J. R.; Slade, R. C. T. *Fuel Cells* **2005**, *5* (2), 187–200.

(19) Couture, G.; Alaaeddine, A.; Boschet, F.; Ameduri, B. *Prog. Polym. Sci.* **2011**, *36* (11), 1521–1557.

(20) Hagesteijn, K. F. L.; Jiang, S.; Ladewig, B. P. *J. Mater. Sci.* **2018**, *53* (16), 11131–11150.

(21) Dekel, D. R. *J. Power Sources* **2018**, *375*, 158–169.

(22) Duan, Q.; Ge, S.; Wang, C.-Y. *J. Power Sources* **2013**, *243*, 773–778.

(23) Xu, T. *J. Membr. Sci.* **2005**, *263* (1–2), 1–29.

(24) Chen, J.; Li, C.; Wang, J.; Li, L.; Wei, Z. *J. Mater. Chem. A* **2017**, *5* (13), 6318–6327.

(25) Arges, C. G.; Wang, L.; Parrondo, J.; Ramani, V. *J. Electrochem. Soc.* **2013**, *160* (11), F1258–F1274.

(26) Gopi, K. H.; Peera, S. G.; Bhat, S. D.; Sridhar, P.; Pitchumani, S. *Int. J. Hydrog. Energy* **2014**, *39* (6), 2659–2668.

(27) Jeong, S.; Lee, J.; Woo, S.; Seo, J.; Min, B. *Energies* **2015**, *8* (7), 7084–7099.

(28) Deavin, O. I.; Murphy, S.; Ong, A. L.; Poynton, S. D.; Zeng, R.; Herman, H.; Varcoe, J. R. *Energy Environ. Sci*. **2012***, 5* (9), 8584.

(29) Sata, T.; Tsujimoto, M.; Yamaguchi, T.; Matsusaki, K. *J. Membr. Sci.* **1996**, *112* (2), 161–170.

(30) Stoica, D.; Ogier, L.; Akrour, L.; Alloin, F.; Fauvarque, J.-F. *Electrochimica Acta* **2007**, *53* (4), 1596–1603.

(31) Hibbs, M. R. *J. Polym. Sci. Part B Polym. Phys.* **2013**, *51* (24), 1736–1742.

(32) Jangu, C.; Long, T. E. *Polyme*r **2014**, *55* (16), 3298–3304.

(33) Yan, X.; Gu, S.; He, G.; Wu, X.; Zheng, W.; Ruan, X. *J. Membr. Sci*. **2014**, *466*, 220–228.

(34) Zhang, B.; Gu, S.; Wang, J.; Liu, Y.; Herring, A. M.; Yan, Y. *RSC Adv.* **2012**, *2* (33), 12683.

(35) Zha, Y.; Disabb-Miller, M. L.; Johnson, Z. D.; Hickner, M. A.; Tew, G. N. J. Am. Chem. Soc. 2012, 134 (10), 4493–4496.

(36) Ran, J.; Wu, L.; He, Y.; Yang, Z.; Wang, Y.; Jiang, C.; Ge, L.; Bakangura, E.; Xu, T. *J. Membr. Sci.* **2017**, *522*, 267–291.

(37) Varcoe, J. R.; Atanassov, P.; Dekel, D. R.; Herring, A. M.; Hickner, M. A.; Kohl, Paul. A.; Kucernak, A. R.; Mustain, W. E.; Nijmeijer, K.; Scott, K.; et al. *Energy Env. Sci* **2014**, *7* (10), 3135–3191.

(38) Liu, Y.; Wang, J.; Yang, Y.; Brenner, T. M.; Seifert, S.; Yan, Y.; Liberatore, M. W.; Herring, A. M. *J. Phys. Chem. C* **2014**, *118* (28), 15136–15145.

(39) Lin, B.; Dong, H.; Li, Y.; Si, Z.; Gu, F.; Yan, F. *Chem. Mater.* **2013**, *25* (9), 1858–1867.

(40) Lin, B.; Qiu, L.; Qiu, B.; Peng, Y.; Yan, F. *Macromolecules* **2011**, *44* (24), 9642–9649.

(41) Tao, R.; Simon, S. L. *J. Phys. Chem. B* **2015**, *119* (35), 11953–11959.

(42) Hou, H.; Sun, G.; He, R.; Wu, Z.; Sun, B. *J. Power Sources* **2008**, *182* (1), 95–99.

(43) Pérez-Prior, M. T.; Várez, A.; Levenfeld, B. *J. Polym. Sci. Part Polym. Chem*. **2015**, *53* (20), 2363–2373.

(44) Qiu, B.; Lin, B.; Qiu, L.; Yan, F. *J Mater Chem* **2012**, *22* (3), 1040–1045.

(45) Li, X.; Yu, Y.; Liu, Q.; Meng, Y. *Int. J. Hydrog. Energy* **2013**, *38* (25), 11067–11073.

(46) Ran, J.; Wu, L.; Varcoe, J. R.; Ong, A. L.; Poynton, S. D.; Xu, T. *J. Membr. Sci.* **2012**, *415–416*, 242–249.

(47) Hugar, K. M.; Kostalik, H. A.; Coates, G. W. *J. Am. Chem. Soc*. **2015**, *137* (27), 8730–8737.

(48) Wright, A. G.; Fan, J.; Britton, B.; Weissbach, T.; Lee, H.-F.; Kitching, E. A.; Peckham, T. J.; Holdcroft, S. *Energy Environ. Sci*. **2016**, *9* (6), 2130–2142.

(49) Long, H.; Pivovar, B. *J. Phys. Chem. C* **2014**, *118* (19), 9880–9888.

(50) Hibbs, M. R.; Fujimoto, C. H.; Cornelius, C. J. *Macromolecules* **2009**, *42* (21), 8316–8321.

(51) Gu, F.; Dong, H.; Li, Y.; Si, Z.; Yan, F. *Macromolecules* **2014**, *47* (1), 208–216.

(52) Thomas, O. D.; Soo, K. J. W. Y.; Peckham, T. J.; Kulkarni, M. P.; Holdcroft, S. *Polym. Chem*. **2011**, *2* (8), 1641.

(53) Thomas, O. D.; Soo, K. J. W. Y.; Peckham, T. J.; Kulkarni, M. P.; Holdcroft, S. *J. Am. Chem. Soc*. **2012**, *134* (26), 10753–10756.

(54) Wright, A. G.; Holdcroft, S. *ACS Macro Lett*. **2014**, *3* (5), 444–447.

(55) Saxer, S.; Marestin, C.; Mercier, R.; Dupuy, *J. Polym. Chem*. **2018**, *9* (15), 1927–1933.

(56) Fan, J.; Wright, A. G.; Britton, B.; Weissbach, T.; Skalski, T. J. G.; Ward, J.; Peckham, T. J.; Holdcroft, S. *ACS Macro Lett*. **2017**, *6* (10), 1089–1093.

(57) Yamamoto, T.; Uemura, T. *J. Polym. Sci. Part Polym. Chem*. **2002**, *40* (15), 2686–2688.

(58) Schmidt, J.; Werner, M.; Thomas, A. *Macromolecules* **2009**, *42* (13), 4426–4429.

(59) Dierschke, F.; Müllen, K. *Macromol. Chem. Phys*. **2007**, *208* (1), 37–43.

(60) Yamamoto, T.; Koizumi, T. *Polymer* **2007**, *48* (19), 5449–5472.

(61) Grigalevicius, S.; Ma, L.; Qian, G.; Xie, Z.; Forster, M.; Scherf, U. *Macromol. Chem. Phys.* **2007**, *208* (4), 349–355.

(62) Asawapirom, U.; Scherf, U. *Macromol. Rapid Commun*. **2001**, *22*, 746-749.

(63) Grünberg, M. F.; Gooßen, L. J. *Chem. - Eur. J*. **2013**, *19* (23), 7334–7337.

(64) Boominathan, S. S. K.; Chen, C.-Y.; Huang, P.-J.; Hou, R.-J.; Wang, J.-J. *New J. Chem.* **2015**, *39* (9), 6914-6918.

(65) Mio, M. J.; Kopel, L. C.; Braun, J. B.; Gadzikwa, T. L.; Hull, K. L.; Brisbois, R. G.; Markworth, C. J.; Grieco, P. A. *Org. Lett.* **2002**, *4* (19), 3199–3202.

(66) Vo, T. H.; Shekhirev, M.; Kunkel, D. A.; Orange, F.; Guinel, M. J.-F.; Enders, A.; Sinitskii, A. *Chem Commun* **2014**, *50* (32), 4172–4174.

(67) Francke, R.; Little, R. D. *J. Am. Chem. Soc*. **2014**, *136* (1), 427–435.

(68) Reich, H. J.; Green, D. P.; Phillips, N. H.; Borst, J. P. *Phosphorus, Sulfur, and Silicon* **1992**, *76*, 3-97.

(69) Bailey, W. F.; Luderer, M. R.; Uccello, D. P.; Bartelson, A. L. *J. Org. Chem*. **2010**, *75* (8), 2661–2666.

(70) Sharma, G. V. M.; Jyothi, Y.; Lakshmi, P. S. *Synth. Commun*. **2006**, *36* (20), 2991–3000.

(71) Chinchilla, R.; Nájera, C. *Chem. Soc. Rev*. **2011**, *40* (10), 5084.

(72) Park, K.; Bae, G.; Moon, J.; Choe, J.; Song, K. H.; Lee, S. *J. Org. Chem*. **2010**, *75* (18), 6244–6251.

(73) Lee, D. G.; Chang, V. S. *J. Org. Chem*. **1979**, *44* (15), 2726–2730.

(74) Miao, Y.; Dupé, A.; Bruneau, C.; Fischmeister, C. Eur*. J. Org. Chem*. **2014**, *2014* (23), 5071–5077.

(75) Rihter, B.; SriHari, S.; Hunter, S.; Masnovi, J. *J. Am. Chem. Soc*. **1993**, *115* (10), 3918–3924.

(76) Li, P.; Cheong, F. H.; Chao, L. C. F.; Lin, Y. H.; Williams, I. D. *J. Mol. Catal. Chem.* **1999**, *145* (1–2), 111–120.

(77) Rogatchov, V.; Filimonov, V.; Yusubov, M. *Synthesis* **2004**, *2001* (07), s-2001-14558.

(78) Nagarapu, L.; Apuri, S.; Kantevari, S. J. *Mol. Catal. Chem*. **2007**, *266* (1–2), 104–108.

(79) Jheng, L.; Hsu, S. L.; Lin, B.; Hsu, Y. *J. Membr. Sci*. **2014**, *460*, 160–170.

(80) Iravaninia, M.; Azizi, S.; Rowshanzamir, S. *Iran. J. Hydrog. Fuel Cell* **2015**, *2* (1).

(81) Lin, B.; Xu, F.; Chu, F.; Ren, Y.; Ding, J.; Yan, F. *J. Mater. Chem. A* **2019**, *7* (21), 13275–13283.

(82) Huang, X. L.; Lin, C. X.; Hu, E. N.; Soyekwo, F.; Zhang, Q. G.; Zhu, A. M.; Liu, Q. L. *RSC Adv*. **2017**, *7* (44), 27342–27353.

(83) Wang, J.; Li, S.; Zhang, S. *Macromolecules* **2010**, *43* (8), 3890–3896.

(84) Lin, B.; Qiu, L.; Lu, J.; Yan, F. *Chem. Mater*. **2010**, *22* (24), 6718–6725.

(85) Schmidt-Rohr, K.; Chen, Q. *Nat. Mater*. **2008**, *7* (1), 75–83.

(86) Choi, P.; Jalani, N. H.; Datta, R. *J. Electrochem. Soc*. **2005**, *152* (3), E84-E89.

(87) Guo, M.; Fang, J.; Xu, H.; Li, W.; Lu, X.; Lan, C.; Li, K. *J. Membr. Sci*. **2010**, *362* (1–2), 97–104.

(88) Ngo, H. L.; LeCompte, K.; Hargens, L.; McEwen, A. B. *Thermochim. Acta* **2000**, *357–358*, 97–102.

Appendix A. Supporting information for PAIM-RR-1

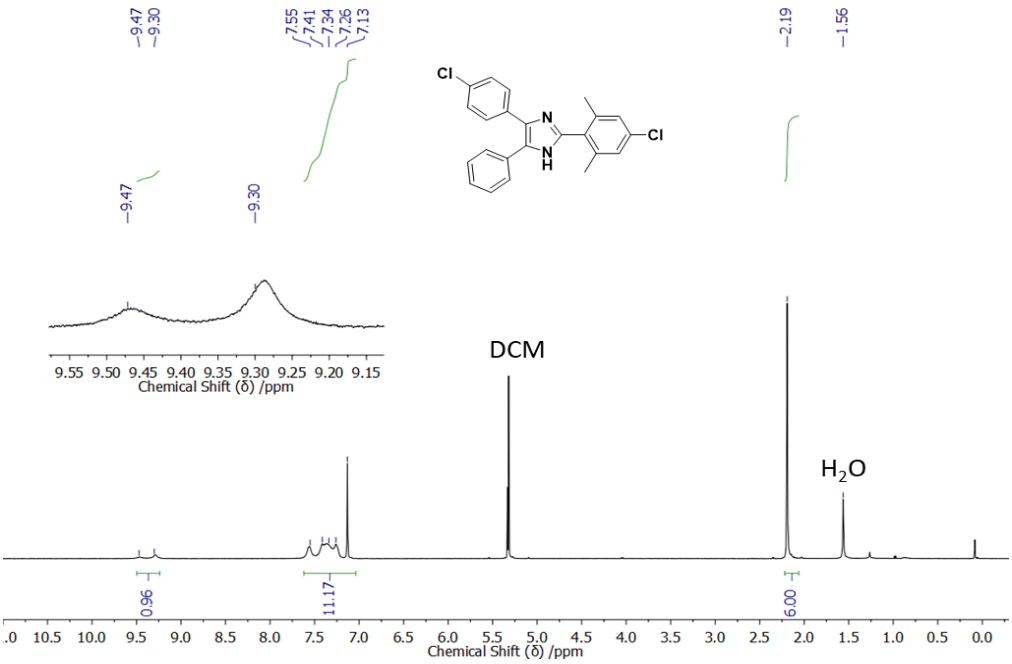

Figure A1. ***^{1}H NMR spectrum (400 MHz, CD_2Cl_2-d_2) of 2-(4-chloro-2,6-dimethylphenyl)-4-(4-chlorophenyl)-5-phenyl-1H-imidazole***

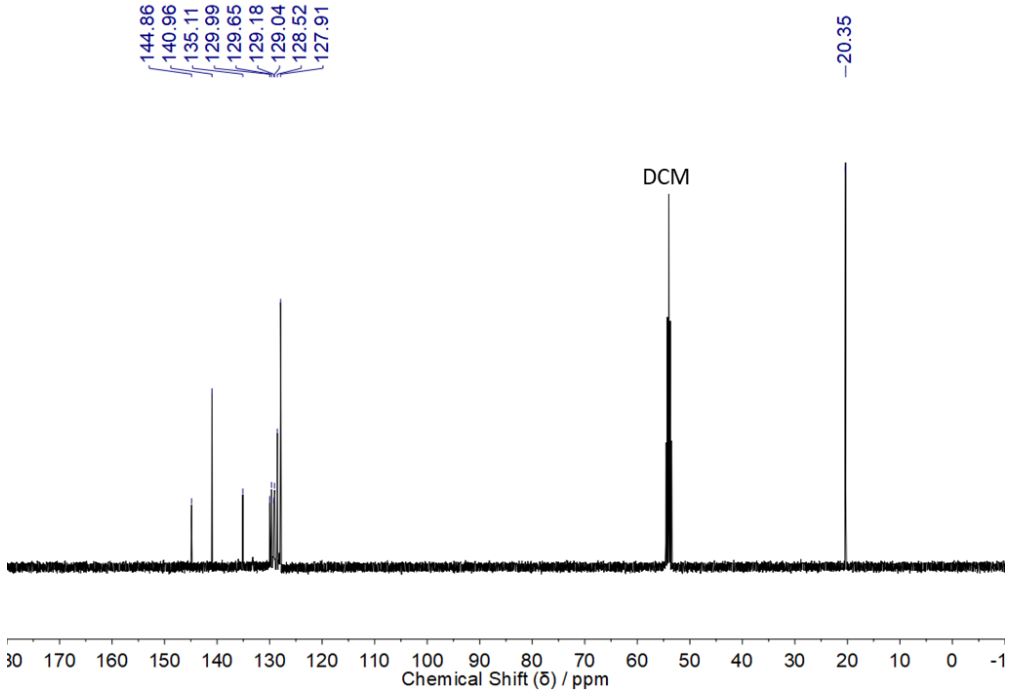

Figure A2. ***^{13}C NMR spectrum (125 MHz, CD_2Cl_2-d_2) of 2-(4-chloro-2,6-dimethylphenyl)-4-(4-chlorophenyl)-5-phenyl-1H-imidazole***

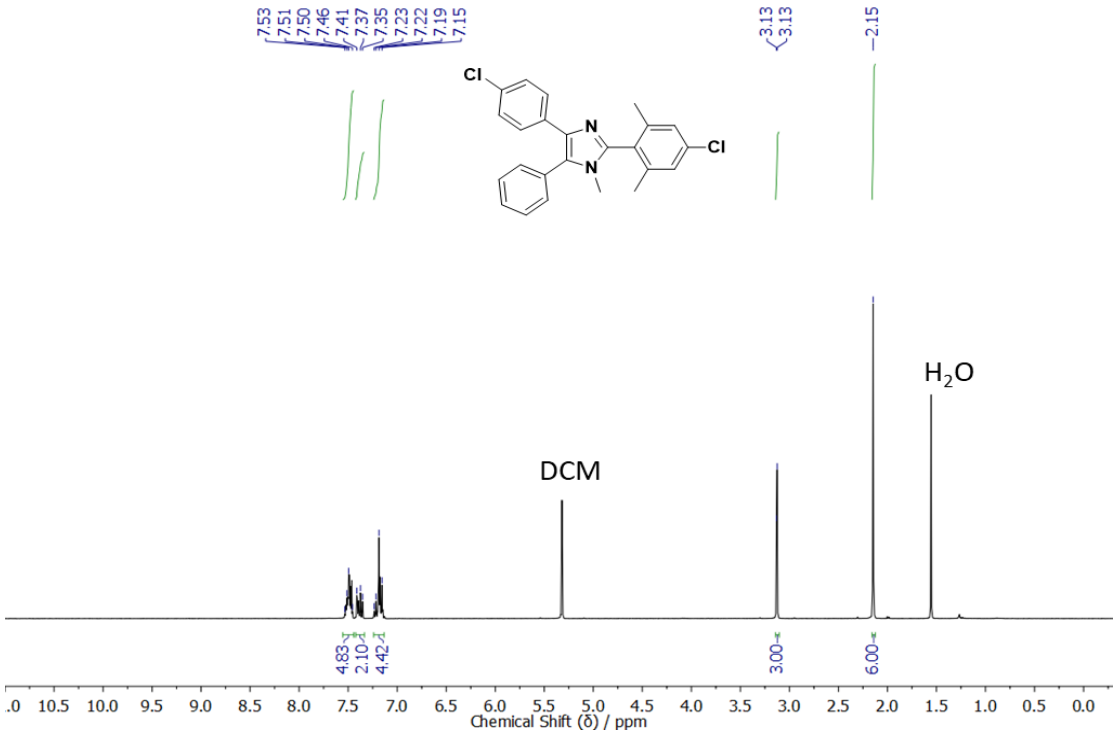

Figure A3. ***^{1}H NMR spectrum (400 MHz, CD_2Cl_2-d_2) of 2-(4-chloro-2,6-dimethylphenyl)-4-(4-chlorophenyl)-1-methyl-5-phenyl-1H-imidazole***

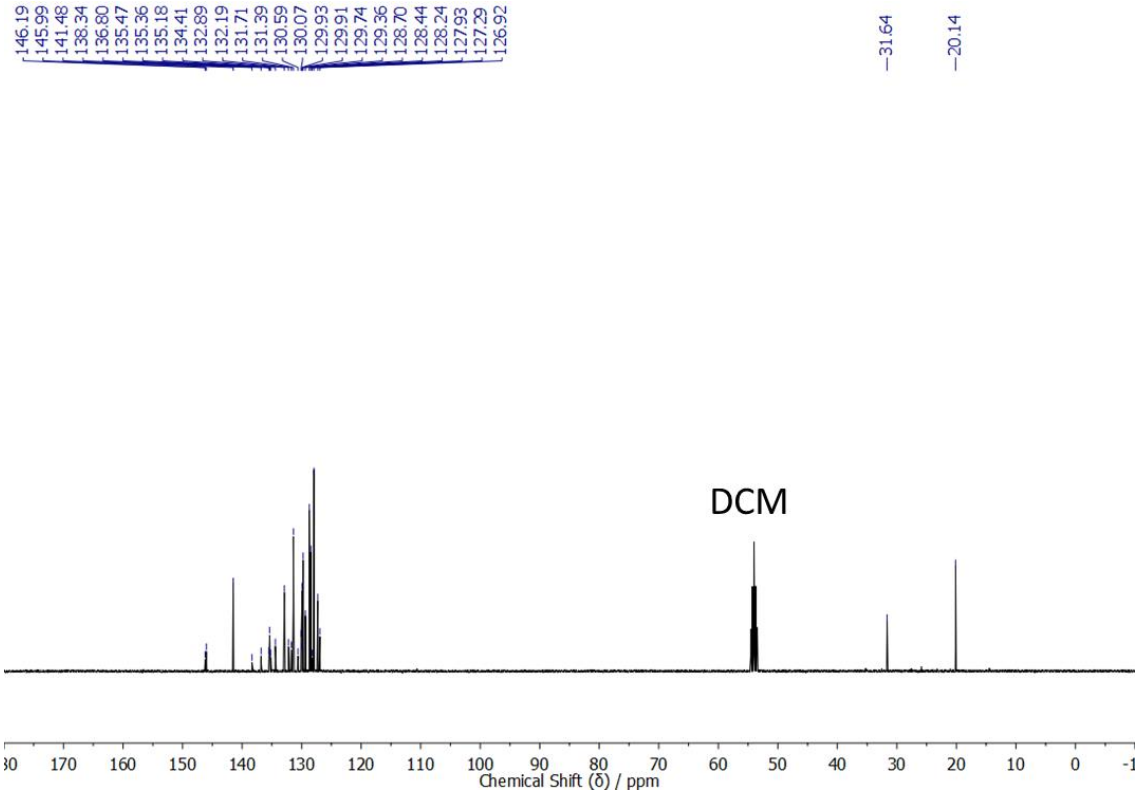

Figure A4. ***^{13}C NMR spectrum (125 MHz, CD_2Cl_2-d_2) of 2-(4-chloro-2,6-dimethylphenyl)-4-(4-chlorophenyl)-1-methyl-5-phenyl-1H-imidazole***

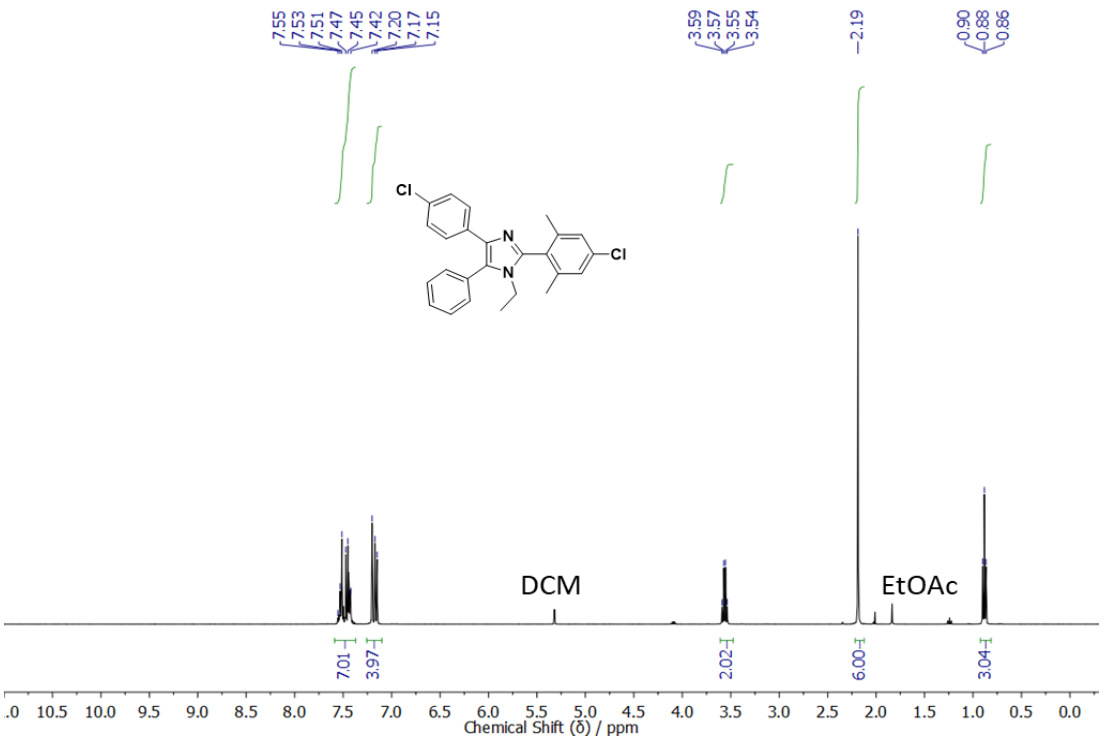

Figure A5. ***^{1}H NMR spectrum (400 MHz, CD_2Cl_2-d_2) of 2-(4-chloro-2,6-dimethylphenyl)-4-(4-chlorophenyl)-1-ethyl-5-phenyl-1H-imidazole***

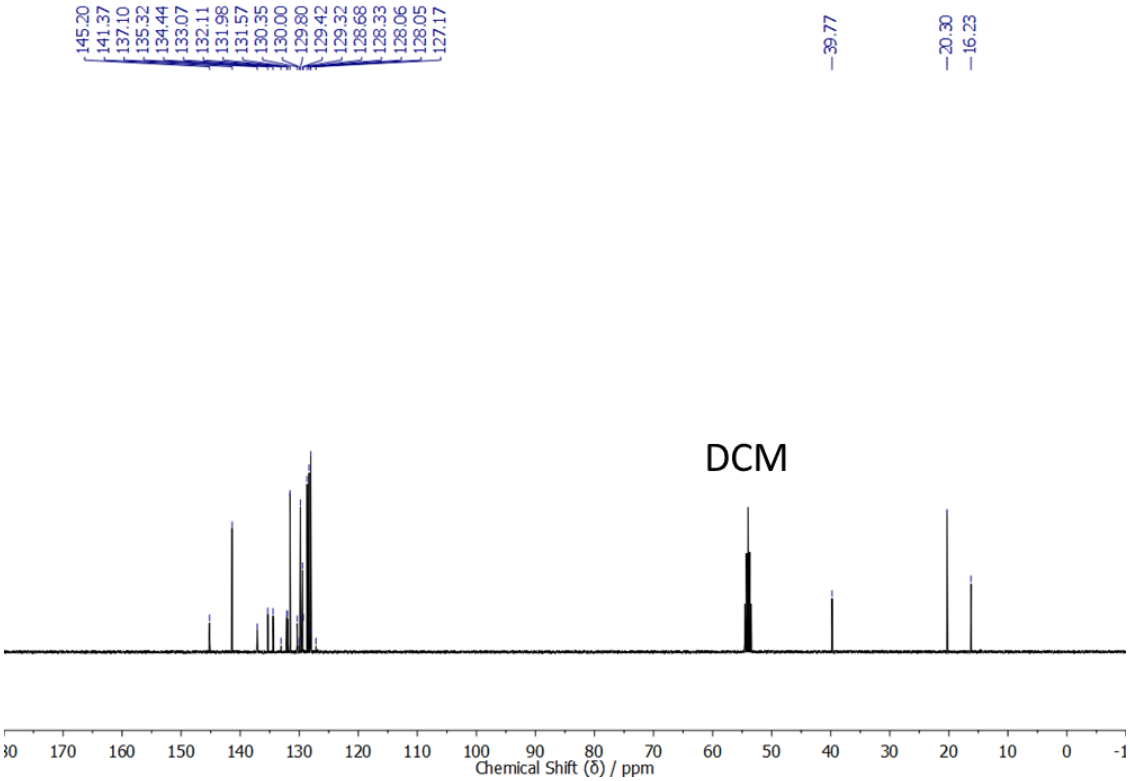

Figure A6. ***^{13}C NMR spectrum (125 MHz, CD_2Cl_2-d_2) of 2-(4-chloro-2,6-dimethylphenyl)-4-(4-chlorophenyl)-1-ethyl-5-phenyl-1H-imidazole***

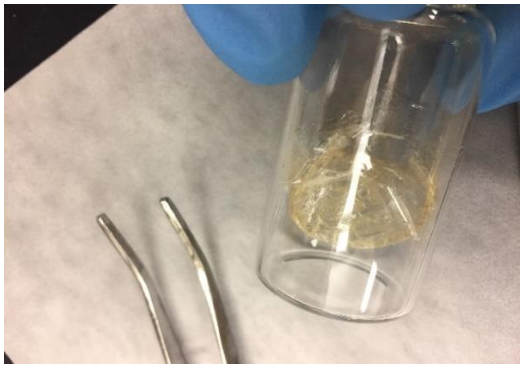

Figure A7. ***PAIM-MX polymer formed as membrane after evaporation of methylene chloride***

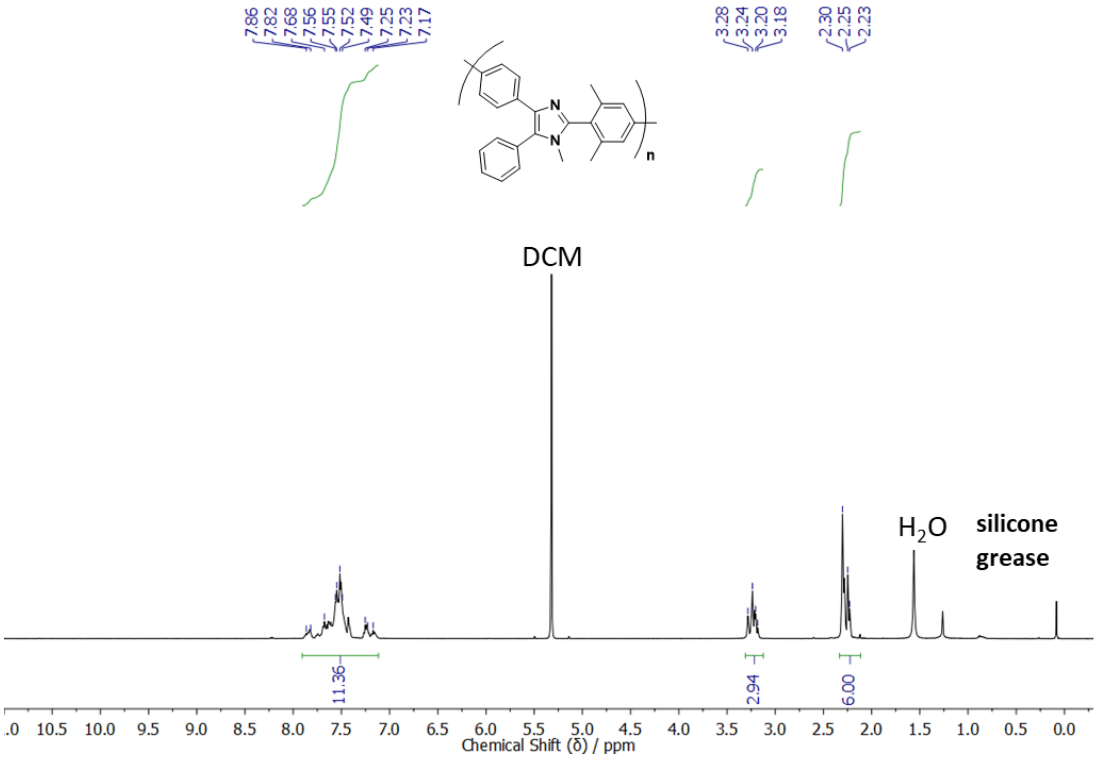

Figure A8. ***^{1}H NMR spectrum (400 MHz, CD_2Cl_2-d_2) of PAIM-MX polymer***

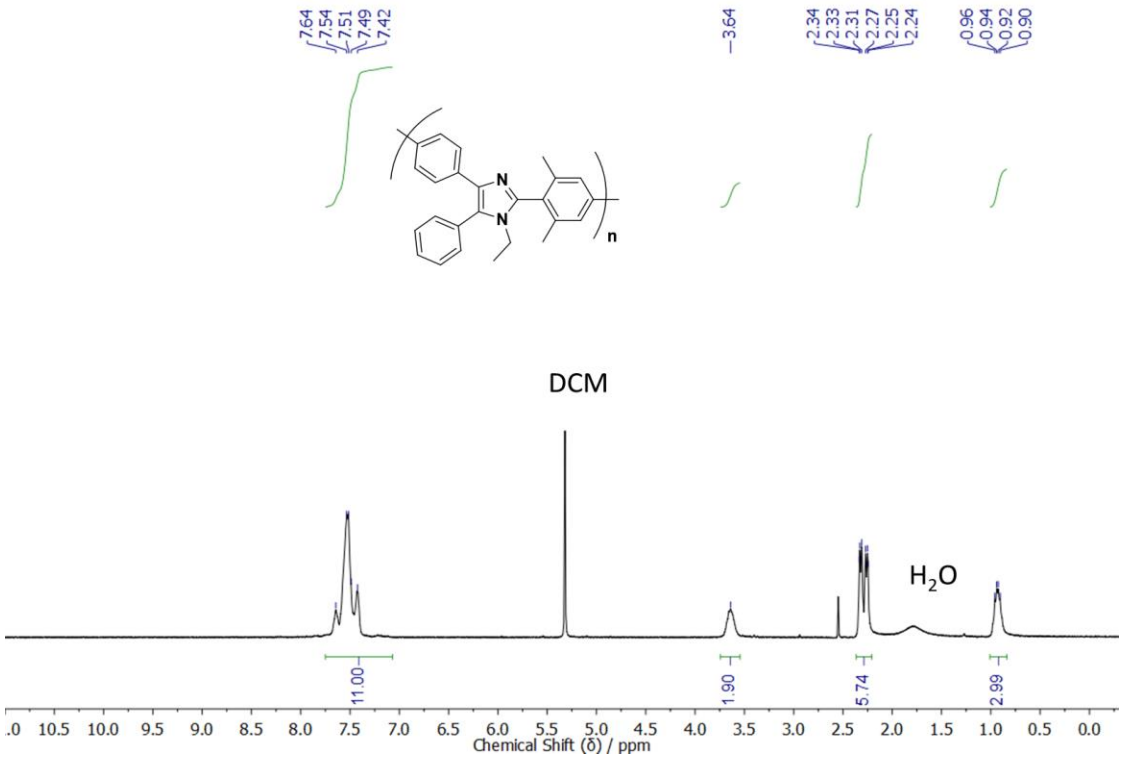

Figure A9. ***^{1}H NMR spectrum (400 MHz, CD_2Cl_2-d_2) of PAIM-EX polymer***

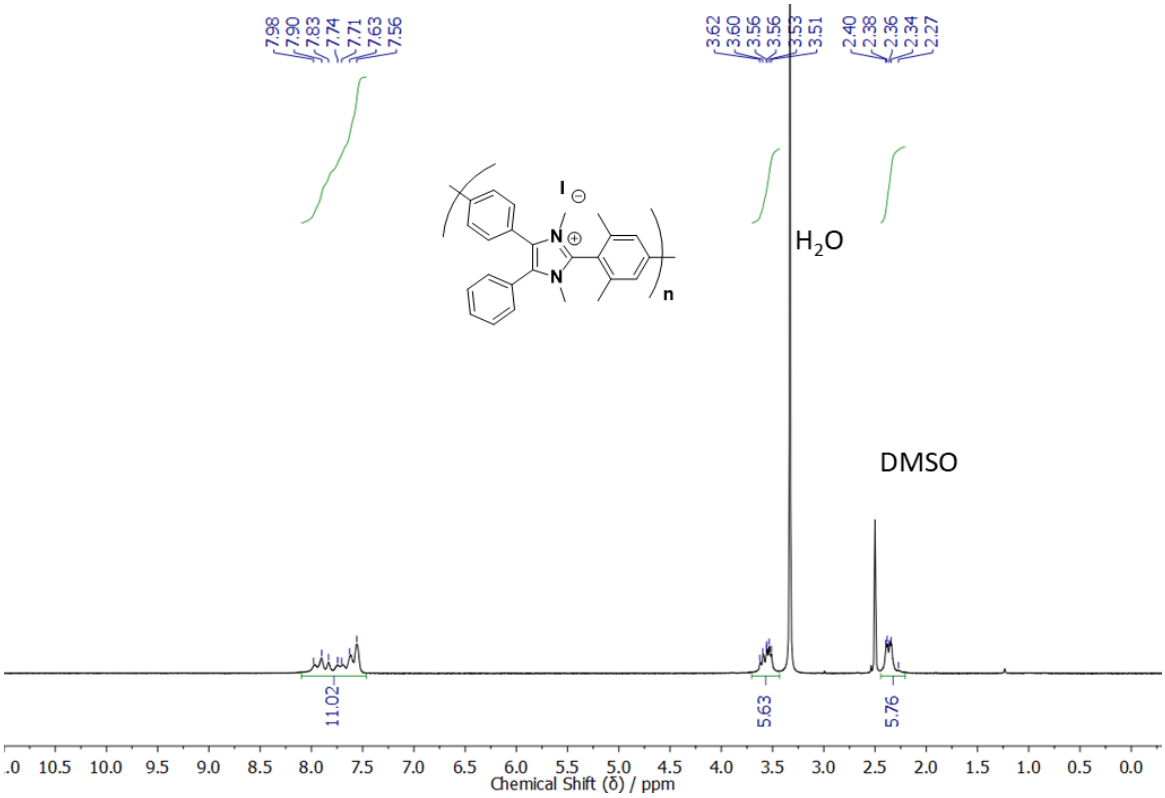

Figure A10. ***^{1}H NMR spectrum (400 MHz, DMSO-d_6) of PAIM-MM polymer***

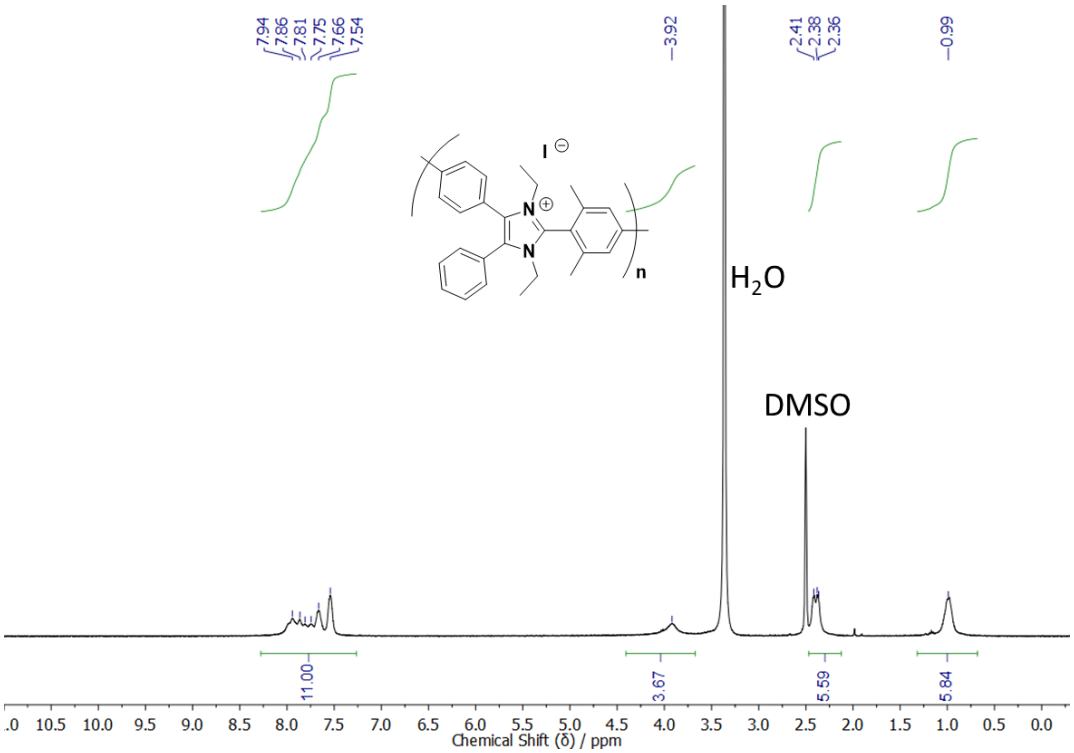

Figure A11. ***^{1}H NMR spectrum (400 MHz, DMSO-d_6) of PAIM-EE polymer***

Table A1. Conditions of equivalent of MeI, temperature and time for different degree of methylation

Trial	Equivalents of MeI	Temperature (°C)	Time (hours)	Degree of Methylation (dm)	IEC (mmol·g^{-1})
1				50	
2	2	23	18	66	0.91
3	11	23	18	78	1.53
4	13	23	18	79	1.56
5	14	23	18	80	1.64
6	20	23	18	84	1.83
7	20	40	20	87	1.98
8	20	40	35	94	2.31
9	20	40	48	97	2.45

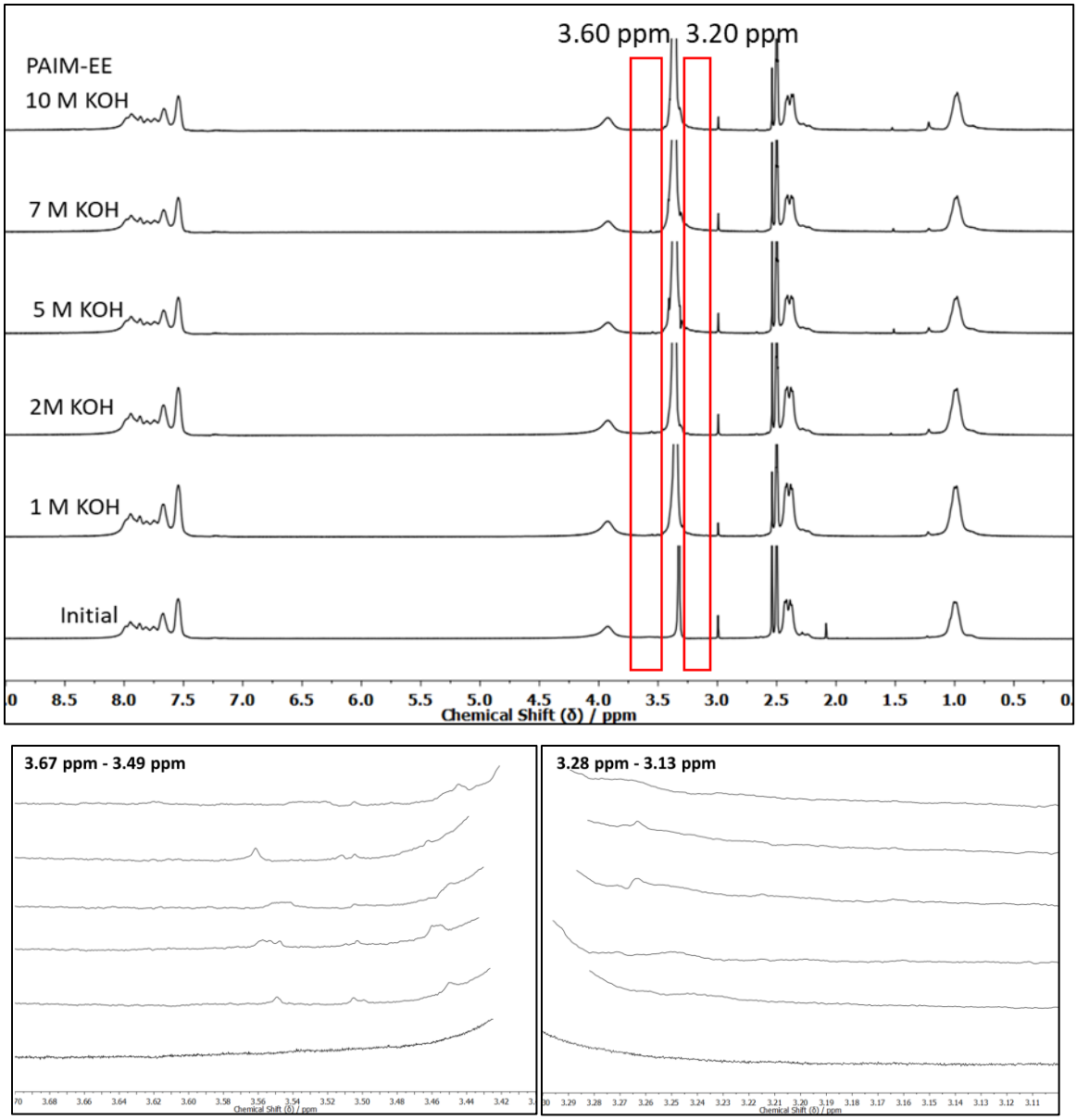

Figure A12. De-ethylation degradation of PAIM-EE in 1M to 10M KOH

Appendix B. Supporting information for PAIM-RR-2, PAIM-RR-3, and PAIM-RR-4

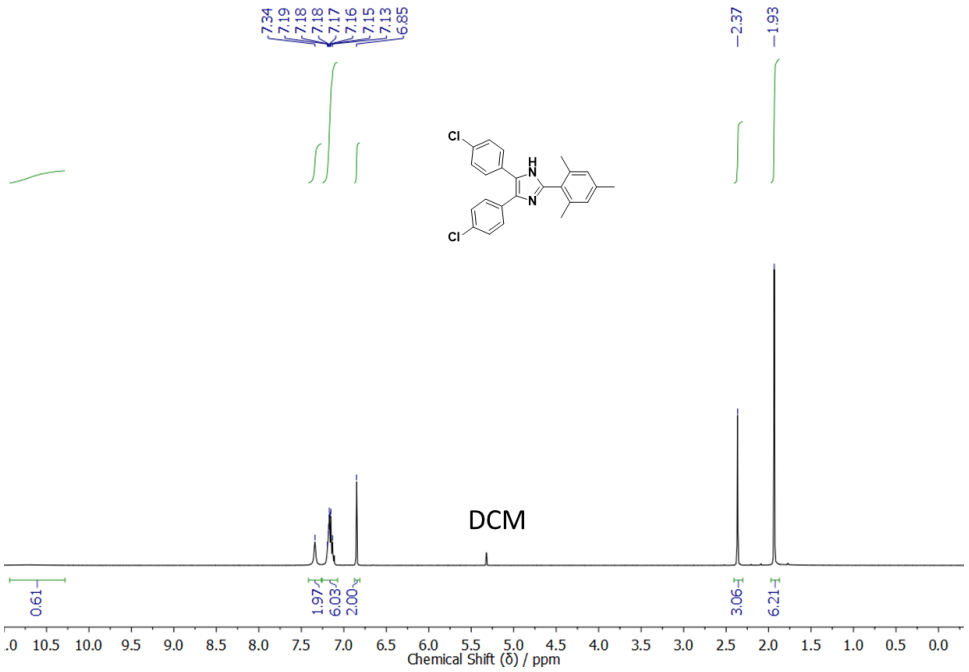

Figure B1. *^{1}H NMR spectrum (400 MHz, CD_2Cl_2-d_2) of 4,5-bis(4-chlorophenyl)-2-mesityl-1H-imidazole*

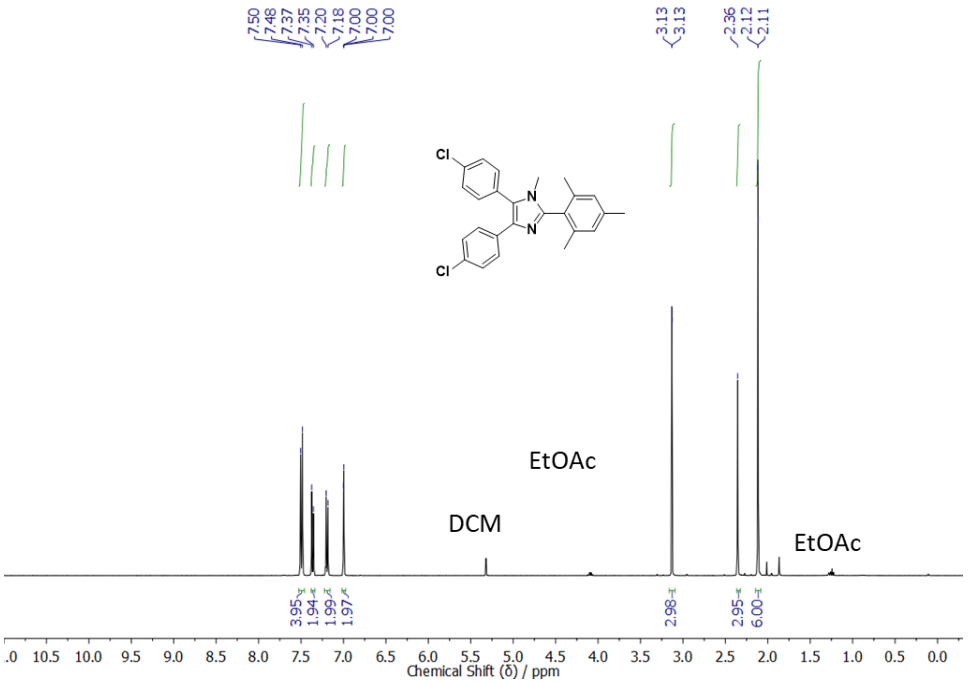

Figure B2. *^{1}H NMR spectrum (400 MHz, CD_2Cl_2-d_2) of 4,5-bis(4-chlorophenyl)-2-mesityl-1-methyl-1H-imidazole*

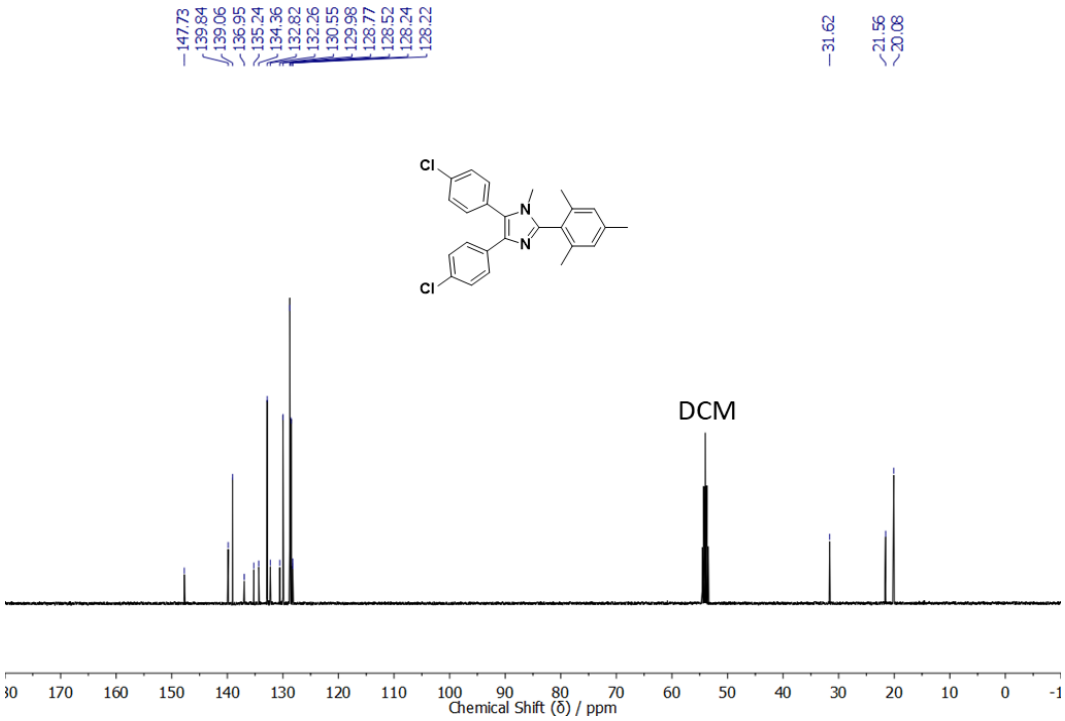

Figure B3. ***^{13}C NMR spectrum (125 MHz, CD_2Cl_2-d_2) of 4,5-bis(4-chlorophenyl)-2-mesityl-1-methyl-1H-imidazole***

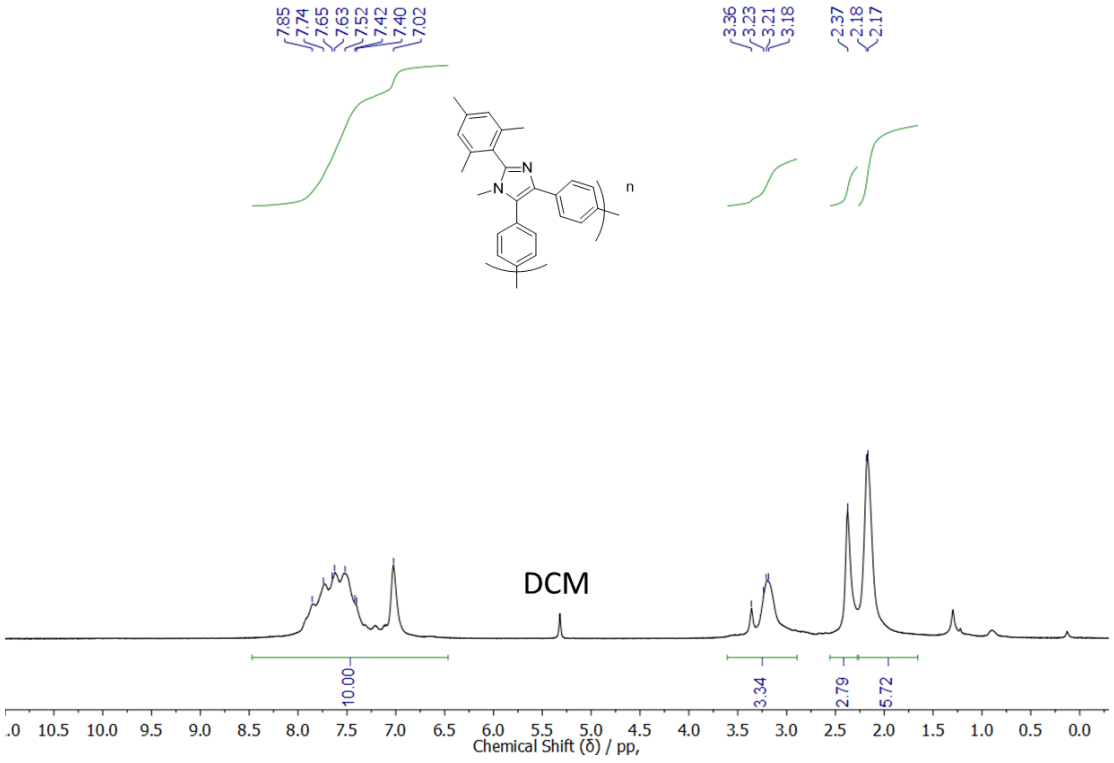

Figure B4. ***^{1}H NMR spectrum (400 MHz, CD_2Cl_2-d_2) of PAIM-MR-2***

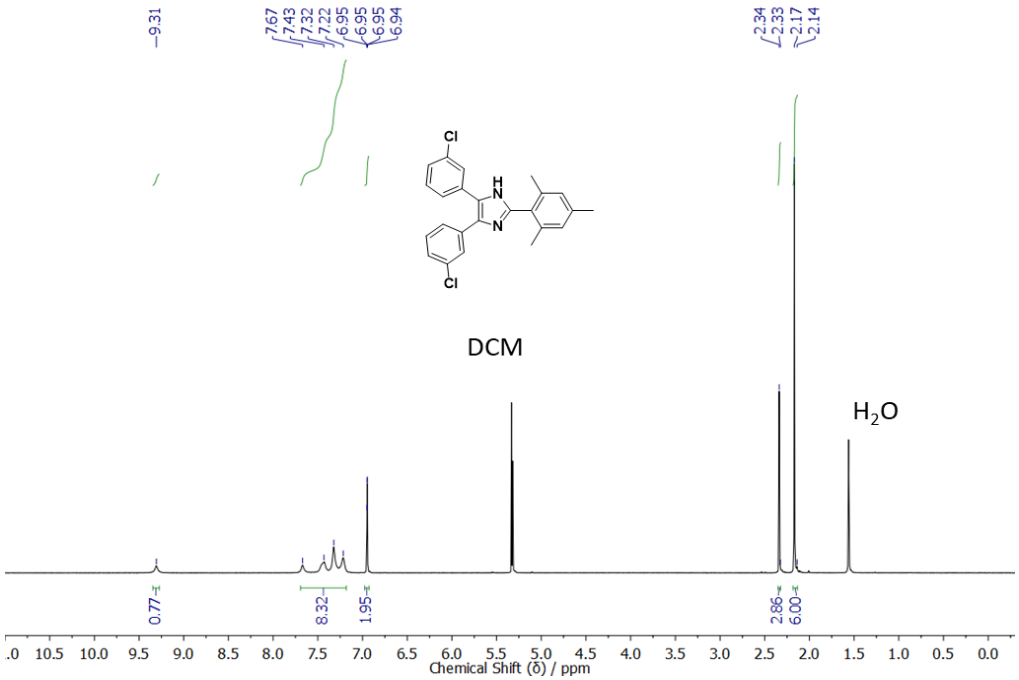

Figure B5. ***^{1}H NMR spectrum (400 MHz, CD_2Cl_2-d_2) of 4,5-bis(3-chlorophenyl)-2-mesityl-1H-imidazole***

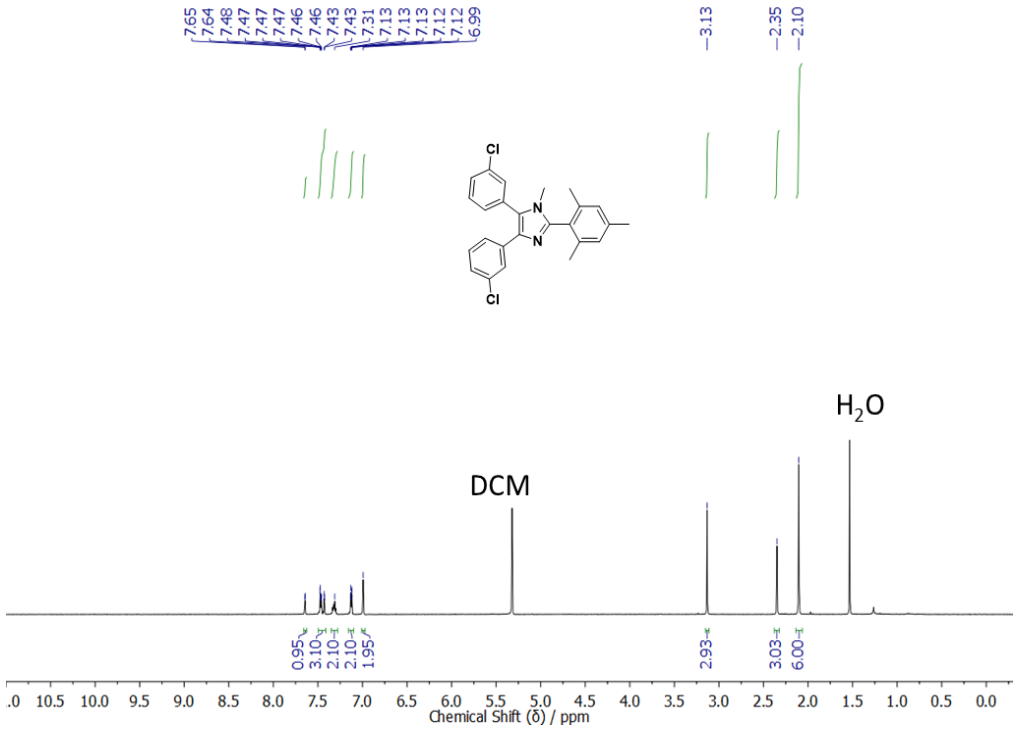

Figure B6. ***^{1}H NMR spectrum (400 MHz, CD_2Cl_2-d_2) of 4,5-bis(3-chlorophenyl)-2-mesityl-1-methyl-1H-imidazole***

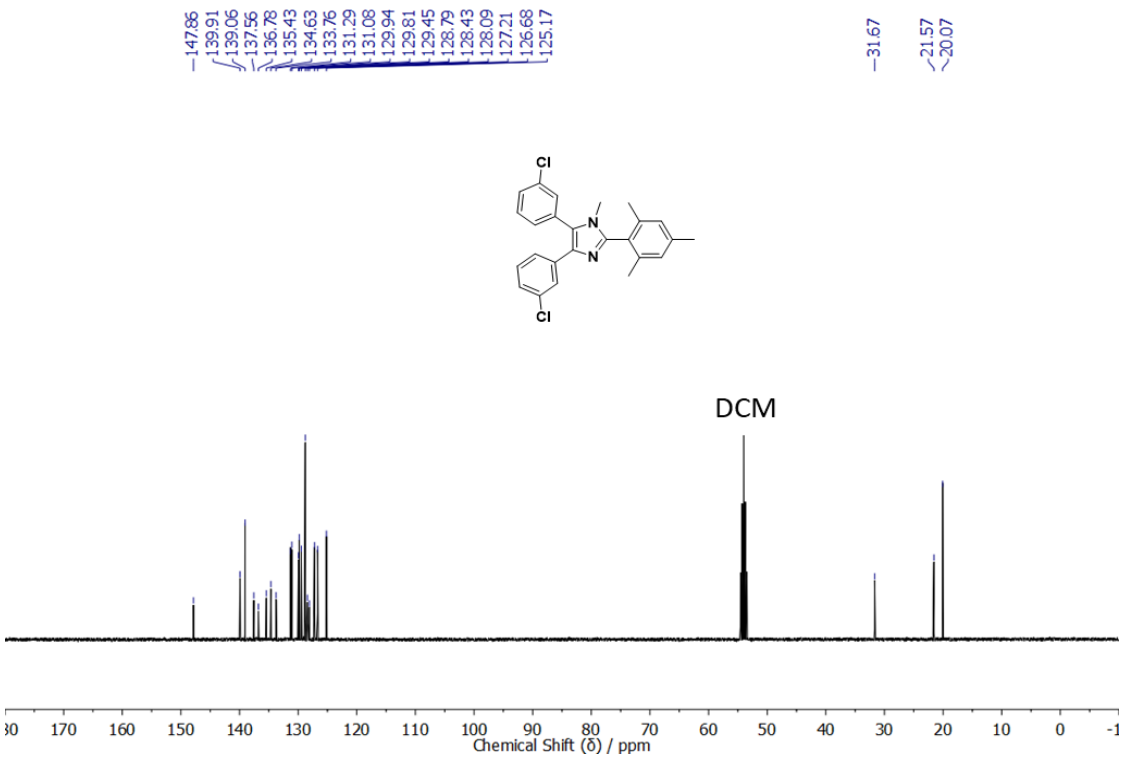

Figure B7. ***^{13}C NMR spectrum (125 MHz, CD_2Cl_2-d_2) of 4,5-bis(3-chlorophenyl)-2-mesityl-1-methyl-1H-imidazole***

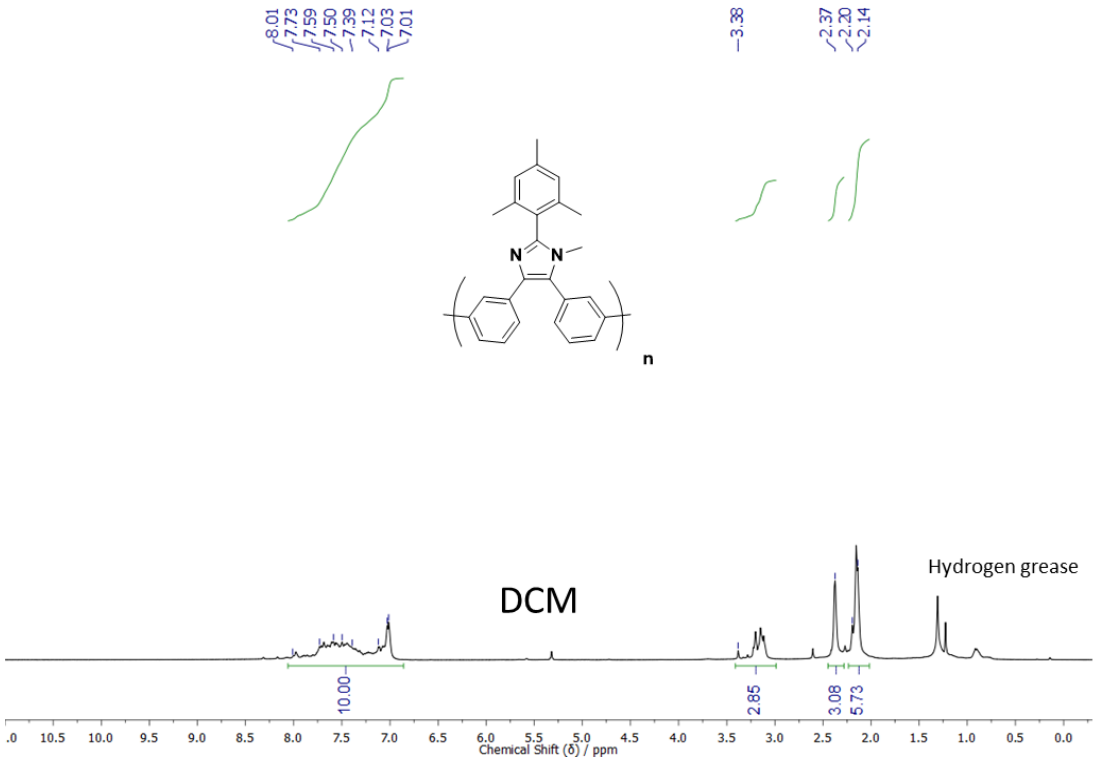

Figure B8. ***^{1}H NMR spectrum (400 MHz, CD_2Cl_2-d_2) of PAIM-MR-3***

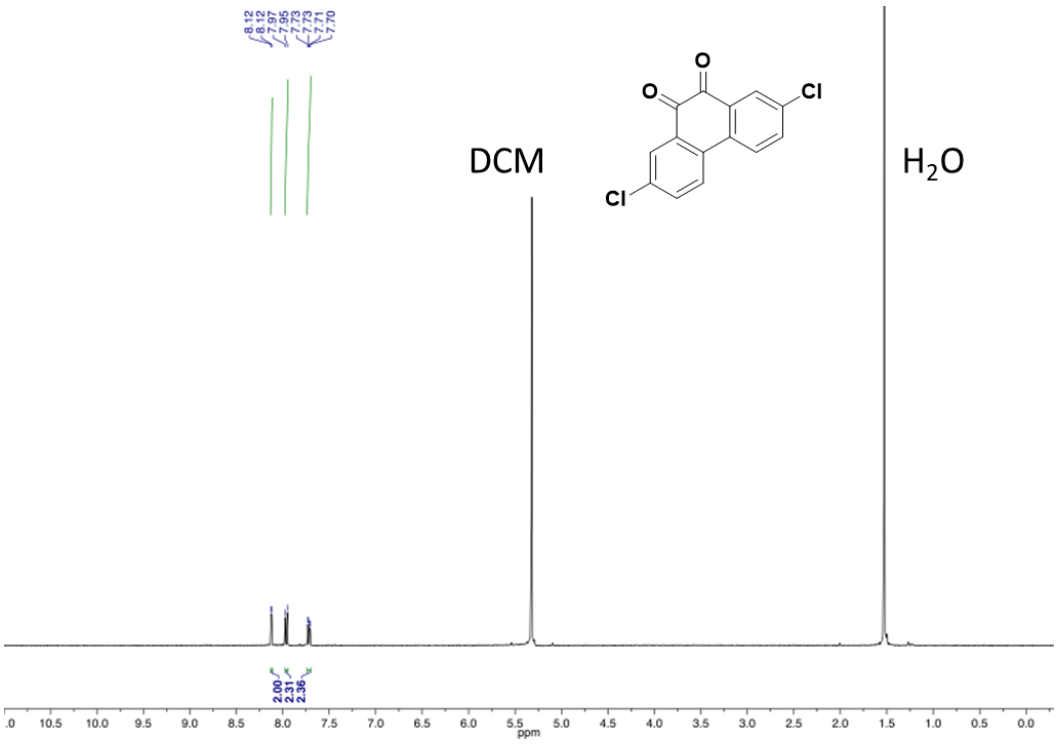

Figure B9. ***^{1}H NMR spectrum (400 MHz, CD2Cl2-d2) of 2,7-dichlorophenanthrene-9.10-dione***

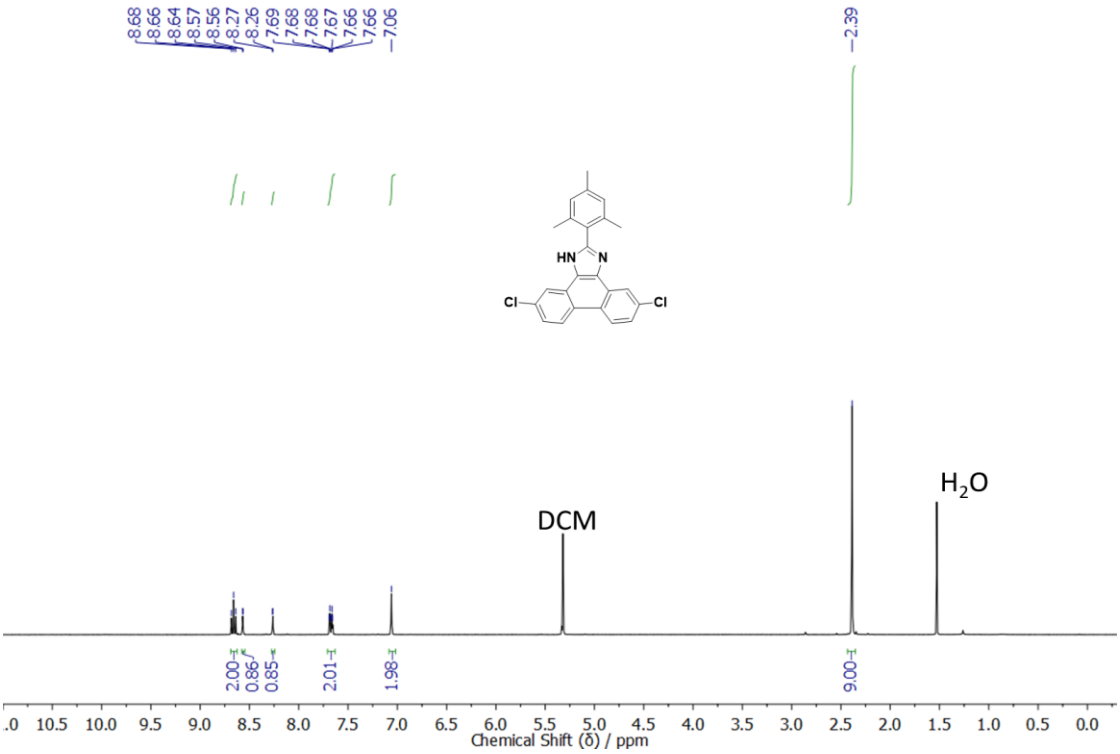

Figure B10. ***^{1}H NMR spectrum (400 MHz, CD_2Cl_2-d_2) of 5,10-dichloro-2-mesityl-1H-phenanthro[9,10-d]imidazole***

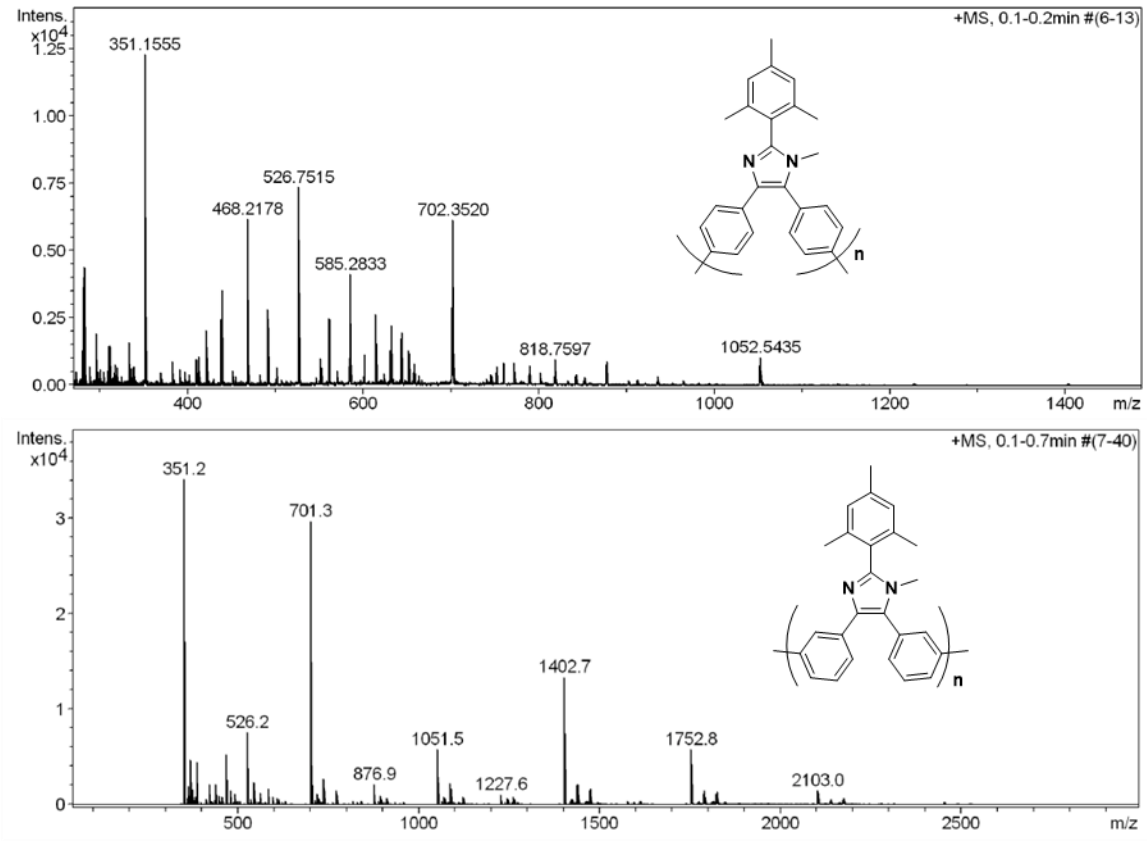

Figure B11. ESI Mass spectra of PAIM-RR-2 and PAIM-RR-3